# Optimization of Clinical Application and User-Friendliness of High-Resolution Impedance Manometry Analysis

R.J.P. van Heugten

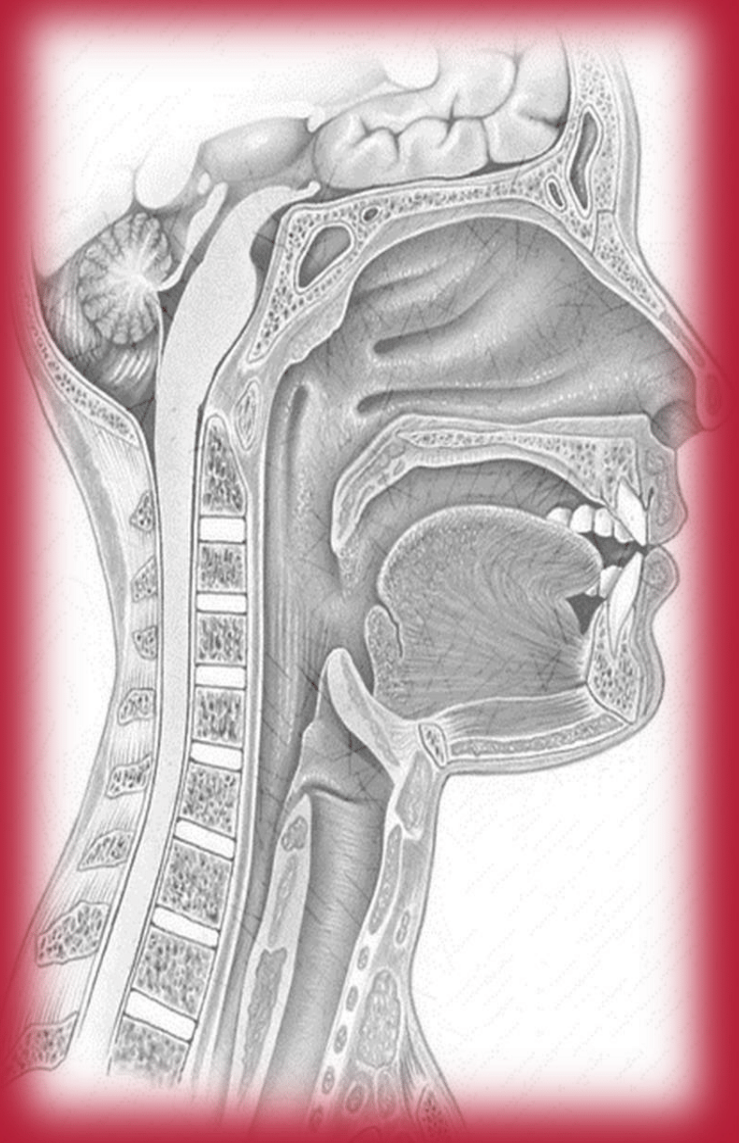

UNIVERSITY OF TWENTE
ANTONI VAN LEEUWENHOEK
TECHNICAL MEDICINE - MASTER THESIS
RUTH VAN HEUGTEN

# Optimization of Clinical Application and User-Friendliness of High-Resolution Impedance Manometry Analysis

July, 2023

ANTONI VAN LEEUWENHOEK FOUNDATION

UNIVERSITY OF TWENTE.

Graduation committee:

| | |
|---|---|
| *Chairman* | *prof.dr.ir. B. ten Haken* |
| *Medical supervisor* | *prof.dr.ir M.W.M. van de Brekel* |
| *Technical supervisor* | *dr. F.J. Siepel* |
| *Process supervisor* | *drs. A.G. Lovink* |
| *Additional member* | *dr. M.J.A. van Alphen* |
| *Additional member* | *dr. L. van der Molen* |
| *Additional member* | *MSc. M. Neijman* |
| *External member* | *MSc. J.R. Abbing* |

# Acknowledgement

The last year of my Master Technical Medicine, I have spent at the Antoni van Leeuwenhoek in Amsterdam. I started here by doing a short internship in September 2021 which was a great experience and motivated me for coming back to this place for my master thesis. The people at the Verwelius 3DLab and the head-neck oncology department were one of the main reasons for this. Therefore, I want to thank you all.

First and foremost, I want to express my appreciation to Marise. She has been a crucial source of advice and assistance, always approachable and infecting me with enthusiasm for research. It really felt like her door was always open for me, which was the same as her interaction with patients. I learned so much from the patience, respectful, and even loving way she interacted with them. In this interaction, it was visible that her patients respected her very much and enjoyed her presence. And of course, I cannot forget the enjoyable moments we shared over coffee (with sweets), a beer at social gatherings, and the memorable three-day trip to Leuven, where privacy was only found during showers.

Then, I want to thank Maarten for your persistent positivity. He always showed me endless possibilities and helped me see the brighter side of things. Whenever I became overly negative or critical, he was there to put things in a more positive perspective, ensuring that I left your office with a renewed sense of optimism. Next to this advice, it was not possible to leave your office without enjoying other stories about your personal life.

I also greatly want to thank Lisette, her critical eye has been vital, particularly in the final stages of writing. I have learned a lot from her expertise in structuring and organizing my thoughts into coherent and well-presented text. Her ability to deliver constructive feedback with tact and without discouraging my motivation is truly remarkable. Not only while writing my final thesis but also in the way I express myself and present myself in the hospital. Furthermore, I want to express my gratitude for the trust she gave me in performing the manometry assessments and other logopaedic measurements.

Then of course Michiel, I want to thank him for the trust he instilled in me when it came to performing various procedures in the clinic. While we didn't have a biweekly like with my other supervisors at the AvL, his prompt responses when needed were highly appreciated. His wise words during our concise feedback and update sessions, like the reminder that significant deviation from the expected often just indicates error, are always remembered.

Then Francoise, during our concise meetings, you always gave me lots of new inspiration to work with and offered me encouraging words that reassured me that everything would turn out fine.

Thanks to my process supervisors, especially Ruby, who enabled me to gain profound self-insight. Despite initially thinking about the intervision sessions as boring and unproductive, I must admit that they are truly worthy. Thanks to intervision, I believe that I have grown into a better professional, and Ruby played a significant role in this by always challenging me to my best.

Then, my chairman Bennie, who was so helpful to jump in during the last months of my thesis period. Without this help, defending my thesis in the summer of 2023 would not have been possible. So, lots of thanks for that. But also, for the reachability, prompt responses by mail when it was needed, and the meaningful conversation we had via mail and phone.

Then one of the most important aspects which made this thesis a success are the fellow student at the Verwelius 3DLab. Without you, I think I would have given up this project lots of times. They showed me relentless support, a safe space to vent struggles, and more importantly also just 'gezelligheid'. It was thanks to all of you that I traveled each day again to Amsterdam with joy and new spirit. I also really cherished all the enjoyable activities we had together outside of the internship. It truly feels like new friendships have started here.

Last but not least, my family, friends, teammates, and other people who were there for me when I needed to vent, even when they didn't even understand at all what I was talking about, and for just being there to do other fun stuff on the weekends!

# Summary

Approximately 0.6% of the Dutch population has some form of dysphagia, especially in patients with head- and neck cancer (HNC). This leads to physical problems, like malnutrition, dehydration, or pneumonia, and psychological burdens, like anxiety, low self-esteem, and social isolation. Therefore, it is important for patients to improve the quality of swallowing after HNC treatment. Videofluoroscopy swallow study (VFSS) is a clinically applied method to evaluate the swallowing problems of a patient thoroughly. However, objective assessment is challenging. Furthermore, VFSS evaluates mainly anatomical problems without considering physiological problems. A new promising tool in this area that can evaluate physiological problems is high-resolution impedance manometry (HRIM). A catheter with closely consecutive pressure and impedance sensors, which is placed via the nose in the pharynx of the patient, is used to measure generated pressure and bolus motion. This technique potentially gives more insight into the physiological problems of bolus propagation. Furthermore, HRIM has real data measures as outcomes, potentially making it easier to objectify the outcomes. However, the technique is not yet widely applied in the clinical care of the HNC patient population. Therefore, several steps must be investigated.

**Chapter 1** gives a clinical introduction to the anatomy and physiology of swallowing and the impact of HNC cancer on this mechanism. Additionally, it contains in-depth background on the measurement and analysis of VFSS and HRIM.

In **Chapter 2**, a review of the current literature on the application of HRIM in HNC patients and the experience that we have gained during the measurement of HRIM in HNC patients are compiled into a measurement protocol for HRIM in HNC patients in the AvL.

In the experience that is gained with measuring HRIM in HNC patients, it is found that HNC patients might exhibit altered pressure patterns while swallowing. For the analysis of HRIM, anatomical regions must be defined on the pressure topography plots, which is challenging due to these altered pressure patterns. Therefore, the potential of VFSS as a supportive tool for HRIM analysis is explored in **Chapter 3**. An automated catheter segmentation and sensor counting algorithm is developed. The catheter segmentation is accurate with mostly less than 1/6th sensor off. Additionally, no significant difference ($p=0.01$) was present between manually and algorithmically counting sensors in defined regions on the VFSS images.

Anatomical region definition for the analyses in HRIM is regularly performed in SwallowGateway (SWG). However, a training course must be followed before analysis can be done, and SWG does not provide insight into which sensor is where on the pressure topography plot. Customizing software does provide the information but is never used or tested for HRIM. At last, it is possible to determine regions on VFSS images, which is hypothesized to be easier due to better visible anatomical landmarks. Additionally, anatomical structures and the catheter undergo movement during swallowing, making it possible to determine anatomical regions on the images pre- and peri-swallowing. These four possibilities of anatomical region definition are compared to each other in **Chapter 4** on interrater variability and deviation between the methods. The interrater variability is the smallest in the VFSS pre-swallow images. The deviation in landmark definition between the same modality is accurate ($<1.5$ sensors) but between two different modalities is not accurate, which indicates a systematic difference between the landmark definition on pressure topography plots compared to VFSS images.

**Chapter 5**, gives a general conclusion and recommendations for future research. The analysis of HRIM could be optimized by incorporating the anatomical information from the VFSS images into the pressure topography plots. This provides deeper insights into the anatomical location on the topography plots and has the potential to enhance the comprehensiveness of HRIM data for less-experienced users, as well as improve the accuracy of landmark definition. Future research should primarily focus on determining the optimal method for defining anatomical landmarks on VFSS images and investigating the underlying reasons for the current deviation between anatomical landmarks on the pressure topography plots and VFSS images. Subsequently, the analysis of HRIM data using VFSS images as anatomical references could be further implemented in clinical practice.

# Contents

# 1

# Introduction

Approximately 0.6% of the Dutch population has some form of dysphagia. In people with pathologies, this number raises to 50%. [1] Dysphagia is especially common in patients with head and neck cancer (HNC). In 2019, 3.130 persons in the Netherlands were diagnosed with HNC. Treatment of HNC involves surgery, radiation, chemotherapy, or a combination of these. This leads to tissue damage, which alters the physiology of normal swallowing. Patients with swallow problems have an increased risk of malnutrition, dehydration, and pneumonia, leading to premature death. On top of the physical problems, patients have psychological burdens, like anxiety, low self-esteem, and social isolation. Therefore, it is important for patients to improve the quality of swallowing after HNC treatment. [2] An assessment of the swallowing function is needed to target the therapy.

Videofluoroscopy swallow study (VFSS) is the standard imaging modality to assess the anatomy during the swallowing of a patient. [3] The assessment of VFSS relies on visual observation, making it difficult to assign a quantifiable score and to objectify the assessment of a patient. Different efforts are made in objectifying the VFSS assessment. For example, a video-fluoroscopic dysphagia scale (VDS) to quantify the quality of different physiological occurrences is developed. [4] This showed a low to moderate inter-rater reliability. Other metrics developed in an attempt to objectify VFSS are the 8-point penetration-aspiration scale (PAS) and a 6-point residue scale (BRS). The PAS showed a wide range of scores for the intra class reliability. It scores between 0.33 and 0.65 for different volumes, consistencies, and amount of training of physicians. [5], [6], [7] The BRS shows a higher consensus among raters, between the 0.53 and 0.78 [8] [6]. Besides this fluctuating reliability, VFSS can only evaluate the movement of anatomical structures and boluses. It cannot evaluate the generated pressure or opening and closing mechanisms of ports that propagate boluses. The low reliability and absence of physiological information show that assessment with VFSS is suboptimal.

A promising technique that could solve both disadvantages is high-resolution impedance manometry (HRIM). This uses a catheter with sensors to measure bolus motion and pressure generated in the pharynx and larynx. This gives the user insight into the mechanisms that propagate a bolus in the patient. Mechanisms that do not work properly can be identified and the patient can receive targeted treatment exercises for those areas. Furthermore, HRIM has real data measures as outcomes, so is more likely to have higher intra- and inter-rater reliability. Besides these advantages, HRIM doesn't require radiation or contrast agents and is portable for application in bed-ridden patients or in the outpatient clinic. A high-resolution pharyngeal manometry international working group of Omari et al. has developed an online analysis platform for the HRIM data, SwallowGateway [9]. Users need to define different anatomical and physiological landmarks after which the software calculates metrics regarding the swallowing quality.

## 1.1 Clinical background

### 1.1.1 Anatomy of the pharynx and physiology of swallowing

To interpret the pressure pattern and bolus motion that is measured with the HRIM, it is important to understand the anatomy and physiology of the head and neck area and the swallowing mechanism. Before food enters the pharynx, it must be ingested into the mouth. Food must be kept in the mouth for

chewing and preparation before it is propagated to the pharynx. The tongue mixes the food and seals the pharynx from the oral cavity to prevent spillage of food into the pharynx. The mandible provides movement and the food bolus is mixed with saliva, so the food bolus is ground. When the food bolus is ground, the tongue curves the lateral edges upwards and contracts from anterior to posterior. The food bolus is pushed into the pharynx. The pharynx is divided into different anatomical regions, see figure 1.1.

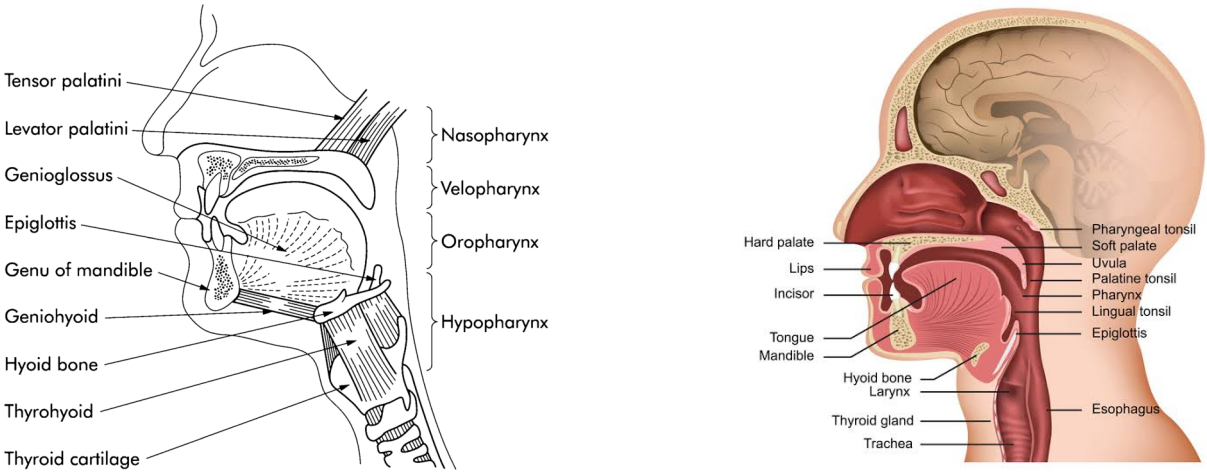


Figure 1.1: The different regions and structures of the pharynx [10] (left) and [11] (right).

### Velopharynx

The velopharynx is bound by the velum, the lateral pharyngeal walls, and the posterior pharyngeal walls. The velum and the pharyngeal walls have the most important function during swallowing and speaking in the velopharyngeal area. The velum consists of a mixture of tendinous, muscular, adipose, and connective tissue along the velar length, with the most functional components in the anterior two-thirds of the velum. It is a valve that extends from the hard palate's posterior surface into the velopharynx in the direction of the posterior pharyngeal wall. The space between the pharyngeal walls and the velum is called the velopharyngeal port. During nasal breathing, the oral surface of the velum points downwards and rests against the back of the tongue. The velopharyngeal port is open. A tight seal in the velopharyngeal port must be made during swallowing to separate the nasal and oral cavities. Two mechanisms accomplish the tight seal. The first mechanism involves the contraction of the levator veli palatini and the musculus uvulae. The levator veli palatini originates from both sides of the skull's temporal bone and is inserted in the middle of the velum. It pulls the velum up at 45 degrees to close the velopharyngeal port. The musculus uvulae runs between both sides of the levator veli palatini as the only intrinsic muscle of the velum, see figure 1.2. It assists in filling the velopharyngeal port by creating bulk to the nasal surface of the velum and providing the velar knee (where the velum bends). The second mechanism involves the movement of the pharyngeal walls in a sphincter-like pattern by the superior pharyngeal constrictor. The superior pharyngeal constrictor is the superior one of the three pharyngeal constrictors (superior, middle, and inferior). Together, they make up the length of the pharynx. The superior pharyngeal constrictor displaces the lateral pharyngeal walls medially and the posterior pharyngeal walls anteriorly. Thereby narrowing the velopharyngeal port. This improves the tight seal between the velum and pharyngeal walls. The amount of contribution of both mechanisms differs among individuals. [12] [13] The tight seal in the velopharyngeal port contributes to increased pressure in the velopharynx. It may display a sustained bimodal or peak-plateau pressure wave. The velopharyngeal pressure increases with increased bolus volume and inverted body position. [14] [15] [16]

Besides the levator veli palatini, the musculus uvulae, and the superior pharyngeal constrictor, more muscles are involved in the functioning of the velopharynx. The tensor vili palatini isn't involved in the swallowing function but is responsible for the opening of the Eustachian tube for drainage of fluids from the middle ear and pressure equalization across the eardrum. The palatopharyngeus has different variations in the course of its bundles among people, resulting in different functions. It could facilitate the overall position of the velum, contribute to the inward placement of the lateral pharyngeal wall and/or elevate the pharynx or larynx. The palatoglossus originates from the lateral margins of the velum and

inserts onto the lateral aspect of the tongue. It is a direct antagonist to the levator veli palatini, so is involved in the opening of the velopharyngeal port. The muscle also attributes to elevating the tongue and constrict the faucial isthmus. This assists in moving the bolus toward the esophagus during a swallow. The last muscle in the velopharyngeal area is the salpingopharyngeus. This muscle terminates in the lateral pharyngeal wall. It probably has no real contribution to the velopharyngeal mechanism because the size and presence differ among individuals. If present, it could provide a superior pull on the lateral pharyngeal walls. All muscles are innervated by the pharyngeal plexus formed by the nervus vagus (CN X) and the nervus glossopharyngeus (CN IX), except for the tensor veli palatini which is innervated by the mandibular branch of the nervus trigeminus (CN V). [13] [12]

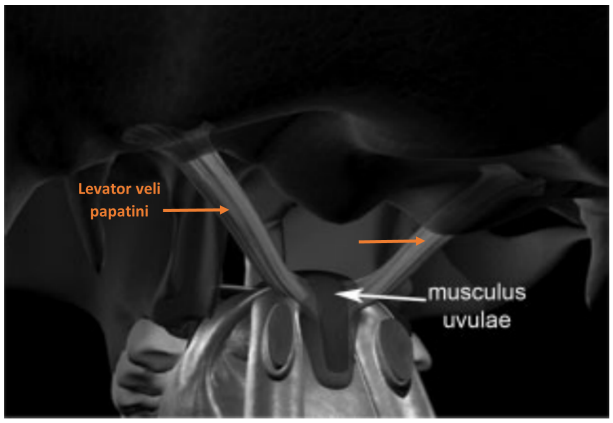


Figure 1.2: Musculus uvulae is running between both levator veli palatini in the velum. [13]

### Oropharynx/mesopharynx

The oropharynx, or mesopharynx, is located posterior to the oral cavity and inferior to the velopharynx. It extends from the soft palate to the level of the hyoid bone (C3). The oropharynx is divided into four distinct components: the base of the tongue, the soft palate, the palatine tonsillar fossae, and the lateral and posterior pharyngeal walls. The base of the tongue is one of the most important parts of the swallowing mechanism. It generates together with the oral tongue the pressures to drive food through the oral cavity into the pharynx and esophagus. The base of the tongue is innervated by the pharyngeal plexus of the nervus glossopharyngeus (CN IX). [17] [18] The pressure peak in this area is mostly unimodal with the same onset and offset time over the whole region. The pressure is generated at the tail of the bolus by the tongue base and the pharyngeal constrictors. The pressure drives the bolus and therefore, the bolus presence is ahead of the pressure. [15]

### Hypopharynx/laryngopharynx

The hypopharynx, or laryngopharynx, is superiorly bound by the mesopharynx indicated by the pharyngoepiglottic fold. The hypopharynx is inferiorly bound by the upper esophageal sphincter (UES) and the vocal cords. It refers to the area where the pharynx divides into the esophagus and larynx (with the trachea). The hypopharynx is essential in propelling food posteriorly into the esophagus. Several components play a crucial role in this mechanism. Contraction of the thyrohyoid and suprahyoid muscles causes the hyoid bone and larynx to elevate and move anteriorly. The epiglottis slopes backward, thereby sealing off the larynx. The vocal folds close, sealing off the glottis. The arytenoid tilts forward. The palatopharyngeus, the stylopharyngeus, and the salpingopharyngeus muscles pull the larynx up, thereby protecting the airway and improving bolus passage. The aryepiglottic and thyroepiglottic muscles are responsible for pulling down the epiglottis to prevent aspiration. [19] [20] [21] The pressure waveform starts in this area with an onset peak after the peak of the tongue-base pressure. Secondary, irregular peaks are present. They reflect cartilaginous laryngeal and epiglottic structures against the catheter. [15].

### Upper esophageal sphincter

The UES is located at the superior end of the esophagus. It is constricted during rest, which prevents air from going into the esophagus and reflux from going into the pharynx or larynx. This causes constant

high pressure at the UES during rest. The UES relaxes when a bolus reaches the UES, so it allows the bolus to enter the esophagus. The inferior pharyngeal constrictor, composed of the cricopharyngeus and thyropharyngeus, is responsible for the relaxation. The high resting pressure drops when the UES relaxes. The pressure rapidly increases when the UES constricts again after the bolus has propagated through the UES. After this, the pressure decreases to resting pressure. The pressure tracing of the UES is captured over multiple pressure sensors because of the movement of all pharyngeal structures. Even pressure sensors that didn't measure the resting pressure.

### 1.1.2 Pathology and pathophysiology

In the Netherlands, each year occur approximately 3000 new cases of HNC and this number has been rising since 1989. [22] Those cases are often caused by excessive smoking, HPV infection, and alcohol abuse. Often used therapies for HNC, depending on the stage and patient variables, are radiation therapy, chemotherapy, surgery, or a combination of some of those. All these therapies damage the structures that are lying close to the region of interest. [23] This leads in most cases to some degree of dysphagia. Aspiration is an example of a common problem in these patients. Aspiration can be divided into three different causes. First, before the swallow due to reduced oromotor control or delayed or absent reflex. Second during the swallow due to reduced laryngeal closure, epiglottic inversion, or laryngeal elevation. Third, after the swallow due to reduced pharyngeal peristalsis, cricopharyngeal sphincter dysfunction, reduced laryngeal elevation, and structural abnormalities. HNC has a lot of different subtypes. The most common subtypes in the Netherlands are oral, oropharyngeal, and laryngeal cancer. [22]

#### Oral and oropharyngeal cancer

Oral and oropharyngeal cancer includes tumors in the tongue, the floor of the mouth, hard palate, soft palate, tonsils, salivary glands, cheeks, and throat. Radiation of tumors in these areas often results in xerostomia (dry mouth) ulceration in the mouth, bleeding, and pain. Degeneration of the jaw, teeth and surrounding tissue, pharyngeal stricture, and reduced taste sensation could be long-term risks of radiation therapy. Also, the sensation of the larynx is reduced which could lead to silent aspiration. The cytotoxics in chemotherapy could cause short-term nausea, weakness, neutropenia, and mucositis. This could lead to different levels of dysphagia. [24] Surgical resection of the tumor does not reduce the risks of dysphagia. The location of the excised lesion is a better prediction for the severity of dysphagia than the size of the excised lesion. For example, tumors in the tongue base result in more severe dysphagia compared to tumors in the anterior floor of the mouth. [25] [24] Also, sensory and motoric innervation could be lost due to nerve damage during surgery. In oropharyngeal cancers, surgery leads to an increased risk of glossopharyngeal nerve damage. This leads to decreased sensory innervation of the pharynx membranes, palatine tonsil, soft palate, tonsillar pillars, and posterior third of the tongue and decreased motoric innervation of the pharyngeal muscles (except for the tensor veli palatini). This could result in dysphagia and recurrent aspiration. In patients with flap reconstruction, the absence of motoric control could lead to the absence of propulsive forces. Removal of parts of the tongue base results in problems due to its crucial role in swallowing. The tongue base makes contact with the posterior pharyngeal wall, which generates pressure and elevates the hyoïd bone and larynx. Lack of this mechanism results in delayed initiation of the swallow, before swallow aspiration, and post-swallow stasis. Resection of parts of the tongue and palate leads to a reduced velopharyngeal mechanism with a non-tight seal of the velum. This reduces the generated pressure in the velopharynx. This makes it more complicated for the tongue to push the food bolus into the pharynx. That could lead to a residue at the pharyngeal recesses, leading to an increased risk of aspiration. [26] Sacrificing the hyomandibular muscle reduces the protective tilting action of the larynx, which results in an increased risk of aspiration. So, radiation, chemotherapy, and tumor resection could have a tremendous effect on the swallowing function of patients. [24] [27]

#### Laryngeal cancer

A patient group in which the anatomy is tremendously altered due to the treatment of HNC is patients with laryngeal cancers. Each year, approximately 685 persons are diagnosed with laryngeal cancer in the Netherlands. 70% of these patients undergo conventional therapy which is a total laryngectomy (TL) with postoperative radiotherapy (RT). [28] [22] Total laryngectomy involves the removal of all laryngeal structures and the superior part of the trachea. This leads to the disconnection of the trachea to the pharynx. The superior trachea is therefore stitched to a permanent breathing hole in the anterior neck, called a tracheostoma. A voice prosthesis can be placed in these patients between the trachea and

esophagus to enable voice production. This prosthesis functions as a one-way valve, allowing exhaled air from the lungs and trachea to enter the esophagus when the patient occludes the tracheostoma. The air induces vibrations in the esophagus, generating voice. Aspiration is no longer possible in these patients unless there is a leakage in the voice prosthesis, as there is no longer a connection between the pharynx and trachea. Moreover, the altered anatomy also affects the pressure and impedance patterns measured with HRIM.

## 1.2 Technical background

### 1.2.1 Videofluoroscopy

Videofluoroscopy swallow study (VFSS) is considered the gold standard for visualization of the anatomy and physiology of the patient's swallowing function. [29] During VFSS, a patient swallows different amounts and consistencies of contrast agents, omnipaque. A moving X-ray is made from the head and neck area, which follows the contrast between the mouth and the stomach. The examination is repeated for boluses of different viscosities by thickening the contrast agent with Precise-Thick-N-Instantgel of NestleHealthSciences and by adding a dice of gingerbread or cracker to the omnipaque. The viscosities are expressed in International Dysphagia Diet Standardization Initiative (IDDSI) levels, ranging from thin liquid to regular easy to chew food, see figure [30] [31]. IDDSI is a global initiative to provide standardized terminology for describing food textures and drink thickness. The patient can be asked to apply some compensation techniques which can improve the swallowing function. These compensation techniques could for example be swallowing with the chin on the chest or while turning the neck to the right or left. After this examination, a speech- and language pathologist (SLP) and physician evaluate the recordings and decide which intervention is advisable for the patient. This intervention could for example be a change in diet, exercises to increase muscle strength, change in head position while swallowing, lipofilling, or dilatation.

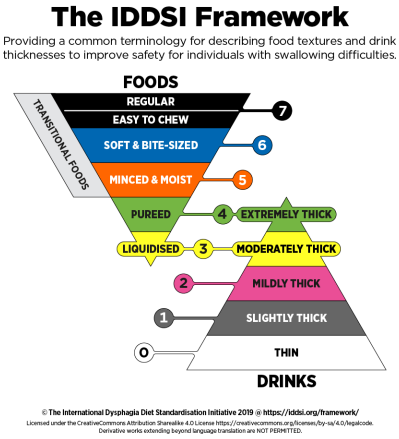


Figure 1.3: The IDDSI framework. [30]

### 1.2.2 High-resolution impedance manometry

HRIM can calculate the bolus motion and pressure generated in the pharynx and larynx. It could be a promising additional or alternative method for the assessment of swallows of patients, with the advantage that no contrast or radiation is needed [32]. In addition, the HRIM is portable, making it possible for bedridden patients and applicable in a regular outpatient clinic. Previous studies have shown a high correlation between parameters in HRIM and VFSS. [33] [34] Two different HRIM catheters exist; a solid-state and a water-perfused catheter. This research will focus on the solid-state catheter because of its availability at the AvL. HRIM catheters contain each 1 to 2 cm a pressure sensor that can measure the real-time pressure from approximately the mouth to the stomach. This makes quantification of the generated pressure in the different anatomical regions possible. In addition, the HRIM catheter has multiple impedance sensors that measure the impedance in approximately the same area. To measure the impedance, NaCl is added to the bolus volume for conductivity. Impedance can be seen as a complex

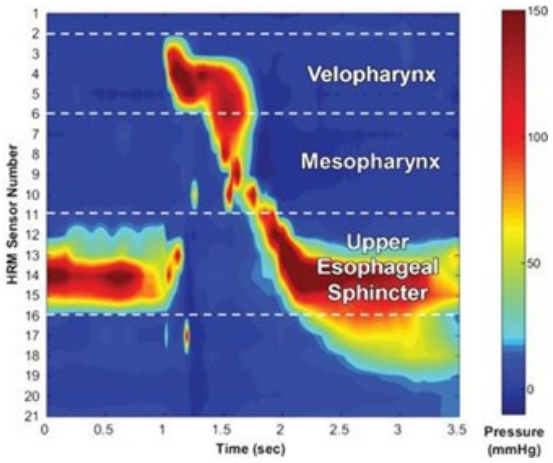


Figure 1.4: Topography plot of HRIM of a pharyngeal swallow. The x-axis is the time, the y-axis is the depth in number of sensors, and the color is the pressure. [36]

resistance. Therefore, it describes the relationship between the current and the potential of an electric circuit, see formula 1.1. When the conducting bolus connects two electrodes, the current increases which decreases the impedance. For easier interpretation, impedance is translated into admittance according to formula 1.2. Admittance has a linear relationship with bolus presence, so gives a higher value when more bolus is present.

$$Z = V/I \tag{1.1}$$

$$Y = 1/Z \tag{1.2}$$

The transducer converts the pressure and admittance into an electrical signal which is amplified, filtered, and digitized to a computer for visualization and recorded to a storage device. [35] Software that is mostly provided by the company of the manometer can visualize the pressures in a 3D spatiotemporal pressure topography plot (x-axis time, y-axis depth, z-axis pressure), see figure 1.4. Some catheters come with the possibility to link VFSS in real-time to the pressure and impedance measurements. [35]

**Swallow Gateway**

Swallow Gateway is an online software program developed by Omari and his working group to analyze HRIM data [9]. The software is compatible with different HRIM catheters and brands. The measured data can be loaded into the software for analysis. This is visualized as a continuous pressure topography plot. On this continuous plot, users are required to select the specific area of a swallow that they want to analyze by drawing a box around it. Once the selection is made, the software opens a new tab where the chosen box is loaded for further analysis. In this analysis, the user needs to identify the following anatomical regions in the pharynx: (1) velopharyngeal proximal margin, (2) hypopharyngeal proximal margin, (3) UES apogee, and (4) UES distal margin. Besides, they need to identify the moment of (5) UES relaxation and (6) UES contraction. From this information, the software defines the depth and time corresponding to activity in the velopharynx, mesopharynx, hypopharynx, UES, and the relaxation time of the UES. Boxes are drawn around these areas and a line indicates the relaxation time, see figure 1.5. The user can adapt the boxes and lines if they are incorrect. The software calculates metrics from this information. These metrics are verified by the high-resolution pharyngeal manometry international working group of Omari et al. via a Delphi consensus process. [16] With this information, swallowing problems can be identified. The measures that are determined by their working are: pharyngeal contractile integral (PhCI), velopharyngeal contractile integral (VCI), mesopharyngeal contractile integral (MCI), hypopharyngeal contractile integral (HPCI), UES integrated relaxation pressure (UES IRP), UES relaxation time (UES RT), UES maximum admittance (UES Max Adm), hypopharyngeal intrabolus pressure (IBP), swallow risk index (SRI), and hypopharyngeal bolus presence time (BPT). The contractile integrals reflect the mean pressure inside the region multiplied by the depth and duration of the corresponding region. They are chosen as pressure metrics because they might display sustained and/or multimodal features. This could indicate whether sufficient pressure is generated in each region to propagate the bolus. The UES IRP is the median of the lowest non-consecutive 0.25 seconds during UES relaxation at the whole UES region. This indicates whether the UES opens sufficiently. The UES RT is

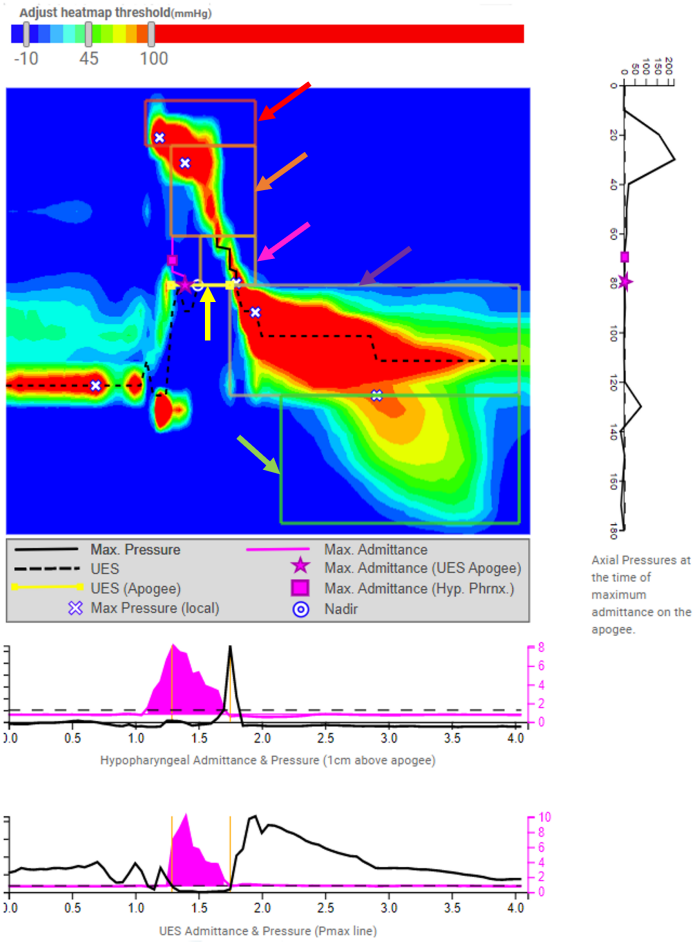


Figure 1.5: Swallow with identified anatomical regions. The upper box identified with a red arrow is the velopharynx. The box indicated with the orange arrow is the mesopharynx. The box identified with the pink arrow is the hypopharynx. And the last box indicated with the purple arrow is the UES. The line indicated with the yellow arrow has as a starting point the relaxation and as the end-point the contraction of the UES.

the time on which the UES pressure is below 50% of the baseline or 35mmHg, indicating whether the UES opens sufficiently long. The UES Max Adm indicates the extent of UES opening because the more bolus could be present between the UES, the bigger the opening diameter is. The IBP indicates UES restriction to bolus flow. An increased IBP shows an increased pharyngoesophageal pressure gradient with could cause increased velopharyngeal and mesopharyngeal pressure. It is defined as the pressure 1 cm above the UES apogee at the moment of maximum hypopharyngeal distension which could be deduced from the impedance. The SRI is a combination of pressure and flow variables, see equation 1.3.

$$SRI = \frac{FlowInterval * PNadImp}{PeakPressure * (TNadImp - PeakP + 1)} * 100 \tag{1.3}$$

The flow interval (FlowInterval) represents the interval on which flow is present through the UES. The pressure at nadir impedance (PNadImp) is the pressure at the moment of lowest impedance, so pressure during bolus presence, during and around the moment of UES opening. The time of nadir impedance (TNadImp) minus the peak pressure (peakP) is the time between the lowest measured impedance (corresponding to bolus presence) and the maximum measured pressure in and around the moment of UES opening. [37]

## 1.3 Research objective

Despite the benefits of HRIM, HRIM is not implemented in the clinical practice of lots of hospitals, also not here in the AvL. This is mainly because of two difficulties. First, the manual landmark definition is hard, especially in HNC patients in which the anatomy and physiology of swallowing are altered. Users need to have extensive knowledge and attended a training course about the anatomical landmark definition. Second, the definition of the anatomical landmarks is time-consuming because every swallow needs to be selected and assessed manually. These difficulties show that the use and analysis of HRIM are not straightforward enough for broad use in clinical practice.

It is expected that simplifying HRIM analyses eases the implementation of HRIM in clinical practice for HNC patients. However, the method to achieve this is currently unknown. Therefore, this thesis aims to identify a possible approach for simplifying pharyngeal HRIM analyses, in order to assess the swallowing quality of HNC patients in a clinical setting. This leads to the following research question: *"How can pharyngeal high-resolution impedance manometry analyses be optimized to asses the swallowing quality of head and neck cancer patients in clinical practice?"*

This research question will be answered by first developing a measurement protocol for the combined application of HRIM and VFSS in clinical practice for HNC patients (Chapter 1). Then, an attempt for automated catheter segmentation and sensor counting in VFSS is done to explore the potential of automating such an analysis method (Chapter 2). Lastly, different methods of anatomical region definition in pressure topography plots and VFSS images are compared to explore the optimal method (Chapter 4).

# 2

# Development of HRIM measurement for HNC patients

## 2.1 Introduction

HRIM is a validated diagnostic tool that can effectively detect swallowing disorders and has the potential to become a standard practice for patient care in the AvL. However, despite its approval, the current clinical practice in the AvL does not yet utilize this tool. As a result, there is a need to establish a comprehensive framework that can support the adoption and implementation of HRIM in the clinical setting. This framework needs to cover several areas like selecting patients, preparing applications and measurements, administering consistently, and communicating effectively with patients and physicians. By developing and implementing this framework, we can ensure that HRIM is used appropriately and consistently, leading to improved patient diagnostics.

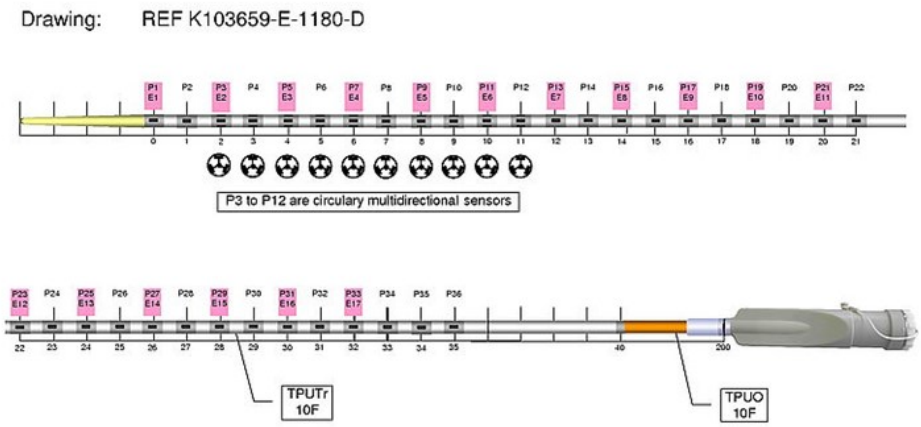


Figure 2.1: The Solar GI K103659-E-1180-D catheter. The catheter from Laborie which is used in the AvL. It has 36 pressure sensors and 16 impedance sensors. The impedance is measured at the even pressure sensors because impedance is measured between two sensors. [38]

In the AvL, the manometry catheter from Medical Measurement Systems/Laborie is purchased. Laborie/Medical Measurements Systems is a medical company specializing in the development of diagnostic tools in gastroenterology, urology, and urogynaecology. They develop a broad range of HRIM catheters. The purchased catheter is a solid-state manometer, the Solar GI K103659-E-1180-D, see figure 2.1. This manometer contains 36 pressure sensors, each 1 cm apart. Sensors P3 to P12 measure the pressure circumferential, which gives as output the mean pressure. The other sensors measure the pressure unidirectional. The impedance is measured at the location between two pressure sensors when the conductive bolus connects the two impedance electrodes. If the bolus connects impedance electrodes E1 (located at P1) and E2 (located at P3), the impedance is measured at the location of P2, and so on for the other

sensors. The catheter has 17 impedance electrodes, so the impedance can be measured at 16 places. These electrodes are located from P1 to P33. All electrodes are made from metal and the impedance is measured with alternating current (AC). [38] The data is real-time loaded into the software of Laborie and a spatiotemporal plot is visualized. During the measurement, swallows can be marked so the users can indicate the bolus size and consistency. All the pressure, impedance, and marker data can be exported as ASC and excel files from the Laborie software.

In the AvL, this catheter is only used in the research setting of the SEATTLE/N21STL study. This study investigates the impact of training with the swallowing exercise aid (SEA) on several swallowing and voice quality outcomes post-TL. A VFSS measurement protocol with HRIM has been developed for this study which may be partly applicable. However, there are several reasons why further research is necessary to explore the applicability of this protocol in the entire HNC population in clinical practice. Firstly, the protocol is specifically tailored for TL patients. Since this population has no larynx (changed anatomy), different swallowing problems compared to a standard HNC population are present. For example, in this population, the airway is distracted from the esophagus so a patient cannot aspirate, while a major problem in other dysphagia patients after HNC treatment is aspiration. This may require adaptations in the method of catheter insertion, measurement techniques, and desired information to be suitable for the entire HNC population. Secondly, this thesis aims to identify a potential approach to optimize the HRIM analysis for clinical practice. To achieve this goal, adaptations in the measurement protocol may be necessary. These adaptations may involve streamlining the analysis process, which may not be required in a research study setting. In a research study, analysis can be conducted at a later time, whereas in clinical practice, immediate and time-efficient analysis is essential. Therefore, more research into a suitable measurement protocol for the clinical practice of the whole HNC population is desired.

Omari et al. [16] conducted an evidence-based study on the key elements of a pharyngeal HRIM measurement protocol to diagnose swallowing disorders in clinical practice. However, their protocol is not specifically tailored to the HNC population, but rather to all dysphagia patients. The potentially altered anatomy and physiology of HNC patients are not accounted for in Omari's protocol. The use of HRIM in patients with HNC has been the subject of little research and there is no specific protocol for the measurement of HRIM in this population. A more detailed search into the current state will lead to more insight into the application for this patient population.

Hence, the objective of this chapter is to address the following research question: *"What should an HRIM measurement protocol for HNC patients, applicable in clinical practice, entail?"* This research into a suitable protocol should take into account the unique characteristics of the HNC population and strive to create a protocol that is practical and efficient for application in routine clinical practice. Therefore, our knowledge, experience, and existing literature about HRIM in the HNC population will be evaluated to answer this question.

## 2.2 Methods

To develop an HNC-specific measurement protocol for clinical practice, two primary sources of information were utilized.

### 2.2.1 Literature review

The first source involved conducting a literature review on HRIM applied to HNC patients to gain insight into existing protocols used in this patient population. A search term was determined as follows: 'TITLE-ABS-KEY ( manometry ) AND TITLE-ABS-KEY ( cancer ) AND TITLE-ABS-KEY ( pharyn* ))'. This search term contains the three essential aspects without being overly specific to avoid excluding relevant articles. PubMed and Scopus databases were utilized for the search, with the former only allowing for searches in titles and abstracts. The identified articles were screened based on predefined inclusion and exclusion criteria, as outlined in table 2.1. Additionally, the snowball effect was employed to include additional relevant articles.

Table 2.1: Inclusion- and exclusion criteria for the analyzed articles.

| **Inclusion criteria** | **Exclusion criteria** |
|---|---|
| People with an age above 18 years | Head and neck patients were not clearly distinguished from other patient categories |
| Cancer in the head-neck area | High-resolution manometry had a sensor spacing higher than 2 cm |
| Treatment is already done. | High-resolution manometry contained less than 12 sensors |
| High-resolution manometry applied in the pharynx | Articles in another language as English |

### 2.2.2 Experience and knowledge

The second source involved utilizing personal experience and knowledge. The SEATTLE/N21STL protocol, which combines VFSS and HRIM measurements, was examined to identify adoptable elements. This protocol is already appropriate for use in the AvL but in a research setting of a specific population, TL patients. Because it is already applicable in the AvL, this protocol was used as a framework to base the measurement protocol for the entire HNC population on. Elements such as catheter connection, setup, and cleaning, how to prepare different IDDSI levels, and VFSS recording settings were easily adapted from the SEATTLE/N21STL. Furthermore, personal experience and knowledge gained from attending relevant courses, engaging in discussions with physicians at the HNC department, and consulting HRIM experts like Taher Omari and Nathalie Rommel were leveraged. In addition, literature from sources beyond the HNC population was mentioned if they were suggested by experts.

To develop a comprehensive measurement protocol, three key steps were undertaken. Firstly, the patient population benefiting from HRIM assessment was identified. Secondly, specific measurements that need to be taken, including volume and consistency, were determined. Lastly, additional adaptations and additions were made. These aspects were determined from the two sources explained above; the literature review and personal knowledge and experience. The protocol developed from this information is tested and optimized by implementing it in clinical practice on patients with HNC patients.

## 2.3 Results

After conducting a search in Scopus and PubMed, 79 articles were found in Scopus and 20 articles in PubMed. Upon scanning these articles and applying the inclusion and exclusion criteria, 14 articles were deemed relevant for analysis. An additional article was identified through the snowball effect, bringing the total number of articles to 15. However, two of the articles only provided a general overview of HRIM and did not provide any information about the specific measurement protocol used, so they were excluded from the analysis. As a result, 13 articles were used for the analysis.

### 2.3.1 Patient population

The cancer types and treatments which are mentioned in the articles (subsection 2.2.1) can be found in table 2.2. The protocols that will be discussed in this chapter will therefore be targeted at those patient populations. All reviewed articles confirm the feasibility and usefulness of HRIM for those populations, despite variations in the severity of swallowing problems among the studies. For instance, Szczesniak [39] emphasizes the importance of HRIM in identifying the underlying pathophysiological mechanism of dysphagia after HNC treatment. This knowledge can lead to more effective management of dysphagia and can also help manage patient expectations regarding treatment outcomes. Similarly, Lippert et al. [40] highlight HRIM as an ideal tool for studying the physiology of pharyngeal swallowing, which is of particular interest in patients after a TLE. By providing a more comprehensive understanding of physiology, HRIM can identify better targets for therapeutic and surgical interventions for swallowing problems, potentially limiting unnecessary interventions and individualizing the treatment.

Table 2.2: Cancer types and treatment of the patient population of the literature review

| **RT with or without CRT:** | **Surgery:** | **All treatments:** |
|---|---|---|
| Nasopharynx [41] | Oropharynx [42] | Oropharynx [43] [44] |
| Larynx [45] | Larynx [46][47][40][48] | All locations [49][39] |
| All locations [50] [6] | | |

Based on the information gathered from the literature (subsection 2.2.1) and additional knowledge and experience (subsection 2.2.2), inclusion and exclusion criteria for applying HRIM have been determined. The analyzed articles did not explicitly mention inclusion and exclusion criteria for HRIM, nor did other literature sources provide clear contraindications to our knowledge. Therefore, criteria were established based on our experience and expertise. At first, patients must have an indication to perform VFSS. Patients must therefore present themselves in the (outpatient) clinic with speech- or swallowing problems, leading to a referral to a speech and language pathologist (SLP) by a physician. VFSS is performed when the outpatient clinic evaluation is inconclusive or additional insights are desired. These patients are all suitable candidates for the HRIM, except when they meet the following exclusion criteria:

1. Patients with a nasogastric tube, as it shares the pathway with the HRIM catheter. Therefore, the nasogastric tube might interfere with the pressure and impedance measurement of the HRIM catheter. However, to the extent of our knowledge, no research into the effect of a nasogastric tube on the HRIM data is presented in the current literature.
2. Patients with aphagia who cannot swallow fluids of IDDSI 3 or lower, experience significant aspiration in these fluids, or cannot swallow at all. Opening the upper esophageal sphincter (UES) is crucial for catheter insertion, and if the patient cannot drink, the UES may not open during the procedure.
3. Patients with compromised esophageal tissue quality resulting from treatments like surgery or radiotherapy in the area. Although a study on the safety and tolerability of HRM showed no complications among 5000 patients, esophageal puncture must be prevented at all costs. [51]
4. Patients with nasal obstruction, as catheter introduction becomes impossible in these patients.
5. Patients before- or during HNC treatment Patients before- or during HNC treatment as minimizing the risk of puncturing the tumor is prioritized. Moreover, HRIM usage primarily focuses on patients who develop swallowing problems as a result of HNC treatment.
6. Patients who cannot follow instructions or cannot understand the procedure.
7. Patients who do not give consent for the measurement of HRIM.
8. Patient with expected stenosis. This is not an absolute exclusion criterion, however, it is necessary

to first conduct VFSS without HRIM to assess the degree of stenosis. If the stenosis is so narrow that a liquid bolus cannot even pass through, catheter insertion will also be impossible.

Furthermore, the following target groups, where HRIM is expected to be particularly important, have been identified:

1. Patients experiencing swallowing problems due to late radiation therapy damage.
2. Patients being considered for surgical treatments like lipofilling, dilatation, or myotomy.
3. Patients before and after participating in intensive swallow exercise boot camps, like the McNeill Dysphagia Therapy Program.
4. Patients pre and post-surgical treatments in which swallowing problems will occur.

### 2.3.2 Volumes and consistencies

When swallowing different volumes and viscosities, sensory modulation of the pharyngeal swallowing response occurs. [52] For this reason, it is important to use a range of volumes and consistencies in the HRIM protocol. The volumes and consistencies listed in Table 2.3 were described in literature for in HNC patients (subsection 2.2.1), see subsection 1.2.2 for elaborated information about IDDSI. Most articles do not give a clear reason why those values are used.

Table 2.3: Volumes and consistencies mentioned in the analyzed articles
*One article mentioned that if the patient is not able to swallow IDDSI 0, IDDSI 1 is used.

| Objective | | Number of articles |
|---|---|---|
| Consistencies | IDDSI 0 | 13* |
| | IDDSI 2 | 2 |
| | IDDSI 3 | 1 |
| | IDDSI 4 | 2 |
| Volumes | 1cc | 1 |
| | 2cc | 4 |
| | 3cc | 1 |
| | 5cc | 7 |
| | 10cc | 8 |
| | 20cc | 1 |

As can be seen, IDDSI 0 (thin) is the most used consistency, IDDSI 2, 3 & 4 (slight to moderately thick) are equally mentioned, and IDDSI 7 (solid food) is not mentioned in any article. Bolus consistency has been shown to affect the pressure and timing of HRIM. How it affects the pressure and timing is still discussed in current literature. Some articles describe that increased bolus consistency leads to increased pharyngeal contraction pressures, delayed pharyngeal clearance, increased nadir pressure on the opening of the UES, and increased intrabolus pressure during transit. [53] [54] However, another article found decreased maximum pharyngeal pressure and decreased pharyngeal pressure duration in healthy volunteers. They stated that swallowing water demands greater physiological control of the bolus. Therefore, the muscles require more contraction to control the bolus speed. [55]

During our participation in the "Non-Profit Course SwallowGateway High-Resolution manometry Course: UES/Pharyngeal Analysis" at KU Leuven, we were instructed by Nathalie Rommel and Taher Omari, two experts in the field of HRIM for pharyngeal dysphagia. They emphasized the importance of measuring HRIM with extremities in order to capture all the various aspects of the patients' swallow. Consequently, they established normal values for IDDSI 0 and IDDSI 4, which are the two extremes within the liquid consistencies according to the IDDSI framework. [30]

Our observations indicate that patients tend to experience the most difficulty with solid foods, which are prone to getting stuck and require more effort to chew due to decreased salivary flow resulting from RT. These difficulties are easily identifiable during VFSS, emphasizing the importance of measuring IDDSI 7 to obtain a comprehensive understanding of the patient's swallowing function. Although IDDSI 7 is not mentioned in any of the HNC articles, IDDSI 7 is probably valuable to add to the protocol as well.

As shown in table 2.3, the most frequently used volumes are 5cc and 10cc. Omari et al. [56] showed that the bolus volume at least changes the peak pharyngeal pressure in patients with severe dysphagia. Jungheim et al. [57] detected temporal adaptations of swallowing dynamics with different volumes.

A larger volume results in a shorter velopharyngeal opening and a longer UES opening. Changes in pharyngeal pressure parameters were not confirmed. They recommend performing HRIM with different bolus sizes to get the best diagnostic result of the complete swallowing process. Lin et al. [58] showed increased UES residual pressure and duration with increasing bolus volume. They did not find an effect on maximum UES pressure pre- and post-UES opening and hypopharynx pressure. Both findings were also observed by [59] et al.

Volumes below 5cc are considered small; the mean sip size for natural drinking in healthy people is 16mL. [60] Based on personal experience (subsection 2.2.2), using even smaller volumes than 5cc does not provide additional insight into the patient's swallowing quality. It is therefore not needed to have smaller volumes in the standard protocol. However, adapting the bolus in these cases to a slightly higher IDDSI level could be useful.

In the SEATTLE/N21STL HRIM protocol (subsection 2.2.2), sips from a cup are included as well to mimic the home situation as best as possible.

In the analyzed literature (subsection 2.2.1), the repetition of the boluses ranges between 12 and no repetition in which most studies applied a repetition of 3 times (6 of 10 studies).

These findings have resulted in using the following consistencies and volumes for the HRIM measurement protocol, which are all repeated twice:

1. IDDSI 0 5cc
2. IDDSI 0 10cc
3. IDDSI 0 from a cup
4. IDDSI 4 5cc
5. IDDSI 4 10cc
6. IDDSI 7

IDDSI 0 will be applied in the HRIM protocol because it is the most used consistency in the analyzed articles. It is also the consistency in which the risk of aspiration is the highest, therefore important to test on the VFSS. If it is already known that a patient aspirates IDDSI0, or clear aspiration is visible in IDDSI0, this consistency could be adapted to IDDSI1, like Komatsu et al. did [43]. A more viscous consistency will be used as well. Due to the recommendation that extremities capture all the different aspects of the swallowing function and the normal values that are determined for IDDSI 4, this is chosen as the second consistency. At last, IDDSI7 is used in the protocol to check the swallowing function with solid food. A combination of HNC literature using mainly 5cc and 10cc and other literature recommending different bolus sizes concluded that 5cc and 10cc are used in this protocol. To replicate the home situation as best as possible, two swallows of IDDSI0 from a cup are included as well. This must mimic the home situation as best as possible, therefore sipping with a straw or directly from the cup is both possible. Based on the literature on HNC patients, three repetitions seem to be a reasonable number. However, we found that three repetitions with three different consistencies and two different volumes are quite extensive in practice. Therefore, the HRIM protocol utilizes a repetition of two times.

### 2.3.3 Other important areas for attention

In addition to considering the patient population and swallow consistencies/volumes, several adaptations or additions to the HRIM protocol used in the SEATTLE/N21STL study need to be implemented. The following items were identified from the literature (subsection 2.2.1) and personal experience (subsection 2.2.2):

1. Prior to the examination, patients should remove visible elements such as jewelry and glasses that may interfere with the VFSS, facilitating the analysis of the measurement.
2. The preference is to administer topical nasal anesthesia in one nostril a few minutes prior to the insertion of the HRIM catheter. This approach is supported by the fact that topical anesthesia is used in at least 10 of the 13 articles, and improved catheter tolerance was observed in patients who received topical anesthesia. Additionally, a study conducted by Kwong et al. [61] demonstrated that topical anesthesia has no impact on swallowing function.
3. To measure impedance, Precise SBMkit Saline Concentrate from Trisco Foods, which contains NaCl, should be added to the bolus. Impedance measurement relies on the bolus' conductivity and enables the assessment of bolus flow and residue, crucial parameters for swallowing function analysis.

4. The catheter's location should be examined with x-ray imaging during insertion in patients with a larynx, and on indication for TL patients. For patients with a larynx, this could prevent the introduction of the HRIM catheter into the trachea, especially in patients with a loss of sensibility in the larynx due to cancer treatment. The larynx is passed at approximately 15cm, therefore the location must be verified at approximately 15 cm. The sensors on the HRIM catheter, each measuring 1cm in length, serve as useful guidance during the insertion process. In all patients, examining the location of the catheter could provide insight into the location of the needed catheter manipulations when the catheter is stuck somewhere. For this, the radiologic technologist should ensure proper positioning of the fluoroscopy tube on the patient before the catheter insertion is started.
5. The last sensor of the catheter should be positioned just in the nose. This ensures that the third until the twelfth sensors, which measure the impedance, are positioned in the pharynx.
6. The bandicam, the recording software for the VFSS video, is recorded as a continuous video and is not paused in between the swallows. This enables synchronization between the time axis of the HRIM and the VFSS recording. A script can be used after synchronization to extract only the relevant portions of the VFSS recording.
7. The cine loop and bandicam should be started at the same time to facilitate synchronization in the post-procedure VFSS analysis. Both should be started after the patient and catheter are clearly visible on the VFSS recording.
8. The radiologic technologist should be instructed to keep all sensors from the nose on the VFSS recording to facilitate post-procedure analysis.
9. The VFSS images should be captured in the lateral position. While the SEATTLE/N21STL study protocol employed an anterolateral position to visualize the voice prosthesis, positioning patients laterally enhances visualization of anatomical regions in HNC patients during VFSS.
10. The marker labels that are set in the Laborie software during the measurement of the HRIM must be set just before the sallow is initiated and when the full bolus is cleared by the patient, approximately the same time as that the X-ray is actively recorded.
11. It is preferred to perform HRIM measurements with at least two members of the manometry team present due to the numerous procedures involved. Additionally, it is preferable to have one SLP with experience in measuring and analyzing VFSS images present for immediate interpretation of the VFSS images.

### 2.3.4 Experience from clinical practice - pilot study

The information stated above is combined into a protocol that can be found in appendix 6.1. This protocol is tested in clinical practice and two major findings were done.

The first thing that is experienced is a problem with the consistencies and volumes of the administered boluses. The HRIM is an addition to the VFSS and should not alter the method on which the VFSS is performed tremendously. For the VFSS, some measurement protocols exist and those are kept in mind while drafting the HRIM protocol. However, when measuring the HRIM/VFSS on new patients, we experienced that it was hard to follow an exact protocol. Clinicians do often also not follow the determined VFSS protocol due to their personal experience. For example, when we start with a bolus of 5cc IDDSI0 and we can see on the VFSS that the patient aspirates a part of the bolus, it is clinically relevant to check whether aspiration occurs in a smaller bolus as well. However, when no aspiration occurs administering a smaller bolus volume is not needed and therefore not done. This happens as well in other situations. For example, when a patient has residue with an IDDSI 4 bolus, it is relevant to check whether residue occurs as well in a bolus of IDDSI 3. Therefore, IDDSI 3 must be tested as well while IDDSI 3 is not mentioned in the protocol. These situations can occur for all different consistencies and volumes. A standardized protocol in which all these situations are covered is therefore impossible. Therefore, a flowchart is added to the measurement protocol which can be an inspiration to follow when specific findings are found based on the VFSS recording. This flowchart works as an example of which clinicians can deviate.

A second element that occurs during the measurement of VFSS is that compensation techniques are tested when it is seen that a patient aspirates. For example, swallowing with the chin on the chest or with a head turn in a certain position will be tested. These compensation techniques are also not covered in the HRIM protocol. Therefore, space for own interpretation the clinician must be present and a standardized protocol is difficult.

## 2.4 Discussion

The results of this chapter indicate that the SEATTLE/N21STL study protocol for combined VFSS and HRIM serves as a suitable framework due to its existing application in the AvL. However, several adaptations are necessary to transform this protocol into one suitable for HNC patients and application in clinical practice. These adaptations involve the patient population, administered bolus volumes and consistencies, and several elements regarding the setup of the measurement system and the generation of the data.

Initially, it was expected that most patients fitting the targeted patient population would be suitable for HRIM measurement. However, in practice, only a few have undergone HRIM measurement. The frequency of VFSS procedures is limited, with an average of four patients per week, primarily scheduled on Wednesdays instead of Tuesdays. Unfortunately, there is a lack of experienced personnel available for HRIM on Wednesdays, resulting in the inability to perform HRIM measurements on those days. Additionally, even when VFSS is conducted on Tuesdays, some patients did not meet the HRIM criteria or declined participation. Patient refusal to undergo HRIM may be due to inadequate prior information about the procedure, resulting in an overwhelming feeling of the HRIM. Therefore, cooperation is expected to improve by informing the patient prior to the VFSS/HRIM appointment. Furthermore, the infrastructure for the HRIM measurement could be improved. There is a need for improved clarity among physicians and SLPs regarding the advantages of measuring HRIM in patients and the process for scheduling these appointments. Enhancing this understanding will lead to an increase in VFSS appointments for the targeted patient population on Tuesdays. So, while the patient population seems to be effectively identified, it is evident that internal infrastructure improvements are required within the hospital to enable HRIM measurements in the desired patient population.

Individualized administration of different consistencies and volumes based on clinical findings presents a challenge in standardizing a single protocol. However, the necessity of a standardized protocol may be questionable since SLPs are proficient in determining the appropriate IDDSI levels for patients based on VFSS findings. Nevertheless, it should be noted that normal values for HRIM are only established for IDDSI 0 and 4. Consequently, deviating from the protocol eliminates the opportunity to compare the outcomes with reference values. However, it is anticipated that the normal values for other IDDSI levels would generally fall within the range between the normal values for IDDSI 0 and IDDSI 4, thereby providing an indication of whether the measurements are within the normal range. An additional important consideration is that HNC patients often require multiple swallowing acts to fully clear the bolus, resulting in the ingestion of smaller volumes at a time. As a result, even the normal values for IDDSI 0 and IDDSI 4 (5cc and 10cc) may not perfectly align with the measurements obtained during IDDSI 0 and IDDSI 4.

Due to the radiation during VFSS imaging, the protocol must be time-efficient and minimize the number of swallows. Most literature articles (subsection 2.2.1) suggest a repetition of three swallows to ensure accurate measurements. However, the protocol already entails two different volumes of three different IDDSI levels, a sip from a cup, and additional boluses when indicated by the SLP. Repeating all these swallows three times would result in excessive radiation exposure for patients. Therefore, repetition of two times is chosen.

It is important to note that this protocol was specifically developed for intern implementation at AvL. Translating the protocol to other centers is challenging due to variations in measurement systems and regulations. Other centers would need to possess HRIM measurement systems, which is currently not the case in many centers. Additionally, they would need to utilize the same software, such as Laborie, and the same VFSS recording software, such as Bandicam. However, a part of the protocol can be generalized and applied to other centers, such as the volumes, consistencies, method of catheter insertion, and the patient population.

This chapter encompasses the design of a measurement protocol for the combined measurement of VFSS and HRIM in the HNC population. However, on top of a measurement protocol, the data must be analyzed and reported to come up with a diagnosis as well. The method of analyzing now is that the HRIM data must be loaded into SwallowGateway where it can be analyzed. SwallowGateway has offered a course in which you learn how to analyze and interpret the HRIM data and parameters that are obtained in SwallowGateway. However, no clear protocol is developed on how this analysis can be done for the HNC population. Additionally, no knowledge about the use of the normal values and these parameters

in the HNC population is present. Therefore, the application of analysis software like SwallowGateway also needs further investigation before it can be applied to the HNC population with certainty.

This chapter presents the design of a measurement protocol for combined VFSS and HRIM in the HNC population. However, beyond the measurement protocol, the analysis and reporting of data are crucial for generating a diagnosis. Currently, the HRIM data must be loaded into SwallowGateway for analysis. Although SwallowGateway offers a training course on analyzing and interpreting HRIM data and parameters, there is no specific protocol developed for analyzing the HNC population. Moreover, the application of the generated parameters and their normal values in the HNC population requires further investigation before confidently applying analysis software like SwallowGateway to this population.

## 2.5 Conclusion

In conclusion, the measurements protocol for application in clinical practice for the HNC population is designed on the framework of the SEATTLE/N21STL VFSS combined with HRIM measurement protocol with several adaptations to be suitable for the clinical practice and HNC population, with defined exclusion criteria for HNC patients for whom the protocol may not be appropriate. The bolus volumes and consistencies are adapted to the most commonly presented in the literature for HNC patients. Deviation from these volumes and consistency is possible when clinically indicated. Additionally, several adaptations are done in the setup of the measurement system and the generation of the data, such as the labeling method, catheter insertion method, and the recording of the VFSS and HRIM for synchronization. This has led to a measurement protocol that is applied in the AvL which improves the measurement and analysis process.

# 3

# Automated VFSS catheter segmentation and sensor counting

## 3.1 Introduction

In the previous chapter, it is mentioned that HRIM and VFSS measurements are always conducted together at the AvL. Figure 3.1 illustrates a VFSS image obtained during the combined measurement, clearly displaying the catheter extending from the nose to the esophagus of the patient. The individual sensors are also visible in the image. Utilizing VFSS in conjunction with HRIM analysis provides the advantage of identifying which sensor is located in which anatomical region based on the VFSS image. In one of our patient cases, VFSS proved to be an essential tool in supporting HRIM analysis. This particular case involved a patient without pressure buildup in the velopharynx. Initially, it was assumed that the velopharynx began around sensor number 15/16 counted from the nose because the first pressure peak is visible at that height, see figure 3.2a. However, upon examination of the corresponding VFSS image during the same swallow, it became apparent that sensor 15/16 was actually positioned inferior to the velopharynx, as shown in figure 3.2b. Consequently, this finding significantly impacted the HRIM analysis in SwallowGateway. Several other patient cases also presented abnormal pressure patterns, making it challenging to define anatomical landmarks accurately.

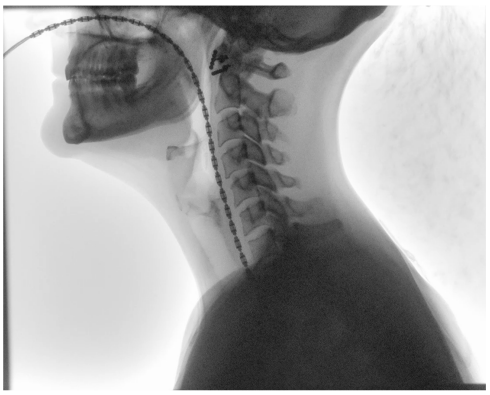

Figure 3.1: A VFSS image of the combined measurement of VFSS and HRIM. The catheter is clearly visible running from the nose to through the pharynx and esophagus.

Singendonk et al. [62] demonstrated the difficulties and reduced interrater reliability of HRIM analysis for severely aspirating patients with abnormal swallowing pressure patterns. Some subjects were even excluded from HRIM analysis due to features in HRIM data that could lead to erroneous readings. Mielens et al.[63] developed an algorithm for automated marker definition on the HRIM topography plots, although it required increased user intervention for disordered subjects. These situations also highlight the difficulty in identifying anatomical landmarks, particularly for pathological pressure patterns. Therefore,

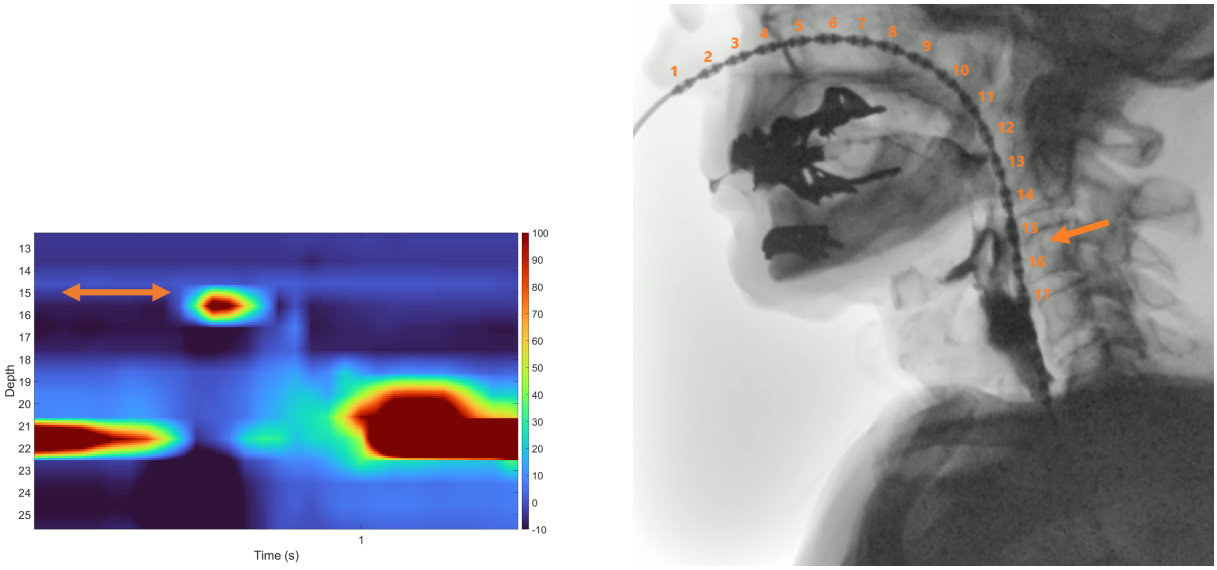


(a) Pressure topography plot of the swallow

(b) VFSS image of the swallow

Figure 3.2: The pressure pattern (3.2a) and the VFSS image (3.2b) from the same swallow. At first, it was thought that the pressure peak between sensors 15 and 16 is the velopharynx. However, when evaluating this on the VFSS images, these sensors showed to be positioned lower than the velopharynx.

there is a need to enhance the analysis by gaining more insight into the positions of anatomical locations within the HRIM topography plots. One potential approach is to incorporate VFSS recordings into the analysis of HRIM data.

Existing literature primarily compares swallowing parameters derived from HRIM data analysis with those obtained from VFSS recordings or focuses on differentiating patients from control groups using VFSS and HRIM, with VFSS considered the gold standard [62] [64] [65]. However, no prior research has investigated the combined use of VFSS and HRIM measurements for analyzing swallowing outcomes.

The previously mentioned cases and literature underscore the importance of improving HRIM analysis by combining it with VFSS, and highlight the existing research gap in this field. Therefore, this chapter aims to develop an analysis method for the combined analysis of HRIM and VFSS. This is done by writing an algorithm that should be able to determine which sensor is positioned in a certain region of the VFSS image. To achieve this, it is crucial to segment the catheter from the VFSS images and count the number of sensors between two predefined markers on the VFSS image. The developed algorithm will be used and validated, addressing the following research question: *"Can VFSS serve as a supportive tool for analyzing HRIM data?"*

## 3.2 Methods

This section outlines the methodology used to count the number of sensors per anatomical region through the development and implementation of an algorithm in MATLAB R2022b. The algorithm will be explained, providing a detailed understanding of the process. Subsequently, the evaluation of the algorithm is explained.

### 3.2.1 Data

The data for this study must meet two conditions. Firstly, all sensors starting from the nose must be visible on the VFSS recording to determine the position of each sensor within specified regions. Secondly, the patients cannot wear any objects which block ionizing radiation, such as glasses and necklaces, because it distracts the VFSS image. Patient data that meets these criteria were collected, resulting in the selection of 36 images. These images comprise 18 pre-swallowing and 18 peri-swallowing images captured during the ingestion of a specific bolus. Detailed information about the swallowed bolus, can be found in table 3.2 and patient characteristics can be found in table 3.1.

Table 3.1: The subjects with their corresponding treatment and primary tumor.
*SND = Selective Neck Dissection, COMMANDO = COMmbined MAndibular and Neck Dissection Operation, FRFF = Free Radial Forearm Flap, PORT = Post-Operative RadioTherapy, TORS = TransOral Robotic Surgery, MRND = Modified Radical Neck Dissection, TL = Total Laryngectomy

| **Subject** | **Relevant treatment** | **Primary HNC tumor** |
|---|---|---|
| **1** | 2021: TORS +SND<br>12/2021-01/2022 CRT | cT2N0M0 oropharyngeal carcinoma |
| **2** | 2020: COMMANDO + FRFF<br>2020-2022: PORT 2022: MRND<br>2022-2022: PORT | cT2N3bM0 orofaryngeal carcinoma |
| **3** | 2014: CRT | T3N2c tonsillar base carcinoma |
| **4** | 2020: TL + MND | cT0N0M1 supraglottic laryngeal carcinoma |
| **5** | 2014: RT 02025: recurrence for which TL<br>2016: laserexcision pseudo-vallecula<br>2017: neopharyngeal reconstruction<br>2017: laserexcision pseudo-vallecula | T2N0 glottic laryngeal carcinoma |
| **6** | 2005: RT<br>2015: TL + faryngectomy + ND + reconstruction with gastric pull-up | T3N0 glottic laryngeal carcinoma |
| **7** | Healthy | - |

Table 3.2: The patient, consistency, and volume corresponding to each selected swallow.
*This swallow is recorded after the patient received excessive swallow training.

| **Number** | **1** | **2** | **3** | **4** | **5** | **6** | **7** | **8** | **9** | **10** | **11** | **12** | **13** | **14** | **15** | **16** | **17** | **18** |
|---|---|---|---|---|---|---|---|---|---|---|---|---|---|---|---|---|---|---|
| **Patient** | P1 | P1 | P1 | P1 | P2 | P2 | P3 | P3 | P4 | P4 | P5 | P5 | P5 | P6 | P6 | P6 | P7 | P1* |
| **IDDSI-level** | 0 | 0 | 4 | 7 | 0 | 7 | 0 | 3 | 0 | 7 | 7 | 0 | 4 | 0 | 4 | 7 | 0 | 4 |
| **Volume** | 10 | 5 | 10 | | 5 | | 5 | 5 | 10 | | | 10 | 10 | 0 | 10 | | 10 | 10 |

### 3.2.2 Catheter segmentation

The VFSS recording is loaded into MATLAB by the videoReader function of MATLAB. This function extracts the video as frames in which the time of the extracted frame can be set. The VFSS video contains the actual X-ray recording surrounded by information on a black background, see figure 3.3. This background interferes with future steps in the image analyses and therefore must be cut off the

image. This is done using a function that finds the highest correlation for four different templates and the VFSS image. The templates are black rectangles with a white line on one long side. The locations with the highest correlation with these templates are cut from the image. See figure 3.3

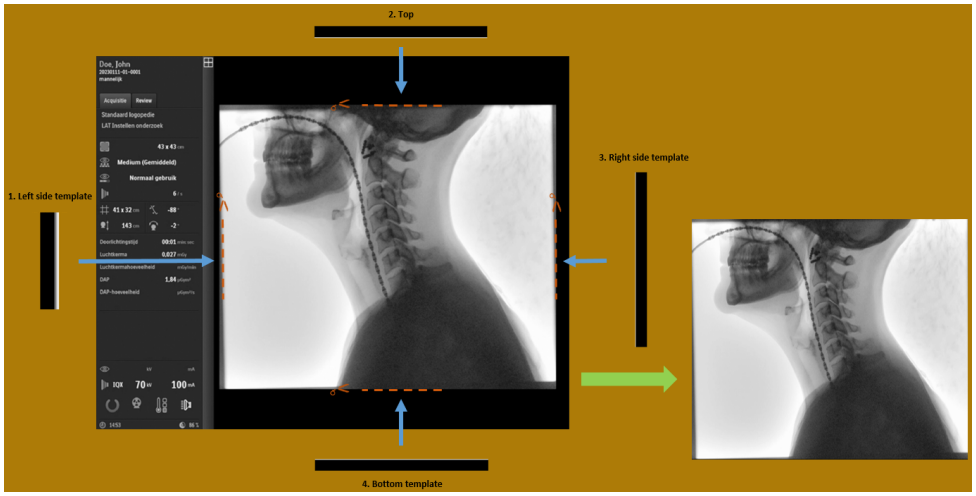


Figure 3.3: The image cropping steps. Four templates consisting of grayscale pixels are cross-correlated with the VFSS image from numbers 1 to 4. The VFSS image is cropped at the line with the highest cross-correlation between the template and the image. This results in the image pointed at with the green arrow.

The cropped images are filtered with a Gaussian high-pass filter and repeatedly closed with a structuring line element of 10 pixels which turned from 160 to 140 degrees. This enhances the differences in pixel values between the catheter and the background and ensures as best as possible that it keeps the catheter in one connected area. Subsequently, the image is binarized with a threshold of 0.07, so only black and white pixels are left in the image. This binarized image is dilated with a structuring line element of 10 pixels in 100 degrees. Next, the two biggest connected areas are selected in the binarized image. The connected area which covers the most image rows is selected as the catheter. This covers already quite well the location of the catheter in the binarized image, see figure 3.4.

### 3.2.3 Length and distances of the catheter

This segmentation of the catheter allows us to determine where the catheter is positioned in the patient. However, on top of the position, the length of the catheter must be determined. This is needed because we want to know the length of the catheter from one point to another in order to count sensors. Therefore, the segmented catheter is reduced to a line of 1 pixel thick by selecting the middle pixel of the longest white area on every row and column, see 3.5. This line often still has gaps and branches that need to be respectively filled and removed which takes a couple of different steps:

1. The catheter line is dilated with a round structuring elemant of 40 pixels in diameter to remove the gaps.
2. A skeleton is made from this binarized white area.
3. All branch- and endpoints of the line are determined.
4. When the distance between an endpoint and a branchpoint is less than 100 pixels, a circle with a radius of the distance between the endpoint and branchpoint is placed on the endpoint.
5. The area under the circle is set to a value of 0 as long as the biggest connected area stays more than 90% of the size compared to before binarizing, see figure 3.5.

The process of determining the branch- and endpoints, placing the circle, and zeroing everything under the circle is repeated until only two endpoints are left because that is the beginning- and end of the catheter. The above-explained steps result in the segmentation of the catheter as a one-pixel width continuous line.

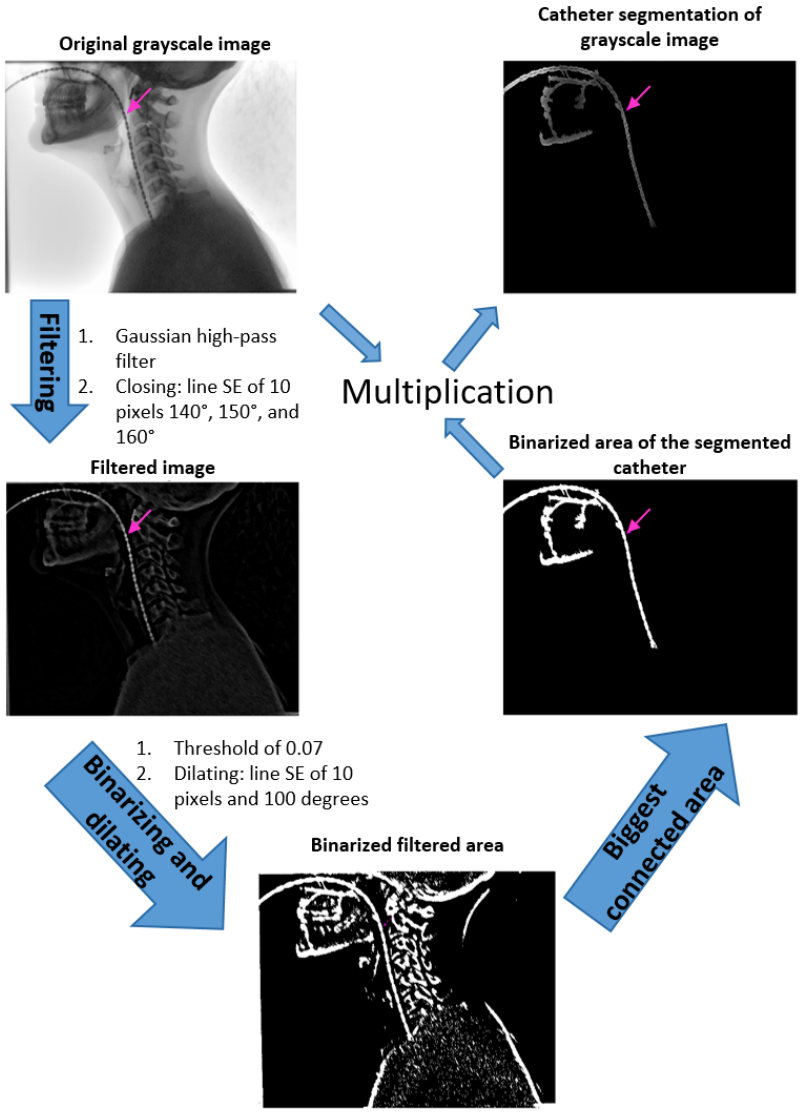


Figure 3.4: The original grayscale is filtered, binarized and the biggest connected area is selected as the catheter. The catheter is indicated by the pink arrows. In the upper right image is visible that the catheter is indeed segmented, however, some more structures than only the catheter are segmented.

### 3.2.4 Determining distances on the catheter

After the catheter is segmented as a continuous line of one-pixel width, it becomes possible to determine distances along the line by counting the number of white pixels between two positions. Firstly, the number of pixels corresponding to one sensor is determined by having the user select the beginning and end points of five sensors of the VFSS image. The closest white pixels of the catheter line to these coordinates are identified, and the number of white pixels between them is calculated. See figure 3.7. This process is repeated for all five sensors, and the average value is used as the number of pixels per sensor. These calculations are performed separately for each pre- and peri-swallow image. Secondly, the number of sensors within specified regions on the VFSS images must be countable. To achieve this, horizontal markers can be placed on the VFSS image to indicate a region. The intersection points between these horizontal markers and the segmented catheter line are determined. The image is then cropped between two consecutive intersection points, resulting in an extracted region. This extracted region is expanded by one row or column as long as there are at least two white pixels in the neighboring rows and columns. Once this criterion is no longer met, the number of white pixels within the extracted region is calculated. By dividing this count by the mean number of white pixels per sensor for that specific image, the number of sensors within the defined region on the VFSS image can be determined.

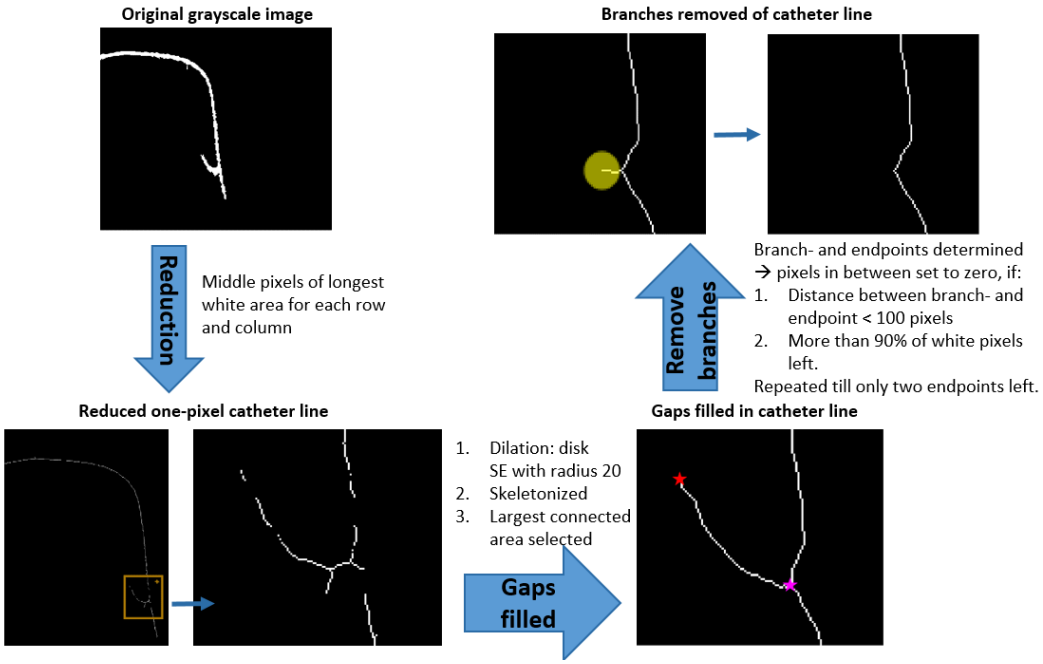


Figure 3.5: The segmented catheter is firstly reduced to a line of 1 pixel thick. This line still contains gaps and branches which need to be respectively filled and removed. The gaps are filled by dilating the line with a round structuring element with a radius of 20 pixels. This area is spurred again. The branches are removed by zeroing all pixels between the endpoint (red star) and the closest branchpoint (pink star).

### 3.2.5 Evaluation of the algorithm

The evaluation of this algorithm focuses on two aspects. Firstly, the accuracy of the catheter segmentation is assessed. To verify the segmentation, ten points are selected on the catheter of the original VFSS image without any knowledge of the segmented catheter line. These points are chosen at regular intervals of every two sensors, or if less than twenty sensors were segmented, the remaining points are randomly placed between the previously selected points. The distance between these points and the closest white pixel of the segmented catheter is then measured. Secondly, the algorithm is evaluated on its ability to determine the number of sensors within indicated regions on the VFSS image. Two users mark five different horizontal lines on the VFSS image, creating five distinct regions, see figure 3.6. The number of sensors in each marked region is manually counted and compared with the algorithm's count. It is crucial that the counts do not significantly differ from each other. This is tested with the paired samples t-test in IBM SPSS Statistics 27. In a clinical context, the manometry data provides pressure and impedance information for each sensor. Therefore, a deviation of more than 0.5 sensors is considered clinically relevant. Deviating by more than half a sensor could result in the misplacement of a sensor in a different region, as determined by the algorithm, compared to manual counting. If the initial step of catheter segmentation is not adequate, minor manual adjustments to the algorithm are allowed before proceeding with the counting of sensors within the distinct regions.

### 3.2.6 Generalization of this method

A limitation of this method is the requirement for manual selection of the beginning and endpoints of five sensors in each VFSS image. This manual selection process is time-consuming and impractical for users. To enhance the clinical application of this method, this manual selection should be eliminated. Therefore, the average number of pixels for a sensor across all VFSS images is calculated. With this number of white pixels, the number of sensors per defined region on the VFSS images is calculated again. The resulting count is compared to the manually counted number of sensors, and the deviation between the two counts is calculated. No significant difference between both should be present. The influence of this alternative approach is compared to the deviation observed when selecting five sensors per anatomical region.

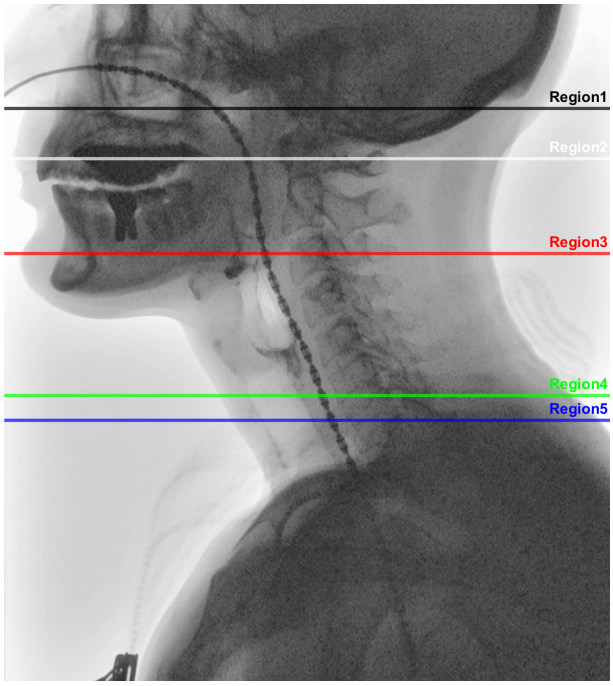


Figure 3.6: What the image looks like after setting five different landmarks on the VFSS images, creating five distinct regions. The number of sensors will be counted manually and by the algorithm in each region.

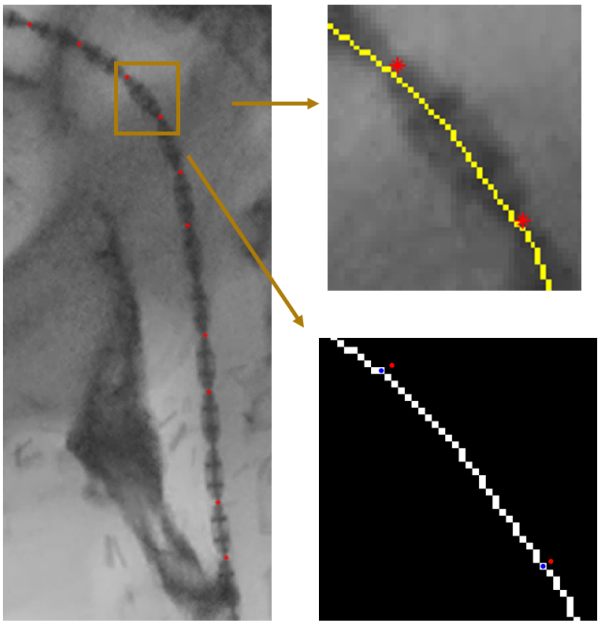

Figure 3.7: To determine how many pixels are in one sensor, the beginning and endpoint of five random sensors are selected (asterisk in red). These points are not always located right on top of the segmented catheter line. Therefore, the closest pixels on this catheter line are selected, the blue circles. The number of white pixels between the selected beginning- and endpoint are calculated.

## 3.3 Results

### 3.3.1 Accuracy of catheter segmentation

Figure 3.8 illustrates an example of the binarized one-pixel-thick segmented catheter overlay on the original VFSS image with the ten selected points on the catheter. In figure 3.9, the mean distance from the ten selected points to the segmented catheter line for each pre- and peri-swallow image is visualized. The average deviation is 5.5 pixels. The mean number of pixels of one sensor is 39 pixels. So, the segmentation is mostly less than 1/6th sensor off. Most images even have an average deviation of less than 2 pixels. For images 1-16, the deviation between the manually selected pixel and the catheter line is much smaller than for images 17 and 18. Also, the distance between the selected pixel and the segmented catheter line is almost in all cases higher for the peri-swallow images compared to the pre-swallow images. Due to the inaccurate catheter segmentation of image 18, a manual adjustment is made in the algorithm by skipping the dilation step in figure 3.4. This led to a comparable small deviation as in the other VFSS images; an average of 1.2 pixels for the pre-swallow, and 2.7 pixels for the peri-swallow image. The large deviation in image 17 was not solvable with minor manual adaptation, so is not changed.

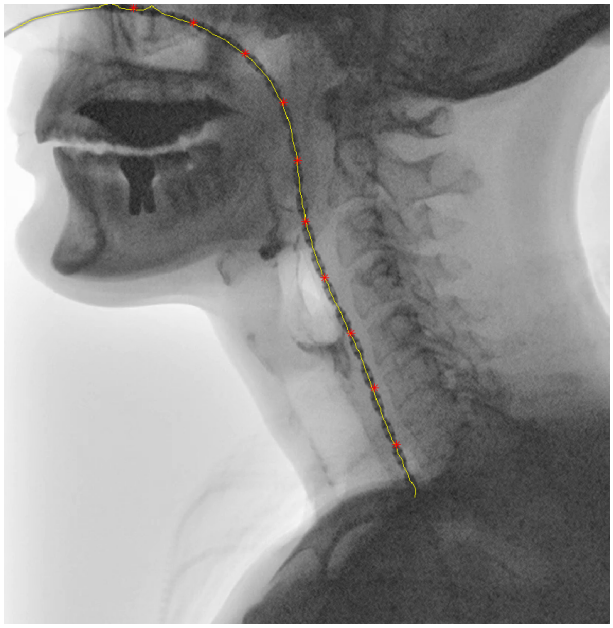

Figure 3.8: An example of a VFSS image with the segmented catheter line in yellow and the ten selected points on the catheter. The distance between these selected points and the segmented catheter line is calculated as a measure of the accuracy of the catheter segmentation.

### 3.3.2 Deviation in manual and algorithm's sensor count

The difference between counted sensors by MATLAB compared to manually counting them is visualized in table 3.3 and 3.4. Manual counting of sensors was not possible for all images and anatomical regions due to various reasons, including poor image quality, anatomical regions being turned due to compensation techniques, or obstruction of sensor visibility by the presence of the bolus. These particular cases are denoted by a dash (-) in the table, and the corresponding measurements are excluded from the analysis. Figure 3.9 illustrates a graph depicting the average deviation between the manually counted number of sensors and the number of sensors counted by MATLAB for each VFSS image. There is no significant difference present between the algorithm's sensor count and the manual sensor count ($p=0.01$). The mean deviation consistently falls below one sensor, almost only below 0.5 sensors.

### 3.3.3 Generalizing sensor count

The average number of pixels per sensor across all images resulted in an average of 38.3 pixels per sensor. Using this value as the sensor size, the comparison of the number of sensors per anatomical region

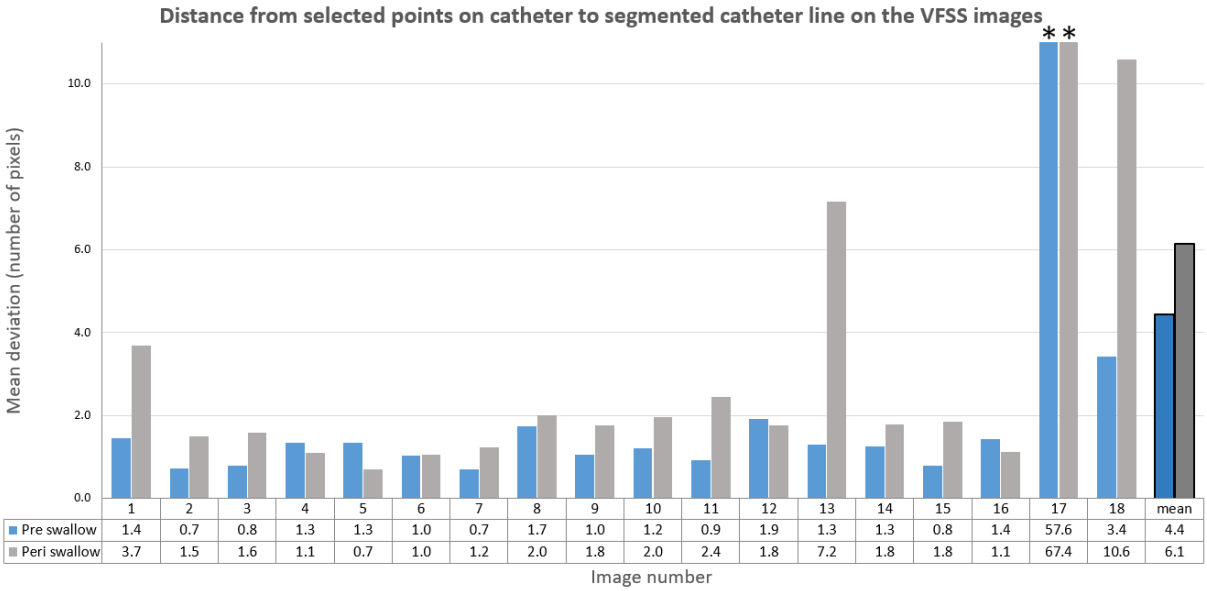


| | 1 | 2 | 3 | 4 | 5 | 6 | 7 | 8 | 9 | 10 | 11 | 12 | 13 | 14 | 15 | 16 | 17 | 18 | mean |
|---|---|---|---|---|---|---|---|---|---|---|---|---|---|---|---|---|---|---|---|
| Pre swallow | 1.4 | 0.7 | 0.8 | 1.3 | 1.3 | 1.0 | 0.7 | 1.7 | 1.0 | 1.2 | 0.9 | 1.9 | 1.3 | 1.3 | 0.8 | 1.4 | 57.6 | 3.4 | 4.4 |
| Peri swallow | 3.7 | 1.5 | 1.6 | 1.1 | 0.7 | 1.0 | 1.2 | 2.0 | 1.8 | 2.0 | 2.4 | 1.8 | 7.2 | 1.8 | 1.8 | 1.1 | 67.4 | 10.6 | 6.1 |

Figure 3.9: The mean distance from selected points on the VFSS image to the segmented catheter line for all pre- and peri-VFSS images.

between manual counting and algorithm counting yields the results shown in figure 3.11. These results indicate that there is no increase in deviation between manual counting and algorithm counting when using the mean sensor length of 38.3 pixels. No significant difference between both methods is present ($p=0.06$). Therefore, this mean sensor length can be considered a suitable value to adopt, improving the user-friendliness of the VFSS image analysis.

Table 3.3: The deviation between the manually counted sensors and algorithm counted sensors per anatomical region for the pre-swallow images. The - means that it was either for the algorithm or for manually not possible to count the number of sensors.

| | **Pre-swallow MN** | | | | | **Pre-swallow LvdM** | | | | | | |
|---|---|---|---|---|---|---|---|---|---|---|---|---|
| | **Region1** | **Region2** | **Region3** | **Region4** | **Region5** | **Region1** | **Region2** | **Region3** | **Rregion4** | **Region5** | **mean** | **SD** |
| **1** | 0,0 | 0,1 | 0,3 | 0,0 | 0,0 | 0,3 | 0,1 | 0,2 | 0,1 | 0,1 | **0,1** | **0,1** |
| **2** | 0,8 | 0,2 | 0,0 | 0,2 | 0,1 | 0,1 | 0,5 | 0,1 | 0,0 | 0,2 | **0,2** | **0,2** |
| **3** | 0,1 | 0,2 | 0,1 | 0,2 | 0,1 | 0,2 | 0,2 | 0,0 | 0,2 | 0,1 | **0,1** | **0,1** |
| **4** | - | - | - | 0,0 | 0,1 | 0,3 | - | - | 0,1 | 0,0 | **0,1** | **0,1** |
| **5** | 0,2 | 0,2 | 0,0 | 0,2 | 0,2 | 0,0 | 0,3 | 0,0 | 0,2 | 0,1 | **0,1** | **0,1** |
| **6** | 0,2 | - | 0,1 | 0,1 | 0,1 | 0,0 | 0,2 | 0,3 | 0,1 | 0,0 | **0,1** | **0,1** |
| **7** | 0,3 | 0,2 | 0,5 | - | - | 0,1 | 0,3 | 0,6 | - | - | **0,3** | **0,2** |
| **8** | - | - | - | - | - | - | - | - | - | - | **-** | **-** |
| **9** | 0,1 | 0,1 | 0,1 | 0,1 | 0,0 | 0,3 | 0,4 | 0,2 | 0,2 | 0,4 | **0,2** | **0,1** |
| **10** | 0,1 | 0,2 | 0,2 | 0,1 | - | 0,1 | 0,3 | 0,3 | 0,2 | - | **0,2** | **0,1** |
| **11** | 0,0 | 0,5 | 0,0 | 0,1 | 0,0 | 0,1 | 0,0 | 0,4 | 0,2 | 0,1 | **0,1** | **0,2** |
| **12** | 0,1 | 0,2 | 0,1 | 1,0 | 0,1 | 0,3 | 0,2 | 0,1 | 0,2 | 0,1 | **0,3** | **0,3** |
| **13** | 0,0 | 0,2 | 0,2 | 0,1 | - | 0,1 | 0,4 | 0,2 | 0,1 | - | **0,2** | **0,1** |
| **14** | 0,2 | 0,2 | 0,0 | 0,1 | 0,1 | 0,1 | 0,0 | 0,2 | 0,0 | 0,2 | **0,1** | **0,1** |
| **15** | 0,2 | 0,2 | 0,2 | 0,1 | 0,2 | 0,3 | 0,2 | 0,2 | 0,1 | 0,1 | **0,2** | **0,1** |
| **16** | 0,1 | 0,1 | 0,1 | 0,1 | - | 0,2 | 0,2 | 0,1 | 0,1 | 0,2 | **0,1** | **0,1** |
| **17** | 0,0 | 0,3 | 0,0 | 0,1 | 0,0 | 0,1 | 0,2 | 0,2 | 0,1 | 0,0 | **0,1** | **0,1** |
| **18** | 0,9 | 0,4 | 0,2 | 0,1 | - | 0,1 | 1,0 | 0,2 | 0,4 | 0,1 | **0,4** | **0,3** |
| **Mean** | **0,2** | **0,2** | **0,1** | **0,2** | **0,1** | **0,2** | **0,3** | **0,2** | **0,1** | **0,1** | **0,2** | |
| **SD** | **0,2** | **0,1** | **0,1** | **0,2** | **0,1** | **0,1** | **0,2** | **0,1** | **0,1** | **0,1** | | |

Table 3.4: The deviation between the manually counted sensors and algorithm counted sensors per anatomical region for the peri-swallow images. The - means that it was either for the algorithm or for manually not possible to count the number of sensors

| | **Peri-swallow MN** | | | | | **Peri-swallow LvdM** | | | | | | |
|---|---|---|---|---|---|---|---|---|---|---|---|---|
| | **Region1** | **Region2** | **Region3** | **Region4** | **Region5** | **Region1** | **Region2** | **Region3** | **Rregion4** | **Region5** | **mean** | **SD** |
| **1** | 0,5 | 0,1 | 0,0 | - | - | 0,1 | 0,4 | 0,3 | 0,0 | 0,1 | **0,2** | **0,2** |
| **2** | 0,1 | 0,0 | 0,1 | 0,2 | 0,1 | 0,2 | 0,2 | 0,0 | 0,0 | 0,0 | **0,1** | **0,1** |
| **3** | 0,1 | 0,0 | 0,0 | - | - | 0,3 | 0,0 | 0,1 | - | - | **0,1** | **0,1** |
| **4** | - | - | - | - | 0,1 | 0,5 | 0,1 | 0,4 | - | 0,1 | **0,2** | **0,2** |
| **5** | 0,3 | 0,1 | 0,2 | 0,2 | 0,1 | 0,3 | 0,0 | 0,1 | 0,1 | 0,1 | **0,2** | **0,1** |
| **6** | 0,8 | 0,3 | 0,1 | 0,2 | 0,0 | 0,8 | 0,1 | 0,1 | 0,2 | 0,1 | **0,3** | **0,3** |
| **7** | 3,7 | 0,1 | 0,2 | - | - | 0,2 | 0,5 | 0,3 | - | - | **0,8** | **1,3** |
| **8** | - | - | - | - | - | - | - | - | - | - | **-** | **-** |
| **9** | 0,2 | 0,4 | - | - | 0,2 | 0,2 | 0,0 | - | - | 0,2 | **0,2** | **0,1** |
| **10** | 0,1 | 0,0 | 0,0 | 0,2 | - | 0,4 | - | 0,3 | 0,2 | 0,1 | **0,1** | **0,1** |
| **11** | 0,3 | 0,4 | 0,1 | 0,1 | 0,4 | 0,5 | 0,1 | 0,0 | 0,1 | 0,0 | **0,2** | **0,2** |
| **12** | 0,6 | 0,2 | - | 0,4 | 0,1 | 0,4 | 0,1 | 0,1 | 0,3 | 0,1 | **0,3** | **0,2** |
| **13** | 0,1 | 0,2 | 0,2 | - | - | 0,0 | - | - | - | - | **0,1** | **0,1** |
| **14** | 0,3 | 0,1 | 0,3 | 0,0 | 0,1 | 0,0 | 0,1 | 0,3 | 0,1 | 0,0 | **0,1** | **0,1** |
| **15** | 0,2 | 0,1 | 0,2 | 0,0 | 0,0 | 0,0 | 0,2 | 0,3 | 0,0 | 0,2 | **0,1** | **0,1** |
| **16** | 0,3 | 0,1 | 0,2 | 0,3 | 0,1 | 0,0 | 0,0 | 0,3 | 0,0 | 0,1 | **0,1** | **0,1** |
| **17** | 0,0 | 0,1 | 0,1 | 0,2 | 0,1 | 0,3 | 0,2 | 1,0 | 0,0 | 0,1 | **0,2** | **0,3** |
| **18** | 3,0 | 0,1 | 0,2 | 0,0 | 0,1 | 3,8 | 0,4 | 1,0 | 0,3 | 0,1 | **0,9** | **1,3** |
| **Mean** | **0,5** | **0,1** | **0,1** | **0,2** | **0,1** | **0,5** | **0,2** | **0,3** | **0,1** | **0,1** | **0,2** | |
| **SD** | **0,9** | **0,1** | **0,1** | **0,1** | **0,1** | **0,8** | **0,1** | **0,3** | **0,1** | **0,0** | | |

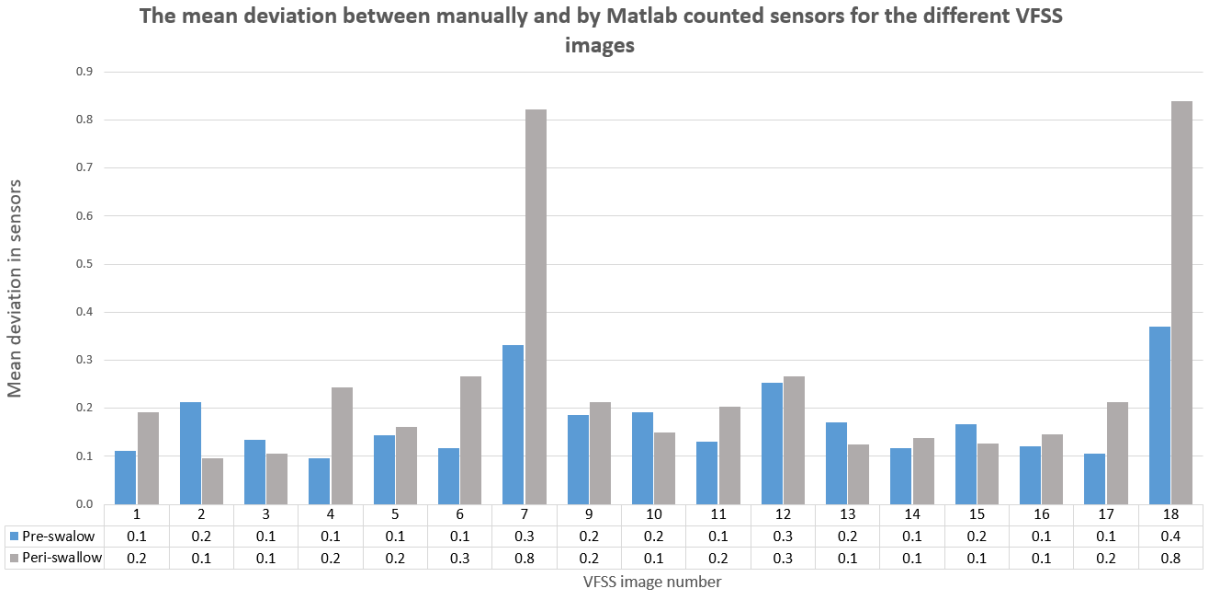


| | 1 | 2 | 3 | 4 | 5 | 6 | 7 | 9 | 10 | 11 | 12 | 13 | 14 | 15 | 16 | 17 | 18 |
|---|---|---|---|---|---|---|---|---|---|---|---|---|---|---|---|---|---|
| Pre-swalow | 0.1 | 0.2 | 0.1 | 0.1 | 0.1 | 0.1 | 0.3 | 0.2 | 0.2 | 0.1 | 0.3 | 0.2 | 0.1 | 0.2 | 0.1 | 0.1 | 0.4 |
| Peri-swallow | 0.2 | 0.1 | 0.1 | 0.2 | 0.2 | 0.3 | 0.8 | 0.2 | 0.1 | 0.2 | 0.3 | 0.1 | 0.1 | 0.1 | 0.1 | 0.2 | 0.8 |

Figure 3.10: The mean deviation between the number of sensors calculated by the algorithm compared to manually counted sensors for 17 pre- and peri-swallow VFSS images.

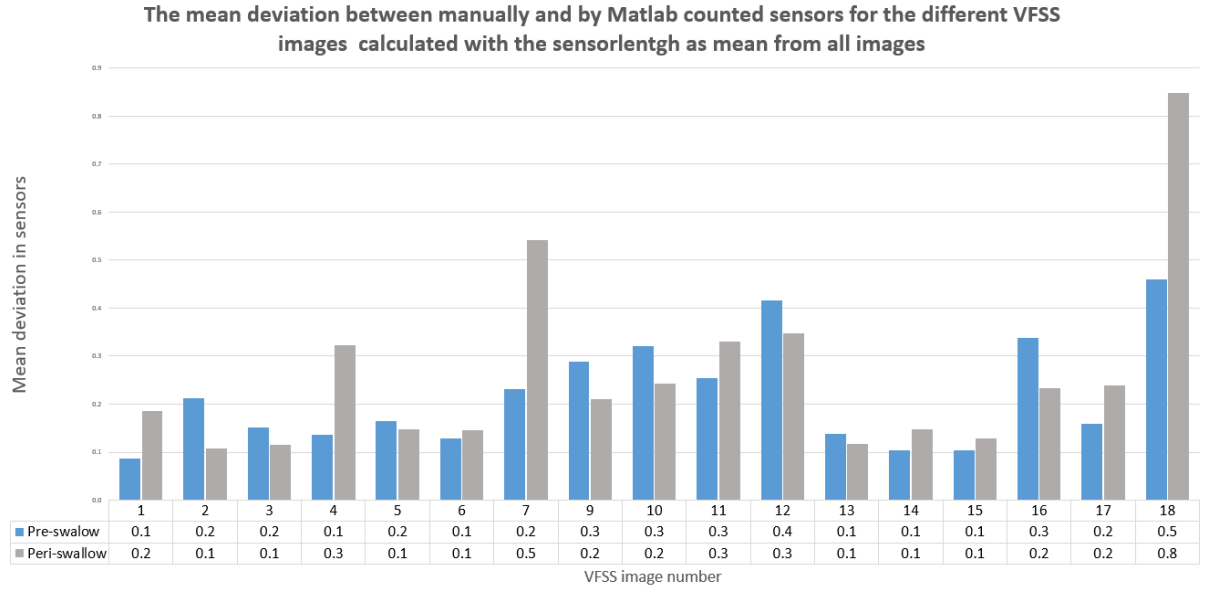


| | 1 | 2 | 3 | 4 | 5 | 6 | 7 | 9 | 10 | 11 | 12 | 13 | 14 | 15 | 16 | 17 | 18 |
|---|---|---|---|---|---|---|---|---|---|---|---|---|---|---|---|---|---|
| Pre-swalow | 0.1 | 0.2 | 0.2 | 0.1 | 0.2 | 0.1 | 0.2 | 0.3 | 0.3 | 0.3 | 0.4 | 0.1 | 0.1 | 0.1 | 0.3 | 0.2 | 0.5 |
| Peri-swallow | 0.2 | 0.1 | 0.1 | 0.3 | 0.1 | 0.1 | 0.5 | 0.2 | 0.2 | 0.3 | 0.3 | 0.1 | 0.1 | 0.1 | 0.2 | 0.2 | 0.8 |

Figure 3.11: The mean distance from selected points on the VFSS image to the segmented catheter line calculated with an averaged number of pixels per sensor for all pre- and peri-VFSS images.

## 3.4 Discussion

In this chapter, the potential of using VFSS as a supportive tool for the analysis of VFSS is explored. To facilitate this analysis, a setup is established for automated catheter segmentation and sensor counting in VFSS images. The accuracy of the catheter segmentation is evaluated by comparing the segmented catheter line with manually selecting points on the actual catheter. The automated sensor counting is compared to manual counting. The results show that the automated catheter segmentation performs well, with an average deviation of 1.4mm between the segmented catheter line and the actual catheter. The deviation is in most cases even below 0.5mm, which is considered to be very small, as it corresponds to 1/20th of a sensor. This deviation is likely not solely due to inaccurate catheter segmentation, but may also be influenced by imprecise manual selection of the catheter. The inaccuracies in segmentation primarily arise from specific challenges, which will be discussed in detail. Furthermore, automated sensor counting across five distinct regions on the VFSS shows no significant difference compared to manual counting. The mean deviation remains below one sensor for all images, indicating a low probability of misidentifying a sensor in the wrong region. These results show the great potential of VFSS as a supportive tool in HRIM data analysis. Finally, the impact of using the mean number of pixels per sensor across all images for automated sensor counting is examined. The findings show no significant difference compared to using a specific number of pixels per sensor for each image. For clinical applications, utilizing a generalized number of pixels per sensor can enhance the user-friendliness of this method, reducing analysis time and requiring fewer user interventions.

### 3.4.1 Catheter segmentation challenges

During the catheter segmentation process, certain images exhibit a large deviation between the real and segmented catheter line. The causes of these high deviations, the problems they pose for further analysis, and potential solutions will be explained.

#### Gaps in the catheter

Figure 3.12a illustrates the overlay of the segmented catheter line and the original VFSS image of pre-swallow 17. It is evident that the catheter is not segmented all the way to the sensor closest to the nose. This results in a large deviation for the four selected points nearest to the nose, as depicted in figure 3.12b. However, the remaining six points exhibit only a small deviation from the segmented catheter line. The incomplete segmentation of the catheter near the nose is caused by the hard palate, which shares a similar gray value with the catheter and is in close proximity to it. Consequently, the catheter segmentation erroneously includes the hard palate, along with the teeth. The middle pixel of each thickest white area is chosen as the line for the segmented catheter. However, these white pixels are not exclusively located on the catheter but also on the teeth, palate, and mandible. As a result, there is a large gap in the catheter line at the width of the teeth. This gap is too large to be closed in a dilatation step of the line. In a later stage of the process, the largest connected area is selected, leading to the exclusion of the catheter portion near the nose. If we skip the dilatation after preprocessing the image, the binarized hard palate and catheter are not connected, causing the exclusion of the hard palate from the binarized area. As mentioned in the results section 3.3, the manual adaptation of skipping this dilating step is used to obtain further results.

#### Contrast-agent-containing bolus

The presence of a contrast-agent-containing bolus affects the accuracy of the catheter segmentation in peri-swallow images. In the VFSS images, both the catheter and the contrast-agent-containing bolus appear as low gray values. Moreover, the contrast agent obstructs the view of the catheter by blocking the ionizing x-ray photons, as shown in figure 3.14a. This leads to challenges in distinguishing the bolus covering the pharynx from the catheter. When the image is binarized, both the bolus and the catheter are included, resulting in a wider segmentation, as shown in figure 3.14b. Consequently, the creation of a binarized line from this segmented area includes white pixels from both the bolus and the catheter. As a result, the segmented catheter line intersects with the bolus and does not align accurately with the actual catheter, see figure 3.14a. This phenomenon contributes to a higher deviation between the real and segmented catheter lines in peri-swallow images compared to pre-swallow images. These factors specifically result in a greater deviation between real and segmented catheter in image 13 and 18, see figure 3.9.

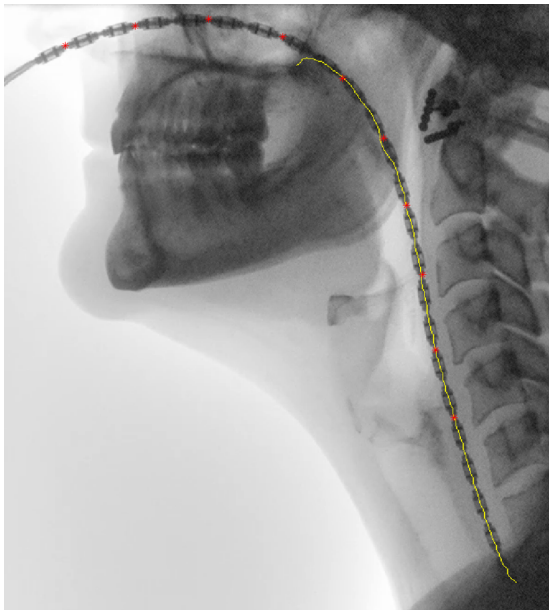

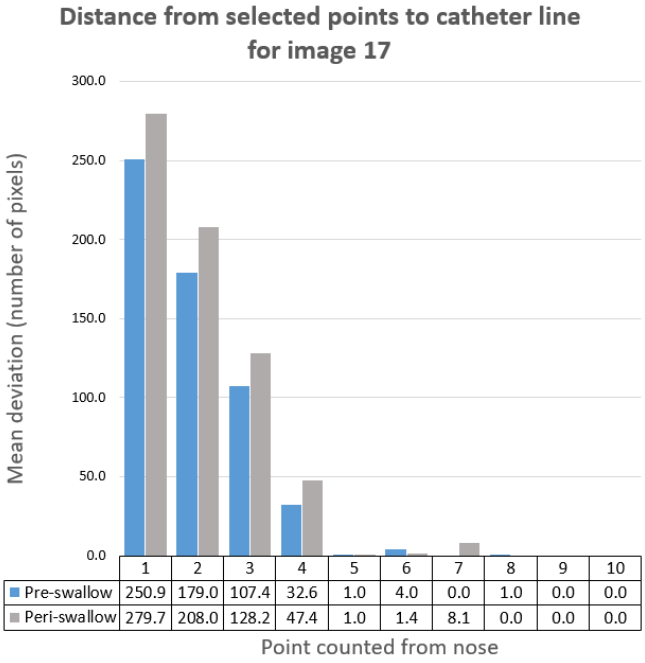


| | 1 | 2 | 3 | 4 | 5 | 6 | 7 | 8 | 9 | 10 |
|---|---|---|---|---|---|---|---|---|---|---|
| Pre-swallow | 250.9 | 179.0 | 107.4 | 32.6 | 1.0 | 4.0 | 0.0 | 1.0 | 0.0 | 0.0 |
| Peri-swallow | 279.7 | 208.0 | 128.2 | 47.4 | 1.0 | 1.4 | 8.1 | 0.0 | 0.0 | 0.0 |

(a) The segmented catheter line in yellow with the selected points on the catheter in red. The catheter is clearly not segmented all the way to the last sensor on the side of the nose.

(b) The distance between the selected points counted from the nose and the segmented catheter line for image 17. The points closer to the nose have a larger deviation because the catheter is not fully segmented until the nose.

Figure 3.12: The incomplete segmented catheter (3.12a) leads to a large deviation between the real and segmented catheter close to the nose (3.12b).

### Branch removal

Another problem encountered during catheter segmentation is the incorrect removal of branches. Structures with similar gray values as the catheter cause branches on the segmented catheter line. These branches are removed with the method explained in subsection 3.2.3. However, when a branch is present close to the start or the end of the segmented catheter line, the current method of branch removal is insufficient. This happened in peri-swallow image 18, see figure 3.13. The distance between both endpoints and the branchpoint is smaller than 100 samples, resulting in the removal of both branches. Therefore, the catheter segmentation reaches not far enough in the direction of the nose. The deviation between the real and the segmented catheter is therefore large for the first selected point on the catheter, contributing to a high mean deviation.

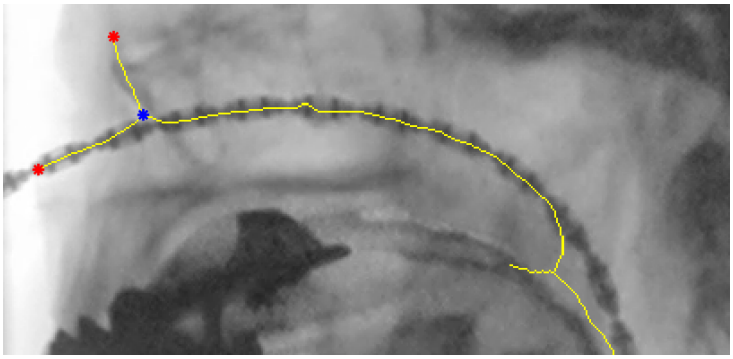

Figure 3.13: The branches labeled with a red asterisk are removed because they are located within 100 pixels of the blue branch point.

### 3.4.2 Effect of the inaccurate segmented catheter on the automated sensor counting

#### Contrast-agent-containing bolus

It is expected that an inaccurate segmentation of the catheter resulting from the presence of the contrast-agent-containing bolus would lead to a large deviation between the manual counting and the algorithm's counting of sensors per region. However, this is not the case. Especially in peri-swallow images 13 and 18 was a large deviation between the real and the segmented catheter line present. However, a closer examination of these images reveals that this did not result in an increased deviation between the manual and the algorithm's sensor count. In fact, for image 13, the deviation between the manual and algorithm's sensor count is even lower for the peri-swallow image compared to the pre-swallow image. While the deviation is higher for peri-swallow image 18, this can be attributed to another factor (paragraph *Branch removal* in subsection 3.4.1). The deviation between the manual and the algorithm's sensor count is only present in region 1 which causes a high mean deviation, see table 3.4. However, no bolus is present in that region. The deviation in the other regions is minimal, indicating that the inaccurate catheter segmentation caused by the bolus does not significantly affect the sensor counting. This limited impact on sensor counting is likely due to the fact that the path followed by the bolus during swallowing overlaps with the region where the catheter is positioned, specifically the pharynx and the esophagus. Consequently, the deviation in counting white pixels within a region is minimal because the segmented catheter line still closely aligns with the actual catheter's trajectory.

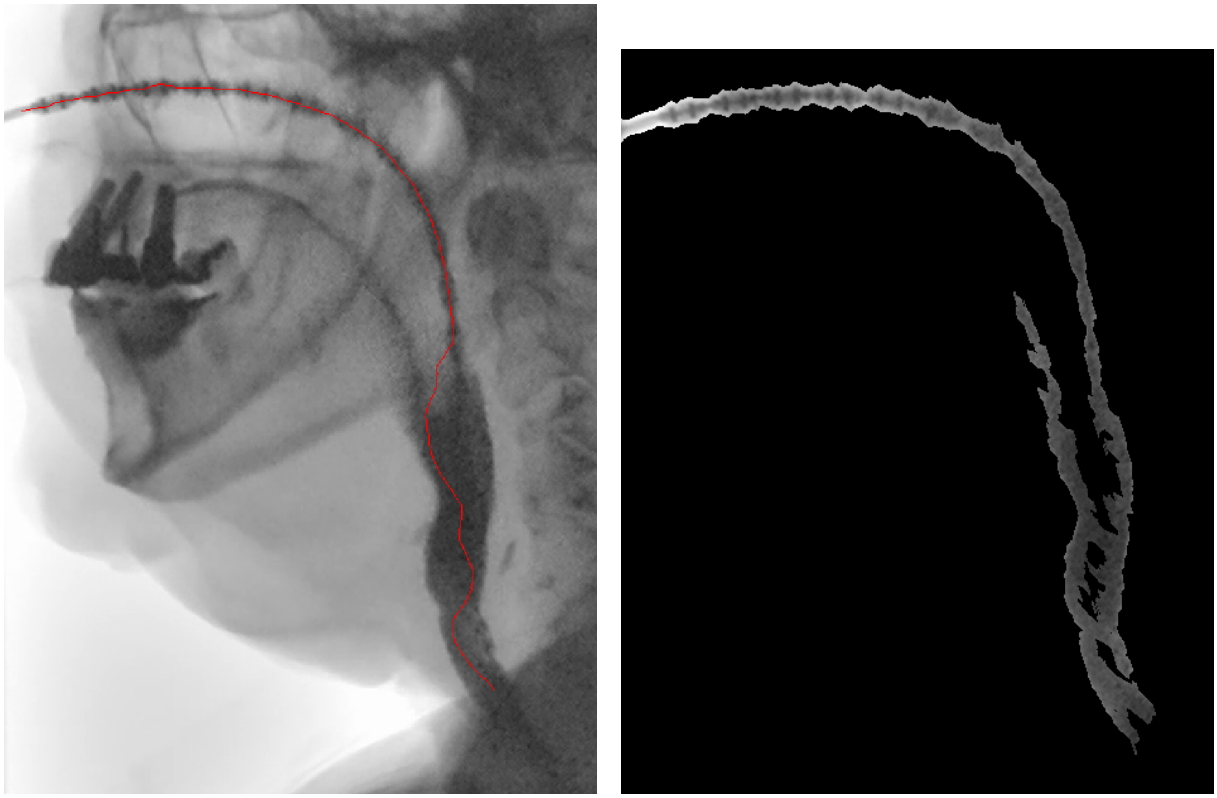

(a) VFSS peri-swallow image 13 with in red the segmented catheter line. The contrast-agent-containing bolus distracts the sight on the HRIM catheter, resulting in inaccurate alignment of the segmented catheter and the real catheter.

(b) The segmented catheter also includes bolus resulting in a higher deviation between the segmented catheter and the real catheter.

Figure 3.14: The contrast-agent-containing bolus (3.14a) distracts the sight on the catheter resulting in a catheter segmentation that also contains bolus (3.14b). The segmented catheter line does not align accurately with the real catheter.

**Branch removal**

As can be seen in peri-swallow image 18, does the wrongful branch removal affect the automated sensor counting in the area where the branch is wrongfully removed. Therefore, the sensor counting in this first area is underestimated by the algorithm, resulting in a high deviation between the manual and algorithm-counted number of sensors. The algorithm could be optimized by adapting the algorithm in a way that the branches are removed from smallest to largest branches. The branches that must be kept are often the largest branches.

### 3.4.3 Cases which make sensor counting challenging

As depicted in table 3.3 and table 3.4, there are numerous cases where counting the sensors, either manually or by the algorithm, is impossible. This is caused by the following aspects:

1. An intersection point between the catheter and all horizontally placed landmarks is required. In VFSS swallow 8, the upper horizontal landmark does not intersect with the segmented catheter. The algorithm therefore already errors and breaks while calculating the number of sensors in the upper region. When patients perform compensation mechanisms, like the chin-tuck (patient 8, see figure 3.15) rotation of the anatomy and catheter is likely, resulting in errors. Therefore, for patients performing a compensation technique, the algorithm needs to be optimized.
2. The segmentation of the catheter in the inferior regions may not extend far enough. This is particularly challenging when segmenting the catheter in the esophagus due to the wider body structure in the thorax region. As a consequence, x-ray photons are more readily absorbed, resulting in lower pixel values. This leads to compromised visibility of the catheter, makings its segmentation difficult, and in some cases, even impossible. As a result, the algorithm fails to define the sensor numbers in the inferior regions. It's worth noting that this issue also arises when manually counting the catheter, as it becomes invisible in the inferior anatomical regions.
3. Contrast agents within the boluses can obstruct the visibility of the catheter. As a result, the catheter becomes less visible as the photons are already absorbed, or the gray values of the catheter and contrast agents are similar. While the algorithm can still count the number of sensors in many cases because the segmented catheter remains continuous, manual counting becomes impossible.
4. Poor overall image quality can pose challenges. In images where the patient moves during the measurement or when the VFSS shows poor contrast, it becomes difficult to distinguish the sensors. Manual counting of the sensors may be impossible in such cases.

Manual counting of the sensors was not possible in 47 regions, whereas algorithm counting failed only in 30 regions. Among these 30 regions, 20 were observed in the pre- and peri-images of swallow 8, in which the algorithm failed consistently. This highlights the advantage of employing a catheter segmentation algorithm for sensor counting. When the visibility of the catheter is compromised by other structures, manual counting becomes impractical. However, the use of a catheter segmentation algorithm often still allows for reliable sensor counting.

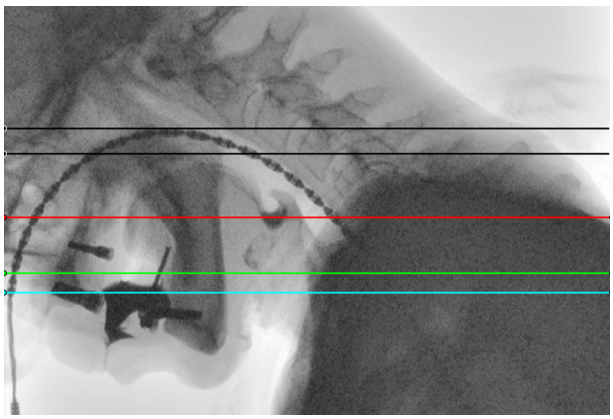

Figure 3.15: The VFSS image during chin-tuck of the patient. The anatomy is almost turned 90 degrees which makes it impossible for the algorithm to properly detect the catheter in each anatomical region.

## 3.5 Conclusion

In conclusion, this chapter demonstrates that accurate catheter segmentation is achievable in most cases, enabling automated sensor counting within defined regions. This advancement has the potential to assist SLPs in analyzing HRIM data, by providing valuable insights into the approximate location of sensors within specific regions. Addressing the research question of this chapter, VFSS proves to be a valuable tool in supporting the analysis of HRIM data. Furthermore, this approach offers the possibility of defining landmarks on VFSS images instead of relying solely on HRIM data. The landmark position can be translated to a location on the HRIM data by the automated sensor counting, providing enhanced insight and consistency on where the markers are placed with respect to the patient's anatomy.

# 4

# Comparison between different methods of anatomical landmark definition

## 4.1 Introduction

The use of HRIM in combination with VFSS is a new method that shows promising results in the diagnosis of swallowing problems. The HRIM data can be analyzed by defining anatomical regions on the pressure topography plots of the swallows. However, in patients after treatment with HNC, this is challenging. These patients have altered anatomy and physiology of their swallows, impacting the pressure patterns in their pressure topography plots. This resulted in mistakenly identified anatomical regions. VFSS recordings provide visual information about the anatomy of the patient in the head-neck area, potentially improving the correct definition of anatomical regions. In the previous chapter, the potential of VFSS as a supportive tool in HRIM analysis through catheter segmentation and automated sensor counting was demonstrated.

The assessment of HRIM data is regularly performed in SwallowGateway. SwallowGateway is an online analysis platform that has been validated to objectively analyze HRIM data [62]. After defining certain anatomical regions on the pressure topography plots in SwallowGateway, verified parameters based on these anatomical regions are generated. SwallowGateway is already often used in research settings and in clinical practice in other hospitals. Additionally, normal values are established which are verified on different patient populations. [16] This information provides us with valuable insight into swallowing problems. At last, SwallowGateway is constantly in development by researchers who also use the HRIM in clinical practice. Attending a course that is specifically developed about how to use and interpret the HRIM data via the SwallowGateway software is obligatory. However, SwallowGateway has some major limitations. At first, it does not provide insight into distances and the location of sensors on the pressure topography plots. Secondly, attendance of the SwallowGateway course is required. This course is time-consuming, and as a result, not many clinicians can perform the HRIM analysis in SwallowGateway.

Another software program in which the HRIM data can be analyzed is the Laborie software, which is used for HRIM measurements. This software provides a bit more insight into the HRIM catheter sensors with respect to the pressure topography plots. However, Laborie was not considered for this study due to its ongoing development at the time of HRIM's introduction in the AvL. It did not provide sufficient analysis options at that stage, and no course is developed on how the analysis should be performed in this software.

Furthermore, it is possible to develop customized software for HRIM analysis, which offers extensive opportunities in data analysis including various displaying options and data manipulation capabilities. This makes it possible to display the sensor numbers on the pressure topography plots and to eventually combine VFSS images with the measured pressure patterns. However, it is unknown how users experience the definition of anatomical landmarks in pressure topography plots in such a software program. No course for such a program is available. Therefore, it is important to investigate whether this can be used effectively for defining anatomical regions.

At last, it is possible to determine anatomical regions on VFSS images. VFSS is a method that is

already regularly used for the diagnoses of swallowing problems in patients, even in patients with altered anatomy or physiology. Due to the better-visualized anatomy on HRIM images, it is hypothesized that the definition of anatomical regions is easier on the VFSS images compared to the pressure topography plots. With the automated catheter segmentation and sensor counting of 3, these regions can be related to the corresponding sensor numbers. This makes relating the anatomical regions on the VFSS images to the pressure topography plots possible. It is important to consider that anatomical structures and the HRIM catheter undergo movement during the swallowing of boluses. As an example, the upward displacement of the UES occurs as a result of laryngeal elevation during swallowing. Consequently, the HRIM catheter also experiences an upward shift at that moment. Nevertheless, the exact relationship between these mechanisms and whether they elevate to the same extent remains uncertain. [66] It is unclear whether the most adequate landmark placement occurs during swallowing when anatomical structures are displaced, or before swallowing when the structures are in a resting position. Consequently, the impact of this movement needs to be investigated.

These methods of defining anatomical regions for the analysis of HRIM data all have advantages and limitations. It is important to test these methods (customized software, VFSS image pre- or peri-swallow) for comparison with the regularly used SwallowGateway. Therefore, this chapter aims to answer the following research question: *"Is there a more consistent and accurate method for identifying anatomical regions for the analysis of HRIM in patients with deviating anatomy than SwallowGateway?"* In order to answer this research question, several subquestions have been formulated:

- *"What is the interrater variability of the different methods of anatomical landmark detection?"*. Assessing interrater variability provides an indication of the reliability of each method individually. On one hand, it is expected that the SwallowGateway software will exhibit the lowest interrater variability because both SLPs attended the same training in analyzing in this software. However, due to the potential deviation in pressure patterns of the HNC population, this analysis is still challenging. Therefore, on the other hand, a low interrater variability is expected by analyzing anatomical regions on the VFSS images because those visualize the anatomy better.
- *"What is the deviation between the different methods of definition of the anatomical landmarks?"* Examining the deviations helps to identify variations and understand the factors contributing to them. A comparison is made with the SwallowGateway software because that is the current clinically applied software.
- *Is it more accurate to determine the position of the anatomical regions on pre-swallow or peri-swallow VFSS images?* To investigate the impact of catheter and anatomical structure movement during the swallow, it is necessary to define anatomical regions on VFSS images at two specific timing moments: just before swallow initiation and during the actual bolus swallowing. The deviation between both methods and the set landmarks on the HRIM topography plots in SwallowGateway and in the customized software. This analysis will reveal insight into which anatomical landmarks should be marked on the VFSS images prior to swallowing and which ones should be marked during the swallowing process.

The above questions will primarily focus on the swallows of HNC patients to assess the potential of all analysis methods specifically for this population. Additionally, in order to answer these questions it must be possible to determine which swallow in the HRIM data corresponds with which swallow on the VFSS recording. Therefore, it is crucial that the HRIM and the VFSS are measured in combination and can be aligned with each other. Additionally, the two conditions mentioned in section 3.2 regarding the visibility of all sensors and the absence of obstructions to ionizing radiation must be met.

## 4.2 Methods

### 4.2.1 Data

For this chapter, the same dataset as chapter 3, containing 18 swallows was used. See table 3.2 and table 3.1 for detailed information about all swallows. The swallows originate from 7 different subjects, of which 6 patients after different treatments of HNC, and 1 healthy volunteer.

The HRIM data was measured with the Solar GI K103659-E-1180-D catheter from Laborie, and the data was exported from their software for each patient individually. For analysis in SwallowGateway, the selected swallows were extracted, labeled with a number, and saved as separate files using Notepad++ v7.9.1. The data for the separate swallows was concatenated, with near-zero pressure and impedance data inserted between each consecutive swallow to clearly separate the swallows. The resulting file was saved in ASCII format, which can be loaded into the SwallowGateway software. For analysis of the swallows in customized software, MATLABR2022b was used. The HRIM data was imported into MATLAB and linearly interpolated to visualize the pressures as a continuous signal in the topography plot. An interpolation factor of 10 was chosen as a consideration between time efficiency and optimal visualization resembling the visualization in SwallowGateway. Subsequently, the data of the selected swallows was extracted, labeled, and saved as separate MATLAB data files. These files could be imported into MATLAB for individual analysis. In addition to the HRIM data, the VFSS data needed to be selected. Similar to the approach in chapter 3, a pre-and peri-swallow image were selected from the VFSS recording. The pre-swallow image was typically selected when the patient had some bolus in their mouth but had not yet initiated swallowing, or just before the bolus entered the mouth. The peri-swallow image was selected at a moment when the bolus was passing through the pharynx. For patients after a TL, the moment of maximum catheter displacement was chosen, while for healthy individuals and other HNC patients, the moment of maximum laryngeal elevation was chosen. These images were extracted using MATLAB's videoReader function, cropped to remove the background with patient information, and saved for further analysis.

### 4.2.2 Data analysis

Two experienced SLPs, MN and LvdM, independently analyzed the 18 swallows. They were asked to place the anatomical markers (explained in chapter 1) corresponding to the proximal margin of the velopharynx (VP PM), the proximal margin of the mesopharynx (MP PM), the proximal margin of the hypopharynx (HP PM), the proximal margin of the UES (UES PM), and the distal margin of the UES (UES DM) on four different methods. These methods are (1) the HRIM data in the SwallowGateway software, abbreviated with HRIM-SWG, (2) the interpolated HRIM data in the customized software (MATLAB in this case), abbreviated with HRIM-custom, (2) the VFSS pre-swallow images, abbreviated with VFSS-pre, and (4) the VFSS peri-swallow images, abbreviated with VFSS-peri, in the rest of this thesis. See figure 4.1 for the visualization of the four methods. For the analyses in HRIM-SWG, both SLPs attended a course for the analysis of pharyngeal HRIM swallows, while for the other three methods, no prior training or consensus was given or applied. First, all HRIM-SWG analyses were performed, subsequently the HRIM-custom, then the VFSS images. The pre-and corresponding peri-swallow images were presented after each other. The swallows were presented in randomized order, the same for both SLPs. The HRIM-custom was presented in the same order as the HRIM-SWG and the VFSS images were presented in a different randomized order.

### 4.2.3 From defined landmarks to sensor numbers

The sensor number of the position of each placed anatomical landmark on the HRIM-custom can be extracted directly from the raw data.

In HRIM-SWG, the sensor number corresponding to the placed landmark cannot be directly obtained. Only the distances between anatomical landmarks can be extracted from the software. Therefore, in HRIM-SWG, the landmark with the clearest position on a characteristic of the swallow, which is specific to each swallow, is set as the reference landmark. This landmark is manually transferred to the same position on the corresponding generated topography plot using MATLAB R2022b. The sensor number corresponding to this landmark is extracted directly such as the landmarks on the HRIM-custom. The positions of the remaining landmarks are calculated based on their distances from this reference landmark, as obtained from HRIM-SWG.

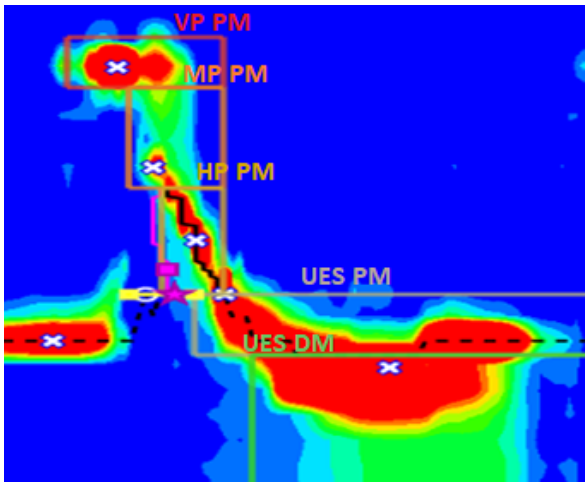


(a) Pressure topography plot with defined landmarks in HRIM-SWG.

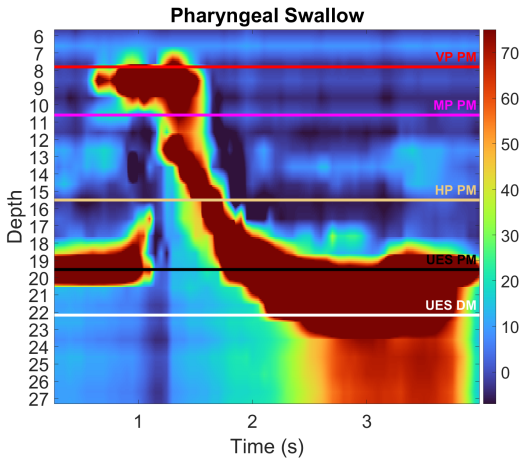


(b) Pressure topography plot with defined landmarks in HRIM-custom

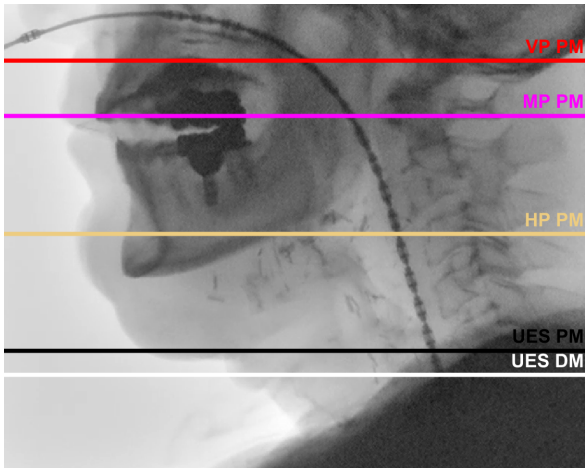


(c) VFSS pre-swallow image with defined landmarks (VFSS-pre)

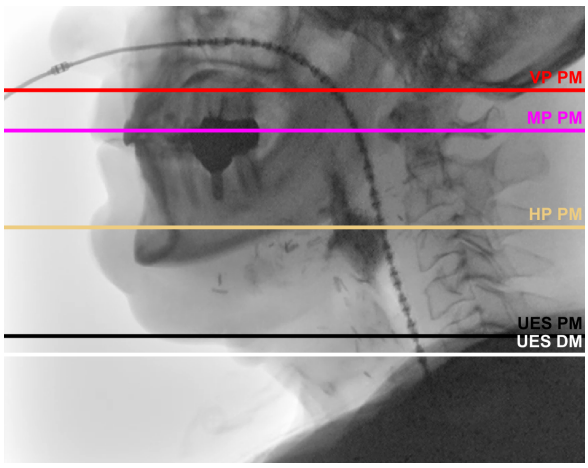


(d) VFSS peri-swallow image with defined landmarks (VFSS-peri)

Figure 4.1: The presentation with set landmarks of the four different analysis methods

For the VFSS images, the algorithm described in Chapter 3 is used to count the number of sensors within each anatomical region and from the first sensor to the first anatomical region. To calculate the landmark position, the number of sensors per anatomical region until that position is added.

### 4.2.4 Variability of all landmarks

The positions of all landmarks with respect to the sensor number are evaluated for inter-observer variability for each method separately. Additionally, the positions of each landmark on the four different methods are averaged for both SLPs, and the deviation for each landmark across the different methods is calculated. In consensus is determined that a deviation larger than 1.5 sensors is considered to be too large to be accurate, especially regarding the small anatomical regions.

## 4.3 Results

### 4.3.1 Inter-observer variability

The interrater variability is assessed across the four different methods of anatomical landmark definition, as depicted in figure 4.2. In general, a deviation between 1 and 2 sensors is present for all landmarks, except the higher deviation for the UES DM as determined in the HRIM-custom. Among the methods, the HRIM-custom exhibits the highest interrater variability, while the VFSS-pre shows the lowest interrater variability.

When considering individual anatomical landmarks, the HP PM exhibits the lowest variability, whereas the UES DM shows the highest variability. The deviation of the UES DM is especially high in swallows 14, 15, and 16 defined on HRIM-custom. In these three swallows, the UES DM differs respectively 8, 9, and 6 sensors between both raters. The deviation of the UES PM is also high, respectively 6 8, and 4 sensors. These three swallows are from the same patient who is treated with a TLE. When looking at those three swallows, it is clearly visible that both SLPs identify the UES on a different position, see figure 4.3. The UES is characterized by a continuous high-pressure zone that is interrupted during the swallow to allow the passage of bolus into the esophagus. Continuous high pressure is present between sensors 14-15 (superior) and between sensors 23-24 (inferior). LvdM identified the superior high-pressure zone, while MN identified the inferior high-pressure zone as UES in HRIM-custom. In HRIM-SWG, both SLPs identify the inferior high-pressure zone as UES, except LvdM on swallow 14. On the VFSS images is the interrater variability for these landmarks only increased for VFSS-pre 15. This results in the high interrater variability in HRIM-custom compared to the other methods. When these swallows are neglected in the calculation of the mean deviation of the UES DM in HRIM-custom, the mean deviation for the UES DM reduces from 2.4 to 1.4 sensors, and the UES PM reduces from 1.8 to 1 sensor.

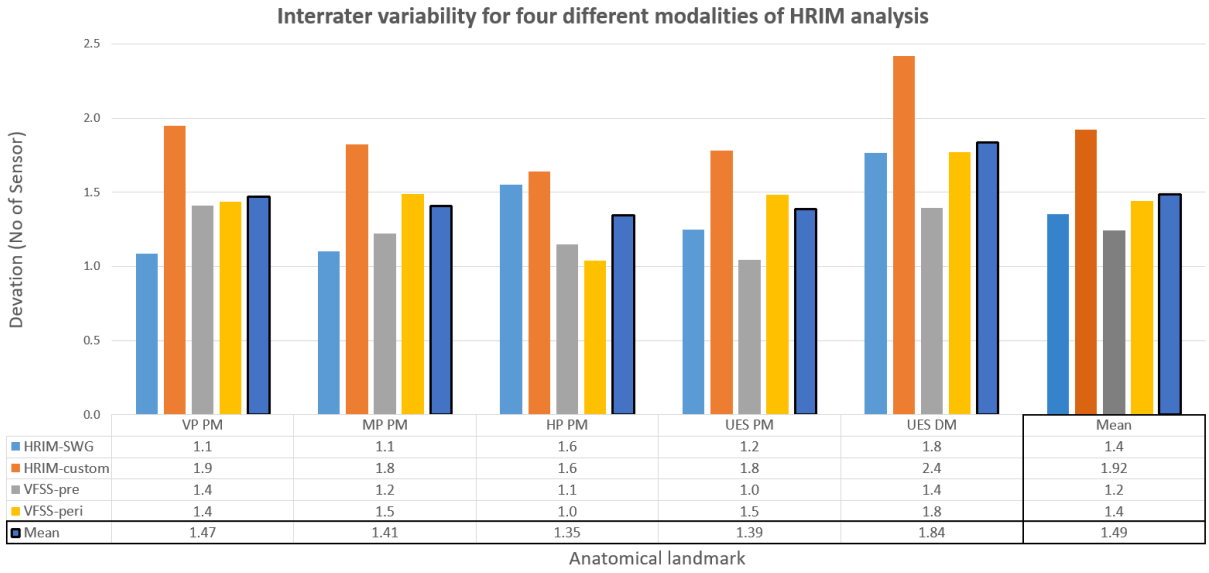


| | VP PM | MP PM | HP PM | UES PM | UES DM | Mean |
|---|---|---|---|---|---|---|
| HRIM-SWG | 1.1 | 1.1 | 1.6 | 1.2 | 1.8 | 1.4 |
| HRIM-custom | 1.9 | 1.8 | 1.6 | 1.8 | 2.4 | 1.92 |
| VFSS-pre | 1.4 | 1.2 | 1.1 | 1.0 | 1.4 | 1.2 |
| VFSS-peri | 1.4 | 1.5 | 1.0 | 1.5 | 1.8 | 1.4 |
| Mean | 1.47 | 1.41 | 1.35 | 1.39 | 1.84 | 1.49 |

Figure 4.2: The interrater variability between the four different modalities in which the HRIM data can be analyzed.

### 4.3.2 Deviation between the different landmark definition methods

The deviation between the four different methods in which the HRIM can be analyzed is depicted in figure 4.4 for both SLPs. The deviation between analyzing the HRIM-SWG and the HRIM-custom, and the deviation between the VFSS-pre and VFSS-peri is always below 1.5 sensors. However, the deviation in position between the landmarks placed on pressure topography plots compared to the VFSS images is higher. This deviation ranges between the 3 and 6 sensors. The variability within analysis on the same modality is similar to the interrater variability. However, the deviation between the different modalities is more than doubled, without an excessive high interrater variability in one of the modalities.

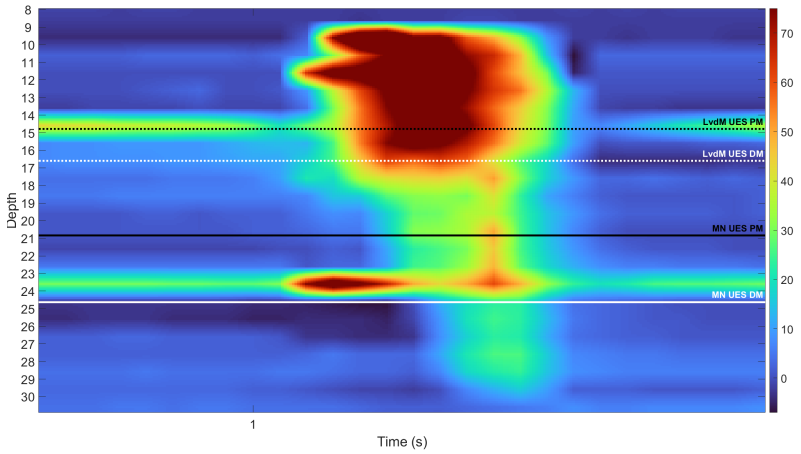


Figure 4.3: The landmark definition of the UES PM and UES DM for both SLPSs. The landmarks deviate a lot. Both SLPs identify a different pressure pattern as the UES.

### 4.3.3 Landmarks on the VFSS-pre compared to VFSS-peri images

The deviation between the landmarks on the VFSS images and the pressure topography plots is lower for the VFSS-pre compared to the VFSS-peri. However, this deviation is shifting per anatomical landmark. For the VP PM and the MP PM, the deviation with the VFSS-pre is higher, while for the UES PM and the UES DM, the deviation with the VFSS-peri is higher. For the HP PM, no clear difference in deviation is noticeable.

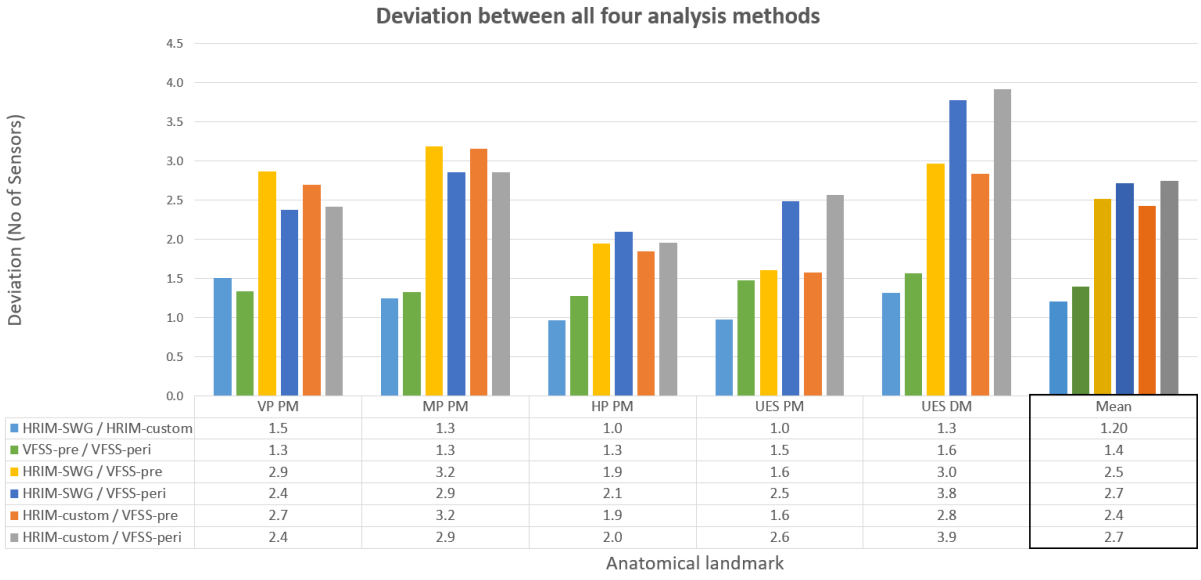


| | VP PM | MP PM | HP PM | UES PM | UES DM | Mean |
|---|---|---|---|---|---|---|
| HRIM-SWG / HRIM-custom | 1.5 | 1.3 | 1.0 | 1.0 | 1.3 | 1.20 |
| VFSS-pre / VFSS-peri | 1.3 | 1.3 | 1.3 | 1.5 | 1.6 | 1.4 |
| HRIM-SWG / VFSS-pre | 2.9 | 3.2 | 1.9 | 1.6 | 3.0 | 2.5 |
| HRIM-SWG / VFSS-peri | 2.4 | 2.9 | 2.1 | 2.5 | 3.8 | 2.7 |
| HRIM-custom / VFSS-pre | 2.7 | 3.2 | 1.9 | 1.6 | 2.8 | 2.4 |
| HRIM-custom / VFSS-peri | 2.4 | 2.9 | 2.0 | 2.6 | 3.9 | 2.7 |

Figure 4.4: The deviation between the position of the anatomical landmarks between two different modalities in which the landmarks can be placed.

## 4.4 Discussion

The objective of this chapter was to determine whether a different method for defining anatomical regions in the analyses of HRIM data performs better than HRIM-SWG. Four different analysis methods (HRIM-SWG, HRIM-custom, VFSS-pre, and VFSS-peri), each with their own limitations and advantages, were assessed in terms of interrater variability and deviation between the methods. Among the four methods, VFSS-pre demonstrated the lowest interrater variability, indicating a higher level of consistency compared to the other methods. Analyzing landmark positions within the same modality (either pressure topography plots or VFSS images) yielded a lower deviation than comparing across different modalities. This finding suggests the presence of a systematic difference between the analysis of VFSS images and pressure topography plots. It has been previously established that errors can occur in the HRIM-SWG analysis. Therefore, a high deviation between the different methods does not necessarily imply that the other methods are more inaccurate. Consequently, it is challenging to determine the optimal method for HRIM analysis based solely on the available data. More in-depth research is required to investigate the sources of this high deviation in order to determine the optimal analysis method.

#### Sensornumbers on pressure topography plots and cross-referencing with VFSS images

In patients with altered pressure topography plots, the inclusion of sensor numbers on the y-axis of the plots appears to be advantageous for accurate analysis, for example in patient 6 who is treated with a TL. In pressure topography plots of non-pathological swallows, the UES is characterized as a continuous high-pressure zone. However, in this patient, there are two distinct high-pressure zones observed, around sensors 15 and 23. One SLP primarily identifies the superior, and the other SLP mostly identifies the inferior high-pressure zone as UES, causing the high interrater variability. A TL causes severe anatomical changes around the UES, causing a decreased UES resting pressure and contraction pressure, which makes identification more challenging. [67] Prior to the TL, the UES is typically located around the C6, aligning more closely to the superior high-pressure zone in this patient. [68] In HRIM-custom, this superior high-pressure zone is more often identified as the UES. The main difference between the analysis on HRIM-SWG and HRIM-custom is that the sensor number is shown on the y-axis of the topography plot in HRIM-custom.

However, reaching this conclusion would not have been possible without cross-referencing the findings with VFSS images. This underscores the vulnerability of anatomical region definition to errors when relying solely on HRIM pressure topography plots in patients with altered anatomy. This vulnerability has been previously demonstrated in the case described in section 3.1, which involved a patient who underwent commando surgery. In contrast, the current patient underwent a TL, highlighting the importance of evaluating HRIM data in conjunction with VFSS images, particularly in patients after treatment of HNC.

#### Difference in anatomical regions between pre-and peri-swallow VFSS images

The timing of the VFSS images (VFSS-pre or VFSS-peri) that corresponds best to the position of landmarks on the pressure topography plots depends on the anatomical landmark. The VP PM and the MP PM align better on VFSS-peri, while the UES DM and UES PM align better on the VFSS-pre. This might be explained by the moment of pressure generation of the structures in the anatomical regions.

The VFSS-peri images are captured at the moment of the highest laryngeal elevation or catheter elevation. This laryngeal elevation occurs immediately after the swallow is initiated. [69] Therefore, the UES is opened while elevating. The continuous high-pressure zone which indicates the UES on the pressure topography plots is therefore captured when no laryngeal elevation is present, so indeed on the VFSS-pre images. This is confirmed by [**berg**] et al. who discovered that the sensor initially located on the high-pressure zone of the UES moves during swallowing with certainly 10mm upwards. In contrast to the UES, the velopharynx and mesopharynx generate pressure during swallowing. The pressure in the velopharynx is due to the tight seal of the velopharyngeal port, and the pressure in the mesopharynx is caused by the tongue base propelling food into the pharynx and esophagus. These pressure increases, on which the landmarks are defined, occur during the swallow, and therefore the VP PM and MP PM correspond better with the anatomical regions on the VFSS-pre images. The pressures in the hypopharynx often reflect cartilaginous laryngeal and epiglottic structures against the catheter. It is not explained yet why this does not matter on which image in time these landmarks are drawn.

However, this study has some findings making the statement that the VP PM and MP PM must be defined on the VFSS-peri images and the UES PM and UES DM must be defined on the VFSS-pre images less conclusive. At first, the deviation between the landmarks defined on the pressure topography plots compared with the VFSS images is overall quite high. A systematic difference seems to be present between both. Secondly, the definition of anatomical landmarks on VFSS-pre- and VFSS-peri is inconsistent; the landmarks are not always placed on the same anatomy. Therefore, it is difficult to determine if the deviation observed between the landmark positions of the VFSS-pre and VFSS-peri is due to shifting displacement of the anatomy or catheter, or simply a lack of consistency in landmark placement by the SLPs.

**Anatomical landmark definition in VFSS images**

The inconsistent definition of anatomical landmarks on the VFSS images and the deviation in landmark position between pressure topography plots and VFSS images can be attributed to several causes.

Firstly, the absence of prior consultation or training in defining anatomical regions in VFSS images made the definition of anatomical regions challenging for the SLPs. It would have been beneficial if the SLPs had discussed and reached a consensus on the definition of anatomical regions before conducting the analysis. Although both SLPs have experience in diagnosing swallow problems from VFSS recordings, defining anatomical regions is not typically required in routine VFSS assessment. Consequently, this method was novel to them, and they were provided with limited opportunities to practice or discuss the position of the anatomical regions. The only resources provided were anatomical images depicting the relevant regions but it is uncertain to what extent they focused on these images. Hence, it can be concluded that establishing a consensus and standardized definition of anatomical regions could improve reliability. Nevertheless, the SLPs themselves expressed the difficulty of this task on the VFSS images, partly due to the limited experience, suggesting potential for improvement.

Secondly, the selection of appropriate frames for VFSS-pre images proved to be challenging due to the nature of the recording process. SLPs administered the bolus to the patient before stepping behind the radiation shielding wall after which the x-ray recording is allowed to start. If the patient does not adhere strictly to swallow initiation instructions or if the X-ray recording started too late, selecting the correct frame for the VFSS- pre image became problematic. In these cases, the swallow was either excluded from analysis or the last frozen frame from the previous swallow was selected as the frame VFSS-pre image. However, selecting the frame when the patient returned to rest after swallowing would yield more accurate results as it still represents the same swallow.

Thirdly, in this study, it is assumed that catheter movement is correlated with laryngeal elevation. However, a study by Isberg et al. [70] revealed that catheter movement is actually correlated with the moment of soft palate lifting during swallowing. This may have contributed to an inconsistency in VFSS-pre image selection between TL patients and non-TL patients. Namely, in TL patients the moment of greatest displacement of the catheter is selected, while in non-TL patients the moment of highest laryngeal elevation is selected as VFSS-peri image. However, its influence on the results is likely minimal given that the same swallows were compared within the study.

Furthermore, some VFSS images are recorded laterally, while others are taken in a left-lateral projection. The left-lateral projection is used for the TL patient because the voice prosthesis becomes better visible. However, the relevant anatomy is better visible and aligned with the catheter on the lateral images. It is therefore recommended to measure at least some swallows in a lateral position to ensure proper visibility of anatomical structures in these images to align them with the pressure topography plots.

Lastly, compensatory swallowing techniques such as chin-tuck or swallowing with the head turned to the left or right posed additional difficulties in anatomical region definition. Figure 3.15 demonstrates the VFSS image while the patient performs a chin-tuck maneuver. It is apparent that the horizontal landmarks used to define the anatomical regions no longer align with the direction of the anatomical structures. Additionally, errors in sensor counting by the algorithm are observed as explained in section 3.4. Swallowing with the head turned resulted in unclear assessment of the catheter's position relative to the anatomy, further complicating landmark definition. Thus, alternative methods need to be developed specifically for analyzing swallowing during compensation mechanisms in VFSS images.

**Evaluation of Analysis Methods and Potential Alternatives**

In this study, four analysis methods were selected: customized software, SwallowGateway, and the utilization of two moments of VFSS image recording. However, it is important to note that the superiority of these methods has not been established, and there are alternative possibilities worth exploring. As mentioned in the introduction of this chapter, Laborie has also developed software that allows for HRIM analysis. Although Laborie was still in the early stages of development at the start of this study, it has since made noteworthy advancements, such as synchronizing VFSS recordings with topography plots. Laborie is therefore another promising tool for HRIM analysis, which justifies further investigation. As an additional benefit, their software is also provided at no cost when purchasing the catheter. However, a drawback is that no accompanying training course is offered. Nevertheless, the landmark definition functions similarly to that of SwallowGateway.

Furthermore, the custom software utilized in this study primarily employed plain topography plots. However, customizing software provides extensive opportunities for data analysis and refinement. For instance, such software could be elaborated by including VFSS images and topography plots in a unified figure. These opportunities were not explored in the present study but hold the potential to improve the precision of anatomical landmark definition. Therefore, it is recommended to consider such enhancements in future research.

## 4.5 Conclusion

This chapter compares the definition of anatomical landmarks between four different methods of which two involve pressure topography (HRIM-SWG and HRIM-custom) plots and two involve VFSS images (VFSS-pre and VFSS-peri). The interrater variability of HRIM-SWG, VFSS-pre, and VFSS-peri, as well as the deviation when comparing the same modalities, remain in an acceptable range ($<$1.5 sensors). However, the deviation between landmark definition on VFSS images and pressure topography plots is too large. This indicates a systematic difference in the landmark definition between the two modalities. This difference could have been caused by the absence of consensus among the SLPs about anatomical landmark definition on the VFSS images or by challenges in selecting the appropriate VFSS images. Furthermore, the added value of cross-referencing the position of the anatomical regions on the topography plots with the VFSS images is demonstrated again. Moreover, the landmarks on the topography plots for the VP PM and MP PM seem to align better with the VFSS-peri, while the UES PM and UES DM align better with the VFSS-pre. Future studies should focus on identifying and reducing the source of the measured deviation, improving the consistency in image selection, and improvement of the analysis methods.

# 5

# General discussion and conclusion

## 5.1 Discussion

Swallowing problems often occur in patients after treatment of HNC due to tissue damage. This does not only result in physical problems, like malnutrition and pneumonia, but also in psychological burdens like anxiety, social isolation, and low self-esteem. To improve the swallowing function in these patients, an assessment of the swallowing is regularly done with VFSS. However, the assessment of VFSS only relies on visual observation. This makes it difficult to objectify the assessment and evaluate physiological problems. HRIM measures generated pressure and bolus motion in the pharynx, potentially solving both disadvantages of VFSS. For the analysis, different anatomical regions must be identified on the pressure topography plots. This is especially challenging in HNC patients, probably leading to not much adoption of this technique in clinical practice.

To overcome this problem, this study aimed to develop an optimized and effective method for analyzing pharyngeal HRIM in patients after treatment of HNC. On top of easier analysis, HRIM should be implemented in the clinical practice for the diagnoses of swallowing problems in HNC patients. Therefore, a measurement protocol is developed based on existing literature, the SEATTLE protocol, and gained experience (Chapter 2). The protocol identified three consistency levels in two different volumes as optimal for clinical diagnostics. However, it is acknowledged that SLPs may need to deviate from the established protocol in certain clinical scenarios. During the HRIM analyses in our patient population, we encountered mistakenly identified anatomical regions when relying solely on the HRIM topography plots in SwallowGateway. Therefore, an additional supportive method had to be developed to improve the adequacy of the HRIM analyses. This led to the investigation of using VFSS recordings as a supportive tool for HRIM analyses because it was hypothesized that anatomical regions could be better identified on the VFSS images (3. (Chapter 3) Moreover, the HRIM catheter is visible on the VFSS images, enabling the correlation of sensor location with patient anatomy. To facilitate this, the topography plots had to be displayed in custom-designed software, as sensor counting is impossible in SwallowGateway. However, manual sensor counting is time-consuming, highlighting the need for an automated approach, which appears feasible when examining the VFSS images. To address this, an automated method for HRIM catheter segmentation and sensor counting in VFSS images is developed. This automated analysis demonstrated the potential for HRIM catheter segmentation and accurate sensor counting. To evaluate this new method, the definition of anatomical regions, similar to SwallowGateway, was performed on VFSS images at two different time points during swallowing, as well as on HRIM topography plots in the custom-designed software (Chapter 4). The landmark positions were compared across the different methods. The findings revealed that interrater reliability was lowest in VFSS-pre. The deviation in landmark definition between the same modality is accurate ($<$1.5 sensors) but between two different modalities not accurate, which indicates a systematic difference between the landmark definition on pressure topography plots compared to VFSS images. Furthermore, upon evaluation of individual swallows, it was observed that some anatomical landmarks were incorrectly identified on the pressure topography plots but correctly identified on the VFSS images. Also, the landmarks on the topography plots for the VP PM and MP PM seem to align better with the VFSS peri-images while the UES PM and UES DM align better with the VFSS pre-images. However, the validity of these conclusions is limited by some limitations in the study setup. In conclusion, this thesis highlights the crucial role of VFSS as a supportive tool for

HRIM analysis, reducing the risk of falsely identified anatomical regions. Additionally, the automation of sensor counting has yielded promising results. Nevertheless, several challenges remain that must be acknowledged and resolved in order to fully implement this novel analysis method.

### 5.1.1 Relation with existing literature

This study represents the first attempt to investigate the use of VFSS as a supportive tool for HRIM analysis. No previous studies examining this specific aspect have been identified in the existing literature. The literature primarily consists of comparative studies that focus on comparing the outcomes of VFSS parameters with HRIM parameters. Most of these studies show a correlation between VFSS and HRIM variables. [71] However, these studies do not synchronize or analyze HRIM and VFSS together. Some studies have used simultaneous VFSS and manometry to confirm sensor position in the desired area [72], or investigate catheter movement during swallowing [70]. Williams et al. [73] correlated manometry with VFSS to display the swallowed bolus on pressure topography plots by establishing a shared coordinate system based on catheter sensors. This allowed them to measure intrabolus pressures with HRIM. However, current manometry catheters incorporate impedance measurement, enabling the measurement of bolus motion already in the same coordinate system as pressure. All identified literature about combining VFSS and HRIM originates from 2001 and earlier, indicating a gap in research on this combination.

Moreover, no prior research has been conducted on topics related to HRIM catheter segmentation or sensor counting for anatomical region definition. However, studies have been performed on automating the segmentation of other structures from VFSS images. Research into automated detection of the position or movement of the hyoid is often reported in the literature on automated VFSS analysis. Various techniques, ranging from conventional semi-automated methods to complex fully-automated segmentation methods, have been reported. These include edge-detection algorithms[74], template matching [75], binary pattern calculation [29], and deep learning with convolutional neural networks [76] [77]. These studies describe accurate results in tracking the hyoid bone but note that challenges when other structures overlap with it. Studies have also focused on automatic detection of the pharyngeal swallow phase[78], detection of airway invasion [79], and segmentation of the bolus [80]. Furthermore, studies that combine these automated segmentation methods have been reported. [81] [82]

However, to the authors' knowledge, automated sensor counting to establish a relationship between anatomy on the VFSS images and pressure features on the topography plots has not been attempted or published yet. Consequently, a comparative analysis between the results of this study and the existing literature is not feasible, emphasizing the originality and unique contribution of this study in the field.

## 5.2 Future perspective

This thesis has demonstrated promising results in optimizing the clinical application of HRIM for HNC patients by developing a measurement protocol and achieving an optimized HRIM analysis method by using VFSS as a supportive tool for the analysis. This makes HRIM analyses potentially more accurate and easier accessible for clinicians without extensive training. In order to successfully integrate this method into patient care, further testing and refinement are necessary. Several key aspects warrant attention in this process. In the following section, we will discuss these aspects in detail and propose strategies for improvement.

### 5.2.1 Increasing HRIM application in clinical practice

In Chapter 2, a protocol for the combined measurement of VFSS and HRIM in clinical practice is designed. This protocol is until this moment applied to six different patients, with each patient revealing aspects for protocol optimization. Ideally, HRIM should be measured in more patients to further refine the protocol. Additionally, increased application of the measurement protocol could enhance standard clinical care by identifying which patients benefit most from HRIM and could provide more patient cases where the added value of HRIM is demonstrated. Even more, larger cohorts of similar patients could facilitate research into affected HRIM variables with corresponding symptoms or treatments.

One obstacle hindering widespread adoption, in the authors' opinion, is the limited knowledge and familiarity among SLPs and physicians. Despite presenting the topic during a consensus meeting attended by the entire department, there still seems to be a lack of compelling evidence that convinces clinicians

to widely adopt manometry in their practice. To strengthen this support, it is crucial to present patient cases where HRIM has resulted in improved treatment outcomes. However, this creates a cycle as the absence of frequent HRIM measurements limits the availability of such cases. While certain cases have provided insights into patients' swallowing problems, determining the most appropriate therapy remains challenging, likely due to the inexperience of the manometry team.

Moreover, the time-consuming and complex nature of HRIM analysis restricts the analysis to those who have attended a course. Other clinicians therefore may perceive it as a cumbersome process that they do not comprehend. Consequently, this further impedes the widespread adoption of HRIM among clinicians, even though clinicians should schedule appointments for the HRIM after assessing the patient in the outpatient clinic and explaining the procedure to obtain informed consent.

Furthermore, HRIM can only be measured when the fluoroscopy room and at least two members of the manometry team are available. Currently, this is limited to Tuesday mornings, which restricts the frequency of HRIM measurement.

Considering these factors, HRIM is not fully utilized to its potential, while if it were, it would accelerate our learning process, expedite the improvement of the measurement protocol, and facilitate the demonstration of its added value. This, in turn, will facilitate opportunities for more research into affected HRIM variables in specified patient groups. This thesis presents a method for a potentially more comprehensive analysis of HRIM data. This method enhances the clinicians' understanding of HRIM topography plots by relating them to the anatomy depicted on the VFSS images, with which they are already familiar. Moreover, this method saves time as it eliminates the need for specialized training. lastly, it offers the potential for more accurate analysis. However, for widespread clinical application of this newly developed method, further research is advised.

### 5.2.2 Improving consistent catheter segmentation

In Chapter 3, the process of segmentation and automated sensor counting is discussed. This initial setup aimed to explore the potential of this process and demonstrated promising results. The proposed method is a simple approach for the segmentation of the catheter, however, this can probably be improved by more elaborated and complicated approaches. One of the problems encountered during the catheter segmentation was the interference caused by objects with similar gray values, such as contrast bolus blocking the sight of the catheter or structures with similar gray values resulting in branches that were mistakenly identified as catheter branches. To address this issue, it is important to better consider the trajectory of the catheter during the segmentation. The VFSS recordings consist of consecutive frames where the catheter does not undergo great displacement. By employing algorithms like Kalman filtering, the catheter's location can potentially be predicted based on its position in the previous frame. This method is used in several applications in VFSS images like tracking the tongue or lumbar vertebrae. [83] [84] This approach ensures smoother movement estimation and helps eliminate noise. Furthermore, even more sophisticated methods such as deep learning show promising results in tracking structures on VFSS frames. Different models reached high accuracy in detecting the location of the hyoid bone in VFSS frames. [76] [85] Also algorithms predicting the bolus location or aspiration are developed. [79] [80] Similarly, developing deep learning models for the detection of the HRIM catheter, which is even more clearly visible compared to other structures, can improve segmentation accuracy. Further investigation into these methods, along with the exploration of alternative techniques, will contribute to advancements in catheter segmentation for VFSS images.

Furthermore, improvement in the quality of the VFSS images can contribute to easier and full catheter segmentation. The quality of the images can on one hand be improved by instructing the patients better in asking to remove all x-ray absorbing objects and move as little as possible during the swallow, resulting in a better image resolution and ensuring that the catheter remains in the same area. On the other, the radiologic technologist could be instructed better by asking to keep the focus of the x-ray on the HRIM catheter and keeping all sensors within the VFSS image. Furthermore, the position of the patient must be considered for the recording of the VFSS video. A lateral position makes anatomical structures clearer on the VFSS images, resulting in easier identification of anatomical structures by the SLPs. These improvements will lead to more robust and accurate catheter segmentation on each VFSS frame, reducing errors in sensor counting. Therefore, further research is required to improve the consistency of catheter segmentation.

### 5.2.3 Changing horizontal landmarks into anatomical locations alongside the catheter

Currently, we have adopted the use of horizontal landmarks as markers to define anatomical regions in VFSS images which is in line with the approach employed in SwallowGateway. However, using horizontal landmarks may not be the optimal approach. When patients perform compensation techniques or change their position, the anatomical regions are no longer horizontal anymore. Moreover, the relevance of identifying complete anatomical regions in VFSS images, especially beyond the catheter's scope (e.g. in the nose or mouth), is questionable. Instead, it would be more advantageous to identify specific anatomical structures near the catheter, such as the velum, tongue base, and cricoid cartilage.

To determine the best anatomical points to identify on VFSS images and establish their precise positions, it is important to initiate a discussion among SLPs or other experts on the VFSS assessment. Once consensus is reached, an in-depth training course, similar to the one developed for SwallowGateway, should be created to teach SLPs how to select these anatomical landmarks on VFSS images. Application of this alternative approach, based on a consensus, could facilitate easier landmark definitions for SPLs, providing more consistent and reliable results. The feasibility of this approach can be evaluated using a similar methodology as described in Chapter 4, which is likely to result in a more consistent definition of the anatomical landmarks. Furthermore, future studies could focus on automatically recognizing relevant anatomical structures in VFSS images, similar as is done for the hyoid bone and cervical vertebrae [76] [86] [85]. By automating the recognition of structures like the larynx, tongue base, and velum, and counting at which sensors they are positioned, the issue of subjective definition of anatomical landmarks by SLPs on VFSS images could be tackled as well. If (some of) the above steps lead to a more consistent definition of anatomical landmarks, the identified structures can be indicated on the corresponding sensor channel in the HRIM topography plots. This will provide greater insight into the pressure patterns associated with specific anatomical regions.

### 5.2.4 Exploring the sources of the deviation between anatomical landmarks on the pressure topography plots and the VFSS images

In this thesis, the underlying cause of the deviation between the landmarks on the pressure topography plots and the VFSS images remains unidentified. Identifying this cause is crucial before further developing the automated sensor counting algorithm, as it would otherwise be of limited utility or require significant adaptation. To determine the source of the deviation, it is important to first reach a consensus in the definition of anatomical landmarks on the pressure topography plots and the VFSS images, as discussed previously. Subsequently, a comprehensive study on healthy subjects is recommended as it is expected that anatomical markers would be more easily identifiable in their data. Anatomical landmarks that are clearly identifiable in both modalities must be defined by multiple raters. Only swallows and anatomical landmarks with minimal interrater variability should be included, as those indicate easy identification of the anatomy. The deviation between the anatomical landmarks on the pressure topography plots and the VFSS images should be calculated. If the deviation is small, it suggests that the anatomical landmark definition used in the patient population of this thesis poses challenges, causing the large deviation. Conversely, if the study with these easily identifiable anatomical landmarks still exhibits high deviation, it may indicate a systematic difference in the identification of anatomical landmarks between the two modalities. Through careful analysis of this data, the source of the deviation and possibly a correction factor can be determined for application in future research or clinical practice.

### 5.2.5 Effect on the verified parameters

The HRIM working group, led by Omari [16], has validated the parameters and their normal values generated by SwallowGateway after the anatomical landmarks are placed. However, this thesis demonstrates that identifying anatomical regions on the pressure topography plots in SwallowGateway can result in misidentified regions in HNC patients. This has the potential to lead to incorrect parameter values and misdiagnoses for patients. Importantly, no research has been conducted on the impact of misplaced anatomical regions on the validated HRIM parameters. Furthermore, those parameters have not been validated specifically for our HNC population. HNC treatment significantly affects the anatomy and physiology of patients' swallowing function, making it unlikely for their swallowing to be entirely normal. It is crucial to determine which swallow parameters can be improved for these patients and which parameters have become abnormal due to their HNC treatment, as this information is vital for the therapy

of these patients. Identifying the parameter values that contribute to optimal swallowing outcomes in different patient groups is essential. To address this, a study can be initiated to categorize patients based on their specific HNC treatments. Subsequently, HRIM measurements can be performed, and patients can provide feedback on their swallowing quality through surveys. Ideally, pre- and post-treatment HRIM measurements would be conducted to investigate the effect of the treatment on swallowing outcomes. This approach would allow us to examine the impact of the categorized treatments on the HRIM parameter values in SwallowGateway.

## 5.3 Conclusion

The possibilities for improving the application of HRIM in clinical practice for patients with HNC have been explored. This resulted in a revised measurement protocol for combined VFSS and HRIM measurement, establishing consistencies and volumes specifically tailored for HNC patients. The protocol also identifies the optimal method for inserting the HRIM catheter, recording VFSS images, and labeling HRIM data for this patient population. Through testing and optimization in clinical practice, the protocol has demonstrated its effectiveness. An automated algorithm for sensor counting in regions on the VFSS images has been developed, showing no significant difference to manual sensor counting. This algorithm has the potential to enhance the time efficiency and accuracy of HRIM analyses. Additionally, different methods for anatomical landmark definition on pressure topography plots and VFSS images have been compared. This showed the lowest interrater variability for VFSS images captured pre-swallowing and substantial deviation between anatomical landmarks on VFSS images and pressure topography plots. This comparison further highlights the limitations of relying solely on HRIM data for the definition of anatomical landmarks in HNC patients, as it may lead to misidentification. In conclusion, the analysis of HRIM could be optimized by incorporating the anatomical information from the VFSS images in the pressure topography plots. This provides deeper insights into the anatomical location on the topography plots and has the potential to enhance the comprehensiveness of HRIM data for less-experienced users, as well as improve the accuracy of landmark definition. Future research should primarily focus on determining the optimal method for defining anatomical landmarks on VFSS images and investigating the underlying reasons for the current deviation between anatomical landmarks on the pressure topography plots and VFSS images. Subsequently, the analysis of HRIM data using VFSS images as anatomical references could be further implemented in clinical practice.

# Bibliography


1. Federatie Medisch Specialisten. *Startpagina - Orofaryngeale dysfagie - Richtlijn - Richtlijnendatabase* Feb. 2017. https://richtlijnendatabase.nl/richtlijn/orofaryngeale%7B%5C_%7Ddysfagie/startpagina%7B%5C_%7D-%7B%5C_%7Dorofaryngeale%7B%5C_%7Ddysfagie.html (2022).
2. Krebbers, I. *et al.* Patients with Head-and-Neck Cancer: Dysphagia and Affective Symptoms. *Folia Phoniatr. Logop.* **73,** 308–315. ISSN: 1021-7762. https://www.karger.com/Article/FullText/508367 (July 2021).
3. Martin-Harris, B. & Jones, B. The Videofluorographic Swallowing Study. *Phys. Med. Rehabil. Clin. N. Am.* **19,** 769. ISSN: 10479651. https://www.ncbi.nlm.nih.gov/pmc/articles/PMC2586156/ (Nov. 2008).
4. Han, T. R., Paik, N.-J., Park, J.-W. & Kwon, B. S. The prediction of persistent dysphagia beyond six months after stroke. *Dysphagia* **23,** 59–64 (2008).
5. McCullough, G. H. *et al.* Inter-and intrajudge reliability for videofluoroscopic swallowing evaluation measures. *Dysphagia* **16,** 110–118 (2001).
6. Szczesniak, M. M. *et al.* Inter-rater reliability and validity of automated impedance manometry analysis and fluoroscopy in dysphagic patients after head and neck cancer radiotherapy. *Neurogastroenterology Motility* **27,** 1183–1189. ISSN: 1365-2982. https://onlinelibrary.wiley.com/doi/full/10.1111/nmo.12610 (8 Aug. 2015).
7. Hind, J. A. *et al.* Comparison of trained clinician ratings with expert ratings of aspiration on videofluoroscopic images from a randomized clinical trial. *Dysphagia* **24,** 211–217 (2009).
8. Rommel, N. *et al.* Bolus residue scale: an easy-to-use and reliable videofluoroscopic analysis tool to score bolus residue in patients with dysphagia. *International journal of otolaryngology* **2015** (2015).
9. Omari, T. *et al. DEVELOPMENT OF SWALLOW GATEWAY (WWW.SWALLOWGATEWAY.COM): AN ONLINE APPLICATION FOR ANALYSIS OF HIGH RESOLUTION MANOMETRY (HRM) AND DIAGNOSIS OF DYSPHAGIA — Taher Omari — 49 updates — 12 publications — Research Project* Feb. 2017. https://www.researchgate.net/project/Development-of-Swallow-Gateway-wwwswallowgatewaycom-An-online-application-for-analysis-of-high-resolution-manometry-HRM-and-diagnosis-of-dysphagia.
10. Leung, R. S., Comondore, V. R., Ryan, C. M. & Stevens, D. Mechanisms of sleep-disordered breathing: Causes and consequences. *Pflugers Arch. Eur. J. Physiol.* **463,** 213–230 (Jan. 2012).
11. MedicalStocks. *Anatomie van de mond en tong medische vector illustratie op witte achtergrond - Illustratie* https://www.istockphoto.com/nl/vector/anatomie-van-de-mond-en-tong-medische-vector-illustratie-op-witte-achtergrond-gm1141280498-305696760?phrase=menselijke%20mond.
12. Raol, N. & Hartnick, C. J. Anatomy and Physiology of Velopharyngeal Closure and Insufficiency. *Adv. Otorhinolaryngol.* **76,** 1–6. ISSN: 00653071. https://www.karger.com/Article/FullText/368003 (2015).
13. Perry, J. L. Anatomy and Physiology of the Velopharyngeal Mechanism. http://dx.doi.org/10.1055/s-0031-1277712..
14. Walczak, C. C., Jones, C. A. & McCulloch, T. M. Pharyngeal Pressure and Timing During Bolus Transit. *Dysphagia* **32,** 104–114. ISSN: 14320460. https://link.springer.com/article/10.1007/s00455-016-9743-5 (Feb. 2017).
15. Jones, C. A. *et al.* Methods for measuring swallowing pressure variability using high-resolution manometry. *Front. Appl. Math. Stat.* **4,** 1–17. ISSN: 22974687 (2018).
16. Omari, T. I. *et al.* High-Resolution Pharyngeal Manometry and Impedance: Protocols and Metrics—Recommendations of a High-Resolution Pharyngeal Manometry International Working Group.

*Dysphagia 2019 35:2* **35,** 281–295. ISSN: 1432-0460. https://link.springer.com/article/10.1007/s00455-019-10023-y (2 June 2019).
17. Gun, R. & Ozer, E. Surgical anatomy of oropharynx and supraglottic larynx for transoral robotic surgery. *J. Surg. Oncol.* **112,** 690–696. ISSN: 1096-9098. https://onlinelibrary-wiley-com.ezproxy2.utwente.nl/doi/full/10.1002/jso.24020 (Dec. 2015).
18. Logemann, J. A. Critical factors in the oral control needed for chewing and swallowing. *J. Texture Stud.* **45,** 173–179. ISSN: 17454603. https://www.ncbi.nlm.nih.gov/pmc/articles/PMC4224116/ (June 2014).
19. Paul Flint *et al.* in *Cummings Otolaryngol. Head Neck Surg.* 7th ed. Chap. 101 (ELSEVIER - HEALTH SCIENCE, Apr. 2020). ISBN: 9780323612166.
20. Bruss, D. M. & Sajjad, H. Anatomy, Head and Neck, Laryngopharynx. *StatPearls.* https://www.ncbi.nlm.nih.gov/books/NBK549913/ (May 2022).
21. Hoerter, J. E. & Chandran, S. K. Anatomy, Head and Neck, Laryngeal Muscles. *StatPearls.* https://www.ncbi.nlm.nih.gov/books/NBK545265/ (Aug. 2021).
22. integraal kankercentreum Nederland (KNL). *NKR Cijfers* https://iknl.nl/nkr-cijfers (2022).
23. Koroulakis, A. & Agarwal, M. Laryngeal Cancer. *StatPearls.* https://www.ncbi.nlm.nih.gov/books/NBK526076/ (Aug. 2021).
24. Gaziano, J. E., Ma, C.-S. & Moffitt, H. L. Evaluation and Management of Oropharyngeal Dysphagia in Head and Neck Cancer. *http://dx.doi.org.ezproxy2.utwente.nl/10.1177/107327480200900505* **9,** 400–409. ISSN: 10732748 (Aug. 2017).
25. Manikantan, K. *et al.* Dysphagia in head and neck cancer. *Cancer Treat. Rev.* **35,** 724–732. ISSN: 0305-7372 (Dec. 2009).
26. Nunn, D. & Goldsmith, T. *Patterns of velopharyngeal closure during speech and swallow: a case study- ASHA 2003* in (Jan. 2003).
27. Kao, S. S. T., Peters, M. D., Krishnan, S. G. & Ooi, E. H. Swallowing outcomes following primary surgical resection and primary free flap reconstruction for oral and oropharyngeal squamous cell carcinomas: A systematic review. *Laryngoscope* **126,** 1572–1580. ISSN: 1531-4995. https://onlinelibrary.wiley.com/doi/full/10.1002/lary.25894 (July 2016).
28. Čoček, A. *et al.* Locally advanced laryngeal cancer: Total laryngectomy or primary non-surgical treatment? *Oncol. Lett.* **15,** 6701. ISSN: 17921082. https://www.ncbi.nlm.nih.gov/pmc/articles/PMC5920282/ (May 2018).
29. Lee, J. W., Randall, D. R., Evangelista, L. M., Kuhn, M. A. & Belafsky, P. C. Subjective Assessment of Videofluoroscopic Swallow Studies: *https://doi-org.ezproxy2.utwente.nl/10.1177/0194599817691276* **156,** 901–905. https://journals-sagepub-com.ezproxy2.utwente.nl/doi/10.1177/0194599817691276 (Feb. 2017).
30. IDDSI. *IDDSI Framework* https://www.iddsi.org/.
31. *Precise Thick-N INSTANT Single Serve 500ml Bottle - BrightSky* https://www.brightsky.com.au/Precise-Thick-N-INSTANT-Single-Serve-500ml-Bottle-1 (2021).
32. Park, C. H. *et al.* Quantitative Analysis of Swallowing Function Between Dysphagia Patients and Healthy Subjects Using High-Resolution Manometry. *Ann. Rehabil. Med.* **41,** 776–785. ISSN: 2234-0645. https://pubmed.ncbi.nlm.nih.gov/29201816/ (2017).
33. Park, D., Oh, Y. & Ryu, J. S. Findings of Abnormal Videofluoroscopic Swallowing Study Identified by High-Resolution Manometry Parameters. *Arch. Phys. Med. Rehabil.* **97,** 421–428. ISSN: 0003-9993 (Mar. 2016).
34. Lan, Y. *et al.* The Correlation Between Manometric and Videofluoroscopic Measurements of the Swallowing Function in Brainstem Stroke Patients With Dysphagia. *J. Clin. Gastroenterol.* **49.** ISSN: 0192-0790. https://journals.lww.com/jcge/Fulltext/2015/01000/The%7B%5C_%7DCorrelation%7B%5C_%7DBetween%7B%5C_%7DManometric%7B%5C_%7Dand.7.aspx (2015).
35. Bredenoord, A. J. & Hebbard, G. S. Technical aspects of clinical high-resolution manometry studies. *Neurogastroenterol. Motil.* **24,** 5–10. ISSN: 1350-1925. https://doi.org/10.1111/j.1365-2982.2011.01830.x (Mar. 2012).
36. *High Resolution Oesophageal and Pharyngeal Manometry service* https://www.melbswallow.com.au/high-resolution-oesophageal-and-pharyngeal-manometry-service/ (2022).
37. Omari, T. I. *et al.* Reproducibility and Agreement of Pharyngeal Automated Impedance Manometry With Videofluoroscopy. *Clin. Gastroenterol. Hepatol.* **9,** 862–867. ISSN: 1542-3565. https://www.sciencedirect.com/science/article/pii/S1542356511005684 (2011).
38. Meek, A. *Manometrie in het AVL [email]*

39. Szczesniak, M. M., Wu, P. I., Maclean, J., Omari, T. I. & Cook, I. J. The critical importance of pharyngeal contractile forces on the validity of intrabolus pressure as a predictor of impaired pharyngo-esophageal junction compliance. *Neurogastroenterology and motility : the official journal of the European Gastrointestinal Motility Society* **30,** e13374. ISSN: 1365-2982 (Electronic) (10 Oct. 2018).
40. Lippert, D. *et al.* Preliminary Evaluation of Functional Swallow After Total Laryngectomy Using High-Resolution Manometry. *The Annals of otology, rhinology, and laryngology* **125,** 541–549. ISSN: 1943-572X (Electronic) (7 July 2016).
41. Fong, R. *et al.* Videofluoroscopic and manometric outcomes of cricopharyngeus balloon dilation for treatment of pharyngo-esophageal dysphagia associated with nasopharyngeal cancer: A case series. *Laryngoscope investigative otolaryngology* **6,** 1077–1087. ISSN: 2378-8038 (Print) (5 Oct. 2021).
42. Fujiwara, K. *et al.* Evaluation of pharyngeal swallowing pressure using high-resolution manometry during transoral surgery for oropharyngeal cancer. *The Journal of laryngology and otology* **135,** 153–158. ISSN: 1748-5460 (Electronic) (2 Feb. 2021).
43. Komatsu, H. *et al.* Blowing time ratio and high-resolution manometry to evaluate swallowing function of patients with oral and oropharyngeal cancer. *Auris Nasus Larynx* **49.** Export Date: 30 November 2022, 477–483 (3 2022).
44. Nativ-Zeltzer, N. *et al.* Autologous Muscle-Derived Cell Therapy for Swallowing Impairment in Patients Following Treatment for Head and Neck Cancer. *The Laryngoscope* **132,** 523–527. ISSN: 1531-4995 (Electronic) (3 Mar. 2022).
45. Yamaguchi, N. *et al.* The influence of radiotherapy on swallowing pressure: A study of 10 laryngeal carcinoma patients using high-resolution manometry. *Acta Medica Nagasakiensia* **61.** Cited By :1¡br/¿¡br/¿Export Date: 30 November 2022, 5–8. `https://www.scopus.com/inward/record.uri?eid=2-s2.0-85016216693&partnerID=40&md5=a91e73413eb87809ac3fe2bb4d991282` (1 2017).
46. Zhang, T. *et al. Modeling of pharyngoesophageal segment during tracheoesophageal phonation in total laryngectomy patients with preliminary validation* in. **2016-Octob.** Cited By :3¡br/¿¡br/¿Export Date: 30 November 2022 (2016), 2917–2920.
47. Búa, B. A., Olsson, R., Westin, U. & Rydell, R. The Pharyngoesophageal Segment after Total Laryngectomy. *Annals of Otology, Rhinology and Laryngology* **126.** Cited By :8¡br/¿¡br/¿Export Date: 30 November 2022, 138–145 (2 2017).
48. Chow, V. L. Y., Chan, J. Y. W., Cheng, I. K. Y. & Chan, K. M. K. Swallowing disorders following free jejunal flap reconstruction of circumferential pharyngeal defect: Does Botox help? *Oral oncology* **104,** 104612. ISSN: 1879-0593 (Electronic) (May 2020).
49. Schar, M. S. *et al.* Pharyngeal tongue base augmentation for dysphagia therapy: A prospective case series in patients post head and neck cancer treatment. *Head neck* **44,** 1871–1884. ISSN: 1097-0347 (Electronic) (8 Aug. 2022).
50. Schaen-Heacock, N. E., Jones, C. A. & McCulloch, T. M. Pharyngeal Swallowing Pressures in Patients with Radiation-Associated Dysphagia. *Dysphagia* **36,** 242–249. ISSN: 1432-0460 (Electronic) (2 Apr. 2021).
51. Oh, J. *et al.* Safety and Tolerability of High-Resolution Esophageal Manometry in Children and Adults. *Clinical and Translational Gastroenterology,* 1–7. ISSN: 2155384X (2023).
52. Cock, C. & Omari, T. Diagnosis of Swallowing Disorders: How We Interpret Pharyngeal Manometry. *Current Gastroenterology Reports* **19.** Cited By :32¡br/¿¡br/¿Export Date: 30 November 2022 (3 2017).
53. Raut, V. V., McKee, G. J. & Johnston, B. T. Effect of bolus consistency on swallowing – does altering consistency help? *European Archives of Oto-Rhino-Laryngology* **258,** 49–53. ISSN: 1434-4726. `https://doi.org/10.1007/s004050000301` (1 2001).
54. Ito, Y. *et al.* The effect of bolus consistency on pharyngeal volume during swallowing: Kinematic analysis in three dimensions using dynamic Area Detector CT. *Journal of Oral Rehabilitation* **47.** https://doi.org/10.1111/joor.13062, 1287–1296. ISSN: 0305-182X. `https://doi.org/10.1111/joor.13062` (10 Oct. 2020).
55. Lan, Y. *et al.* The effect of bolus consistency on swallowing function measured by high-resolution manometry in healthy volunteers. *The Laryngoscope* **127.** https://doi.org/10.1002/lary.26085, 173–178. ISSN: 0023-852X. `https://doi.org/10.1002/lary.26085` (1 Jan. 2017).
56. Omari, T. I., Dejaeger, E., Tack, J., Beckevoort, D. V. & Rommel, N. Effect of bolus volume and viscosity on pharyngeal automated impedance manometry variables derived for broad dysphagia patients. *Dysphagia* **28.** Cited By :34¡br/¿¡br/¿Export Date: 30 December 2022, 146–152 (2 2013).

57. Jungheim, M., Kallusky, J. & Ptok, M. Effect of Bolus Volume on Pharyngeal Swallowing Dynamics Evaluated with Small High-Resolution Manometry Catheters. *Laryngo- Rhino- Otologie* **96.** Cited By :5¡br/¿¡br/¿Export Date: 30 December 2022, 112–117 (2 2017).
58. Lin, T. *et al.* Effect of bolus volume on pharyngeal swallowing assessed by high-resolution manometry. *Physiology Behavior* **128,** 46–51. ISSN: 0031-9384 (Apr. 2014).
59. Gumbley, F., Huckabee, M. L., Doeltgen, S. H., Witte, U. & Moran, C. Effects of bolus volume on pharyngeal contact pressure during normal swallowing. *Dysphagia* **23,** 280–285. ISSN: 0179051X. https://link.springer.com/article/10.1007/s00455-007-9137-9 (3 Sept. 2008).
60. Bennett, J. W., Van Lieshout, P. H. H. M., Pelletier, C. A. & Steele, C. M. Sip-sizing behaviors in natural drinking conditions compared to instructed experimental conditions. eng. *Dysphagia* **24,** 152–158. ISSN: 1432-0460 (Electronic) (June 2009).
61. Kwong, S. L. *et al.* Effect of Topical Nasal Anesthetic on Comfort and Swallowing in High-Resolution Impedance Manometry. *The Laryngoscope* **132,** 2124–2131. https://onlinelibrary.wiley.com/doi/abs/10.1002/lary.30010 (11 2022).
62. Singendonk, M. *et al.* Reliability of an online analysis platform for pharyngeal high-resolution impedance manometry recordings. *Speech, Language and Hearing* **22,** 195–203. https://doi.org/10.1080/2050571X.2018.1535564 (2019).
63. Mielens, J. D., Hoffman, M. R., Ciucci, M. R., Jiang, J. J. & McCulloch, T. M. Automated analysis of pharyngeal pressure data obtained with high-resolution manometry. *Dysphagia* **26.** Cited By :62¡br/¿¡br/¿Export Date: 30 December 2022, 3–12. https://link.springer.com/article/10.1007/s00455-010-9320-2 (1 2011).
64. Lee, T. H. *et al.* High-resolution impedance manometry facilitates assessment of pharyngeal residue and oropharyngeal dysphagic mechanisms. *Diseases of the Esophagus* **27,** 220–229. ISSN: 14422050 (3 2014).
65. Jung, M., Kim, Y.-G., Jeong, K. W., Choi, K. H. & joo song, K. High Resolution Manometry versus Video Fluorography for Evaluating Dysphagia in Patients with Inflammatory Myopathy: A Pilot Study. *Journal of the Korean Dysphagia Society* **10,** 107–112. ISSN: 2233-5978 (1 Jan. 2020).
66. Olsson, R., Nilsson, H. & Ekberg, O. Pharyngeal Solid-State Manometry Catheter Movement During Swallowing in Dysphagic and Nondysphagic Participants. *Academic Radiology* **1,** 339–344. ISSN: 10766332 (4 1994).
67. Choi, E. C. *et al.* Changes of Esophageal Motility after Total Laryngectomy. *Otolaryngology–Head and Neck Surgery* **128,** 691–699. https://aao-hnsfjournals.onlinelibrary.wiley.com/doi/abs/10.1016/S0194-59980300093-7 (2003).
68. Ramaswamy, A. T., Martell, P., Azevedo, R. & Belafsky, P. The upper esophageal sphincter: anatomy and physiology. *Annals of Esophagus* **5.** ISSN: 26162784 (Sept. 2022).
69. Hashimoto, H. *et al.* Non-invasive quantification of human swallowing using a simple motion tracking system. *Scientific Reports* **8,** 5095. ISSN: 2045-2322. https://doi.org/10.1038/s41598-018-23486-0 (2018).
70. Isberg, A., Nilsson, M. E. & Schiratzki, H. Movement of the upper esophageal sphincter and a manometric device during deglutition. A cineradiographic investigation. *Acta Radiol. - Ser. Diagnosis* **26,** 381–388. ISSN: 05678056 (1985).
71. Pauloski, B. R. *et al.* Relationship between manometric and videofluoroscopic measures of swallow function in healthy adults and patients treated for head and neck cancer with various modalities. eng. *Dysphagia* **24,** 196–203. ISSN: 1432-0460 (Electronic) (June 2009).
72. Olsson, R., Nilsson, H. & Ekberg, O. Simultaneous videoradiography and pharyngeal solid state manometry (videomanometry) in 25 nondysphagic volunteers. *Dysphagia* **10,** 36–41. ISSN: 0179051X (1995).
73. Williams, R. B., Pal, A., Brasseur, J. G. & Cook, I. J. Space-time pressure structure of pharyngo-esophageal segment during swallowing. *Am. J. Physiol. Liver Physiol.* **281,** G1290–G1300. ISSN: 0193-1857. https://doi.org/10.1152/ajpgi.2001.281.5.G1290 (Nov. 2001).
74. Kellen, P. M., Becker, D. L., Reinhardt, J. M. & Van Daele, D. J. Computer-Assisted Assessment of Hyoid Bone Motion from Videofluoroscopic Swallow Studies. *Dysphagia* **25,** 298–306. ISSN: 1432-0460. https://doi.org/10.1007/s00455-009-9261-9 (2010).
75. Hossain, I., Roberts-South, A., Jog, M. & El-Sakka, M. R. Semi-automatic assessment of hyoid bone motion in digital videofluoroscopic images. *Comput. Methods Biomech. Biomed. Eng. Imaging Vis.* **2,** 25–37. ISSN: 21681171 (2014).
76. Zhang, Z., Coyle, J. L. & Sejdić, E. Automatic hyoid bone detection in fluoroscopic images using deep learning. *Scientific Reports* **8.** ISSN: 20452322 (1 Dec. 2018).

77. Lee, D. *et al.* Online Learning for the Hyoid Bone Tracking During Swallowing With Neck Movement Adjustment Using Semantic Segmentation. *IEEE Access* **8,** 157451–157461 (2020).
78. Bandini, A. & Steele, C. M. The effect of time on the automated detection of the pharyngeal phase in videofluoroscopic swallowing studies. eng. *Annu. Int. Conf. IEEE Eng. Med. Biol. Soc. IEEE Eng. Med. Biol. Soc. Annu. Int. Conf.* **2021,** 3435–3438. ISSN: 2694-0604 (Electronic) (Nov. 2021).
79. Lee, S. J., Ko, J. Y., Kim, H. I. & Choi, S. I. Automatic detection of airway invasion from videofluoroscopy via deep learning technology. *Appl. Sci.* **10.** ISSN: 20763417 (2020).
80. Ariji, Y. *et al.* A preliminary deep learning study on automatic segmentation of contrast-enhanced bolus in videofluorography of swallowing. *Sci. Rep.* **12,** 18754. ISSN: 2045-2322. https://doi.org/10.1038/s41598-022-21530-8 (2022).
81. Abdelaziz, M. A. *et al. AI-Powered Toolkit for Automated Swallowing Kinematics Analysis in X-Ray Videofluoroscopy* in *2022 4th Nov. Intell. Lead. Emerg. Sci. Conf.* (2022), 71–74. ISBN: VO -.
82. Bandini, A., Smaoui, S. & Steele, C. M. Automated pharyngeal phase detection and bolus localization in videofluoroscopic swallowing study: Killing two birds with one stone? *Comput. Methods Programs Biomed.* **225,** 107058. ISSN: 0169-2607. https://www.sciencedirect.com/science/article/pii/S0169260722004400 (2022).
83. Best, M. D. *et al. Semiautomatic marker tracking of tongue positions captured by videofluoroscopy during primate feeding* in. **2015-November** (Institute of Electrical and Electronics Engineers Inc., Nov. 2015), 5347–5350. ISBN: 9781424492718.
84. Wong, S.-F., Wong, K.-Y. K., Wong, W. .-. K., Leong, C. .-. J. & Luk, D. .-. K. *Tracking Lumbar Vertebrae in Digital Videofluoroscopic Video Automatically* ().
85. Kim, H.-I. *et al.* Hyoid Bone Tracking in a Videofluoroscopic Swallowing Study Using a Deep-Learning-Based Segmentation Network. *Diagnostics* **11.** ISSN: 2075-4418. https://www.mdpi.com/2075-4418/11/7/1147 (7 2021).
86. Zhang, Z., Mao, S., Coyle, J. & Sejdić, E. Automatic annotation of cervical vertebrae in videofluoroscopy images via deep learning. *Medical Image Analysis* **74,** 102218. ISSN: 1361-8415. https://www.sciencedirect.com/science/article/pii/S1361841521002632 (2021).

# 6

# Appendix

## 6.1 Combined VFSS and HRIM measurement protocol for HNC patients

# 6.1 Protocol uitvoering manovideofluoroscopy

*NB: This protocol is written in Dutch due to the clinical application for a Dutch hospital. If desired, the author can request a translation of this protocol.*

## Algemene opmerkingen:

- Viscositeit en volume gelijk houden bij alle patiënten.
- Bolussen aanbieden aan patiënt via spuitjes.
- Stop bij grote hoeveelheden aspiratie.
- Noem de volume en consistenties voor toediening hardop op.
- Neem de röntgen opname in één lange opname op.
- Houd de blootstelling aan röntgen voor de patiënt zo kort mogelijk.
- Degene die de manometrie bedient draagt een loodschort, omdat deze niet achter de wand kan staan. Evt draagt een tweede persoon loodschort als een tweede persoon de bolussen aan de patiënt aanbiedt. Daarnaast draagt degene die de katheter inbrengt een loodschort bij het inbrengen van de katheter. Dit kan een van bovengenoemde personen zijn.
- Bij residu de patiënten met water na laten spoelen, daarna checken of contrast geklaard is.
- Voor de videofluoroscopy beelden de halswervels in beeld brengen, dan belichting vastzetten, dan breder beeld: lippen, zachte gehemelte, bovenste deel slokdarm. NB: beeld constant houden, dus hij moet niet op pulseren staan.

## Benodigdheden:

**Manometrie:**

1. Handschoenen
2. Tissues
3. Manometer Solar GI HRIM SOldi State, Trolley System SN 18710476 (kar met manometrie computer).
4. Katheter Unisensor HRM K103659-E-1180-D
5. 2% Lidocaïne hydrochloride + schoon opzetstuk
6. Tristel Trio Whipes System, incl. zakje 1, 2, 3 + foam en naslagboekje
7. Nasofix fixatie pleister
8. Plastic teil met water op 37 ˚C (sticker schoon)
9. Plastic teil met twee uitgevouwen tissues (sticker vies)
10. Bekertje water met rietje
11. Thermometer
12. Camera

**Slikmateriaal:**

1. Omnipaque
2. Kraanwater
3. Precise SBMkit Saline Concentration
4. ThickenUp Gel Express
5. Twee 10ml spuitjes (#BD305959 )
6. Maatbeker
7. Lepel om door te roeren
8. 4 papieren bekertjes met op de bekertjes geschreven:
    a. IDDSI0
    b. IDDSI4
    c. IDDSI7
    d. IDDSI7

## Voorbereiding:

**Slikmateriaal klaarmaken per patiënt:**

1. Doe 6 pompjes saline in een maatbeker.
2. Voeg hier 20mL kraanwater aan toe.
3. Vul aan met omnipaque tot 200mL.
4. Roer door.
5. Verdeel het mengsel over vier verschillende bekertjes:

| **IDDSI0** | **IDDSI4** | **2x IDDSI7** |
|---|---|---|
| 125mL van het mengsel | 75mL van het omnipaque mengsel | Overig beetje IDDSI4 mengsel |
| Doe hiervan minstens 80mL in een aparte beker | 3 pompjes ThickenUp Gel Express | Halve cracker |
| | Roer het mengsel 30 seconden door | |
| | Laat de beker 5 minuten staan | |
| | Roer nogmaals door | |

| ***Haal hieruit tijdens meeting:*** | ***Haal hieruit tijdens meeting:*** |
|---|---|
| *2 spuitjes van 10mL* | 2 spuitjes van 10mL |
| *2 spuitjes van 5 mL* | 2 spuitjes van 5mL |
| *2 keer een slok uit de beker* | |
| *(hier is dan 95 mL voor over)* | |

**Manometrie:**

1. Maak de CIM-module vast aan de infuuspaal
2. Sluit de katheter aan op de CIM-module
3. Zet de computer van de manometer aan
4. Open het programma “Laborie”
5. Log in: Username: admin
1. Wachtworod: admin
6. Klik op New patient OF new investigation (bij herhaalde meting)
7. Voer de gegevens in OF kies de juiste patiënt
8. Klik op Nieuw Onderzoek
9. Klik op SEATTLE protocol
10. Klik op Oesophagus manometrie
11. Controleer katheter (Unisensor HRM K103659-E-1180-D) en klik op doorgaan
12. Vul een schone plastic teil met water van 37 graden (meten met de thermometer)
13. Leg de katheter in de plastic teil met water (schoon)
14. Zorg dat er 1cm water boven de katheter in de teil zit
15. Laat de katheter minimaal 2 minuten in het water liggen
16. Klik op “Nul alle drukken” (let op: de katheter moet ca. 1cm onder water liggen). Dit moet voordat de katheter wordt ingebracht.
17. Laat de patiënt voorwerpen die duidelijk zichtbaar worden op de röntgen, zoals bril, ketting, e.d. afdoen.

Katheter inbrengen

18. Vraag naar voorkeur neusgat
19. Spray 1 spray lidocaïne in het gewenste neusgat (tenzij patiënt anders aangeeft).
20. Laat de patiënt het hoofd achterover houden (kin de lucht in).
21. Plaats katheter in de neus en begeleid hem naar binnen, houd hoofd en katheter vast.

22. Zodra de katheter achterin is, moet patiënt naar beneden kijken (kin op borst). De katheter zal nu ongeveer 15cm opgevoerd zijn. Controleer de positie van de katheter bij patiënten zonder larynx nu, totdat de tip van de katheter zich met zekerheid in de slokdarm bevindt.
23. Laat patiënt, indien mogelijk, continue slikken met water en een rietje. Als dit niet mogelijk is kan de patiënt droge slikken uitvoeren tijdens het inbrengen.
24. Blijf de katheter zacht begeleidend doorvoeren tot de laatste sensor zich net in de neus bevindt. Als er twijfel is over het inbrengen, altijd kort doorlichten ter controle van de positie van de katheter.
25. Zorg dat de katheter niet te diep ligt. De laatste sensor moet net in de neus liggen, het begin van het oranje gedeelte moet buiten de neus liggen (anders wordt er geen impedantie in de velopharynx gemeten). De katheter ligt zo tot een diepte van 36cm in de neus.
26. Bevestig de katheter aan de neus van de patiënt met de nasofix pleister.
27. Laat de patiënt even rusten.
28. Voer ondertussen het aantal sensoren in software in.
29. Plaats de lijntjes in de software op de correcte plek.

*NB. Stagneert het inbrengen? Dan kan de patiënt vaker kort doorgelicht worden om te zien wat er gebeurt (stenose oid).*

**Camera**

1. Plaats de camera zo dat de patiënt en de Laborie software (dus drukmetingen van de manometrie) goed in beeld zijn.
2. Zet de camera aan.

**Slikvideo**

1. Start de computer op en log in.
2. Open Bandicam
3. Noteer de juiste patiënt.
4. Open HiX
5. Documenteer alle verslaglegging in HiX.
6. Documenteer in een tekstbestand of papier alle informatie over de gegeven consistenties en de manometrie.

## Afname protocol:

1. Laat de patiënt rechtop zitten met de schouders laag, zodat de röntgen lateraal wordt ingeschoten.
2. De combidiagnost staat ingesteld op continue doorlichting en hoge resolutie, zie hieronder:

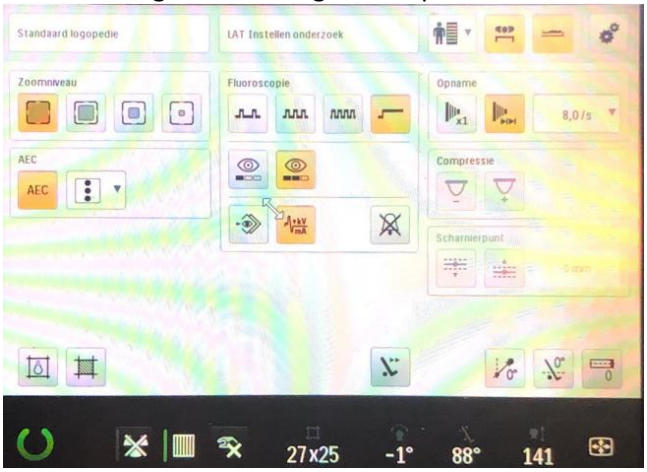


3. Controleer of de camera met videostand aanstaat en alles filmt.
4. Zet de dictafoon bij de patiënt aan.
5. Klik op de manometer op “Start Onderzoek”.

6. Laat de laborant de röntgen instellen. Instrueer de laborant dat de eerste sensor van de katheter tot en met de sensoren onder de UES in beeld moeten blijven tijdens de metingen.
7. Controleer of daarnaast de volgende structuren in beeld zijn:

| | | |
|---|---|---|
| ☐ Oral cavity | ☐ Oropharynx | ☐ UES |
| ☐ Nasopharynx | ☐ Hypoharynx | ☐ HRM Katheter |

8. Zet de Bandicam en de cine loop op hetzelfde moment aan.
9. Laat de Bandicam continue doorlopen
10. *Plaats iets voordat de patiënt de eerste slik uitvoert EN iets nadat de patiënt klaar is met het klaren van de bolus een marker van de juiste consistentie in Laborie.*

**Slikken:**
Laat de patiënt de volgende hoeveelheden en consistenties slikken via een spuit, tenzij anders aangegeven:
*! Indien er bij de eerste slik van 5cc IDDSI0 veel aspiratie is, ga dan naar stap 2 van het stroomdiagram hieronder !*

- ☐ IDDSI0 5cc
- ☐ IDDSI0 5cc
- ☐ IDDSI0 10cc
- ☐ IDDSI0 10cc
- ☐ IDDSI 0 – slok uit beter
- ☐ IDDSI4 5cc
- ☐ IDDSI4 5cc
- ☐ IDDSI4 10cc
- ☐ IDDSI4 10cc
- ☐ IDDSI 7
- ☐ IDDSI 7
  *Draai de patiënt nu zodat de röntgen opname AP ingeschoten wordt.*
- ☐ IDDSI 0 – slok uit beker → *volg deze bolus via de slokdarm naar de maag.*

Totaal 11 bolussen (30cc +2 slokken IDDSI0, 30cc IDDSI4 en 2 halve crackers IDDSI 7)

*Indien diagnostisch wenselijk kunnen er meer slikken van verschillende IDDSI's uitgevoerd worden, eventueel met behulp van onderstaand stroomdiagram.*

# Afname protocol bij onveilige 10cc IDDSI0 slik

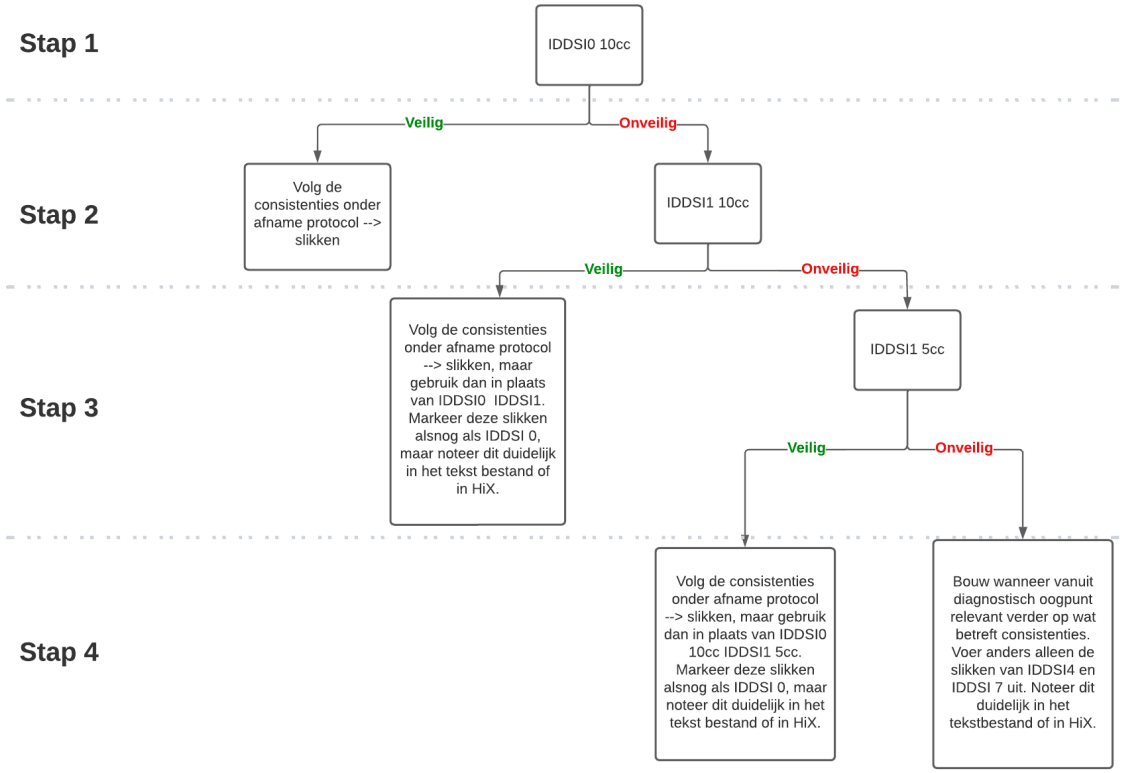


# Afronden en schoonmaken

1. Leg de Tristel Trio Whipes System, incl. zakje 1, 2, 3 + foam en naslagboekje klaar.
2. Vul het naslagboekje in.
3. Trek handschoenen aan.
4. Zet de vieze teil voor de HRIM-katheter klaar.
5. Verwijder de nasofix pleister van de neus van de patiënt.
6. Verwijder de HRIM-katheter in één rustige beweging uit de neus van de patiënt.
7. Verwijder de nasofix pleister van de katheter.
8. Ontkoppel de HRIM-katheter van de CIM-module.
9. Maak de HRIM-katheter schoon met zakje 1 en leg hem op een schone onderlegger.
10. Ontsmet de handen en trek nieuwe handschoenen aan.
11. Spuit twee pompjes schuim op doekje 2, wrijf het doekje 15 seconden over zichzelf, en maak vervolgens de katheter gedurende 30 seconden schoon met doekje 2.
12. Leg de katheter op een schone onderlegger.
13. Ontsmet de handen en trek nieuwe handschoenen aan.
14. Maak de HRIM-katheter schoon met doekje 3.
15. Leg de katheter in de schone bak.